AD-A192 073 FLUID DYNAMICS OF HIGH PERFORMANCE TURBOMACHINES(U) 1/2
MASSACHUSETTS INST OF TECH CAMBRIDGE DEPT OF
AERONAUTICS AND ASTRONAUTICS E M GREITZER ET AL.
UNCLASSIFIED DEC 87 AFOSR-TR-88-0103 F49620-85-C-0018 F/G 20/4 NL

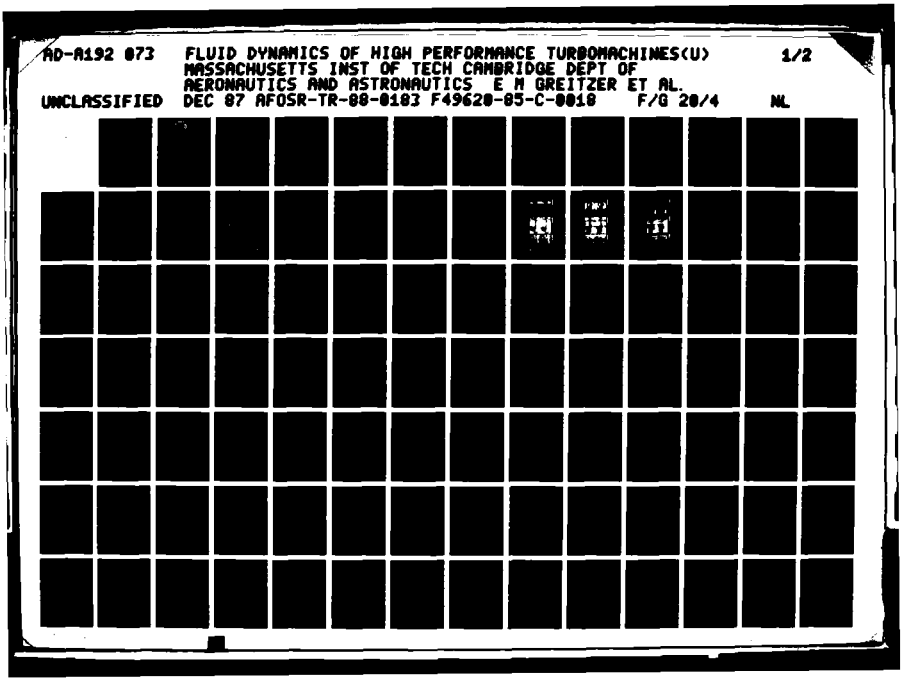

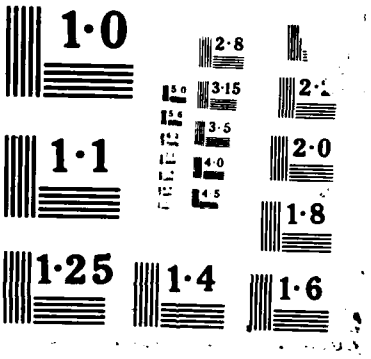
1·0
1·1
1·25
1·4
1·6
1·8
2·0
2·8
3·15
3·5
4·0
4·5

UNCLASSIFIED

SECURITY CLASSIFICATION OF THIS PAGE

OTIC FILE COPY

(2)

REPORT DOCUMENTATION PAGE

AD-A192 073

1a. REPORT SECURITY CLASSIFICATION: Unclassified	1b. RESTRICTIVE MARKINGS: None
	3. DISTRIBUTION/AVAILABILITY OF REPORT: Approved for public release; distribution unlimited.
	5. MONITORING ORGANIZATION REPORT NUMBER(S): AFOSR-TR- 88-0183
6a. NAME OF PERFORMING ORGANIZATION: Department of Aeronautics and Astronautics, MIT	6b. OFFICE SYMBOL (If applicable): 31-264
7a. NAME OF MONITORING ORGANIZATION: See #8 AFOSR/NA Bolling AFB, DC 20332	
6c. ADDRESS (City, State, and ZIP Code): 77 Massachusetts Avenue Cambridge, MA 02139	7b. ADDRESS (City, State, and ZIP Code): See #8 AFOSR/NA Bolling AFB, DC 20332
8a. NAME OF FUNDING/SPONSORING ORGANIZATION: AFOSR	8b. OFFICE SYMBOL (If applicable): NA
9. PROCUREMENT INSTRUMENT IDENTIFICATION NUMBER: Contract F49620-85-C-0018	
8c. ADDRESS (City, State, and ZIP Code): AFOSR Bolling AFB, DC 20332	10. SOURCE OF FUNDING NUMBERS: PROGRAM ELEMENT NO. 61102F; PROJECT NO. 2307; TASK NO. A4; WORK UNIT ACCESSION NO

11. TITLE (Include Security Classification)

Fluid Dynamics of High Performance Turbomachines

12. PERSONAL AUTHOR(S)

E.M. Greitzer, A.H. Epstein, M.B. Giles, J.E. McCune, C.S. Tan

13a. TYPE OF REPORT	13b. TIME COVERED	14. DATE OF REPORT (Year, Month, Day)	15. PAGE COUNT
Annual	FROM 10/19/86 TO 10/18/87	87/12	129

16. SUPPLEMENTARY NOTATION

17. COSATI CODES		
FIELD	GROUP	SUB-GROUP

18. SUBJECT TERMS (Continue on reverse if necessary and identify by block number)

Transonic Compressors, Compressor Stability, Casing Treatment Design, Vortex Wakes, Unsteady Flows in Turbomachines

19. ABSTRACT (Continue on reverse if necessary and identify by block number)

This report gives a summary of work carried out at the Gas Turbine Laboratory at MIT, during the period 10/19/86 to 10/18/87, as part of our multi-investigator effort on high performance turbomachinery fluid dynamics. Within the general topic, four separate tasks are specified. These are, in brief: I. Loss mechanisms and loss migration in transonic compressors, including development of advanced instrumentation for measurements of wake radial transport and analysis of unsteady vortical wake structures. II. Experimental and theoretical study of flows in casing and hub treatment, including mechanisms for stability enhancement in compressors and unsteady fluid dynamic interactions between passage and groove flows. III. Computational techniques for turbomachinery, including inverse (design) calculation procedures for transonic turbomachine blades accounting for viscid/inviscid interaction. IV. Theoretical modelling of stability and unsteadiness in transonic compressor flow fields, including analyses of unsteady temperature fluctuations due to vortex shedding.

20. DISTRIBUTION/AVAILABILITY OF ABSTRACT	21. ABSTRACT SECURITY CLASSIFICATION
☒ UNCLASSIFIED/UNLIMITED ☒ SAME AS RPT ☐ DTIC USERS	UNCLASSIFIED
22a. NAME OF RESPONSIBLE INDIVIDUAL: Captain H. Helin	22b. TELEPHONE (Include Area Code): 202 767 0471 — 22c. OFFICE SYMBOL: NA

DD FORM 1473, 84 MAR — 83 APR edition may be used until exhausted. All other editions are obsolete.

SECURITY CLASSIFICATION OF THIS PAGE

UNCLASSIFIED

GAS TURBINE LABORATORY
DEPARTMENT OF AERONAUTICS AND ASTRONAUTICS
MASSACHUSETTS INSTITUTE OF TECHNOLOGY
CAMBRIDGE, MA 02139

ANNUAL TECHNICAL REPORT

on

CONTRACT NO. F49620-85-C-0018

entitled

FLUID DYNAMICS OF HIGH PERFORMANCE TURBOMACHINES

for the period

October 19, 1986 to October 18, 1987

submitted to

AIR FORCE OFFICE OF SCIENTIFIC RESEARCH

Attention: Dr. James Wilson, Program Manager
AFOSR/NA
Directorate of Aerospace Sciences
Building 410
Bolling Air Force Base, DC 20332

Principal Investigator: Edward M. Greitzer
Professor and Director, Gas Turbine Laboratory

Co-Investigators: Prof. Alan H. Epstein
Prof. Michael B. Giles
Prof. James E. McCune
Dr. Choon S. Tan

December 1987

TABLE OF CONTENTS

1. INTRODUCTION AND RESEARCH OBJECTIVES

This report describes work carried out at the Gas Turbine Laboratory at MIT, as part of our multi-investigator effort on high performance turbomachinery fluid dynamics. Support for this program is provided by the Air Force Office of Scientific Research under Contract Number F49620-85-C-0018, Dr. J.D. Wilson, Program Manager.

The present report gives a short summary of the work for the period 10/19/86 - 10/18/87. For further details and background, the referenced laboratory reports, publications, the previous final report (Ref. [1]) covering the period 10/1/81 - 9/30/84, and the three recent progress reports on the current contract should be consulted (Refs. [2], [3], [4]).

Within the general topic, four separate tasks are specified. These are, in brief:

I. Loss mechanisms and loss migration in transonic compressors, including development of advanced instrumentation for measurements of wake radial transport and analysis of unsteady vortical wake structures.

II. Experimental and theoretical study of flows in casing and hub treatment, including mechanisms for stability enhancement in compressors and unsteady fluid dynamic interactions between passage and groove flows.

III. Computational techniques for turbomachinery, including inverse (design) calculation procedures for transonic turbomachine blades accounting for viscid/inviscid interaction.

IV. Theoretical modelling of stability and unsteadiness in transonic compressor flow fields, including analyses of unsteady temperature fluctuations due to vortex shedding.

The work carried out in each of the tasks will be described in the next section.

References

1. E.M. Greitzer, et al., Final Report, 10/81 - 9/84, on "Current Problems in Turbomachinery Fluid Dynamics."

2. E.M. Greitzer, A.H. Epstein, M.B. Giles, J.E. McCune, C.S. Tan, Annual Technical Report on Contract F49620-85-C-0018, "Fluid Dynamics of High Performance Turbomachines," November 1985.

3. E.M. Greitzer, A.H. Epstein, M.B. Giles, J.E. McCune, C.S. Tan, Research Progress and Forecast Report on Contract F49620-85-C-0018, "Fluid Dynamics of High Performance Turbomachines," March 1986.

4. E.M. Greitzer, A.H. Epstein, M.B. Giles, J.E. McCune, C.S. Tan, Annual Technical Report on Contract F49620-85-C-0018, "Fluid Dynamics of High Performance Turbomachines," November 1986.

TASK I: LOSS MECHANISMS AND LOSS MIGRATION IN TRANSONIC COMPRESSORS
(Investigators: A.H. Epstein, P. Kotidis)

Objectives

The primary objective of this effort is to elucidate and quantify the physical mechanisms which produce loss (entropy) in a high speed compressor, with particular attention to three-dimensional and unsteady effects. The motivations for this work are twofold. The first is the desire to dramatically improve the design point performance of high speed compressors to meet the ambitious Air Force propulsion goals of the 1990's. The second is the realization (spurred by AFAPL data showing apparent efficiencies above 100%) that there are important physical phenomena influencing the behavior of compressors which are not at all understood or accounted for in present design methodologies.

Progress During This Year

Efforts during this year have been concentrated in two areas: (a) experimental mapping of the radial flow in a transonic compressor and analysis of the resultant data, and (b) a parametric cycle calculation of the net effects of radial loss migration on jet engine performance.

Radial Flow Migration in a Transonic Rotor

The structure of the radial flows in a turbomachine can have an important influence on the behavior of a given stage as well as on the performance of subsequent blade rows downstream. These radial flows give rise to spanwise mixing which is a key determinant of multistage compressor performance. The nature of magnitude of this process has recently become a topic of considerable debate (Atkins and Smith versus Gallimore and Cumpsty) fueled by its very real practical importance. In all cases to date, these radial mixing processes have been treated only in the time average. In this work, we are taking time resolved measurements of the flow field using a tracer gas to elucidate the

radial flow transport in the rotor. The motivation is both to unsort the radial flow structure (spanwise vortex coherence, flows in boundary layer separation regions, etc.), and to quantify the radial mixing mechanisms.

The mapping of the radial flow in the AFAPL high thru-flow rotor (a 17 inch diameter, 62 lb/sec machine) has been carried out using gas injection in the MIT Blowdown Compressor Facility. Basically, a circumferential sheet of gas (helium/Freon-12 mixture) is injected upstream of the rotor and the time resolved concentration distribution of the injectant is measured at the rotor outlet. The radial position of the injector is then changed and the experiment repeated. The experimental technique has been developed during previous years of this effort. The layout of the apparatus is shown in Figs. 1 and 2. The injector was first run in the tunnel without the compressor stage to establish a baseline mixing rate for the injectant sheet. The stage was then run with the injector present, with and without the injectant turned on, to indicate the effect of the injector hardware (blockage and viscous wake) on the stage performance. The experiment with injectant was then run.

The experiment has proven considerably more difficult than first expected, with detection sensitivity (and thus accuracy) the principal problem. For this reason, the tracer gas was changed from CO_2 (the best match to the main flow) to helium/Freon which increased the sensitivity by a factor of about 10. (The mixture ratio was chosen to make the injectant neutrally buoyant in the argon-Freon test gas used in the blowdown compressor.)

The aspirating probe developed for this project simultaneously measures concentration, total pressure, and total temperature (and thus entropy) with a spatial resolution of 3 mm in the tangential direction and 6 mm in the radial direction. The frequency response is d.c. to 20 kHz. (The theory and development of this probe is well documented [1] and thus will not be given here.)

The probe is traversed from tip to hub over the 30 millisecond test time. Thus, relative to the rotor, the measurement area prescribes a shallow inward spiral. The probe traverse velocity is slow enough compared to the rotor rotational velocity (10 fps vs. 1200 fps) that a quasi-steady measurement is made at each radial or spanwise position.

Data taken with the injector positioned near the hub, midspan, and tip is presented in three forms - "raw" time trace data of the instantaneous measurement (Fig. 3), five blade passing ensemble averages of the raw data (Fig. 4), and contour maps made from the ensemble averaged data (Fig. 5).

The contour maps show the average concentration, total pressure ratio, and total temperature ratio measured at the rotor exit (the view is looking upstream). The vertical scale represents spanwise position, the horizontal scale is azimuthal position; two blade passages are shown (the annulus is flattened here). The radius at which the injectant would be expected without mixing (i.e. the position of the streamline on which the injector is placed translated through the rotor using a streamline curvature solution) is shown as a horizontal line on the concentration map. Note that the concentration, pressure, and temperature ratio maps are aligned vertically on the page such that the azimuthal (or blade to blade) positions correspond, i.e. they represent simultaneous measurements. The uncertainty in the concentration measurement is at the 1% level.

Examining the contour maps for tip injection (Fig. 5a), we see that, although much of the injectant stays near the injection streamline, there is a distinct "tongue" of fluid which is transported inward all the way to the hub. This corresponds to a similar structure of high temperature fluid in the temperature map. (There is an implication - still to be verified - that the higher temperature in this region represents the higher enthalpy [i.e. work

addition] of the tip fluid.) If we assume that the blade wake location can be defined as the low total pressure regions, then the inward motion of the tip fluid clearly occurs outside the wake close to the suction surface.

A similar conclusion may be drawn from examination of the midspan injection data (Fig. 5b). The inward motion of the fluid is evident in the same location on both the concentration and temperature maps. It is interesting to note, however, that just to the right of the inward moving high concentration region there is a region of lower concentration at the outer radii in the blade wake locations. The same pattern can be seen in the tip injection case where the wake position shows very low concentrations of the tracer, even at the injector location.

At this point, it is useful to examine the ensemble averaged time traces (Fig. 4) from which the maps were drawn and the unaveraged instantaneous data (Fig. 3). The instantaneous time traces for the tip injection experiment (Fig. 3a) show that the convection of fluid inward from the tip is restricted to a few isolated regions (the tall "spikes" in concentration at the midspan and tip). Large upspikes of total temperature can be seen to be coincident with the concentration spikes. These spikes are not aligned with the total pressure minimums of the wakes but rather are in the core flow near the suction surface. With midspan injection (Fig. 3b), the hub measurements exhibit the same spiky structure as for the tip injection. With hub injection (Fig. 3c), the midspan measurement shows the spiky concentration distributions which are coincident with upspikes in total temperature.

The tentative conclusion from this data is that there is a mechanism which moves fluid inward in the core flow near the blade suction surface. In the wakes, there is the flow moves inward from midspan toward the hub and perhaps outward from midspan to tip. The actual data is not what we expected,

which was that the radial motion would be predominately in the wakes with perhaps a vortex street as the convection mechanism.

Now that the experimental data has been taken and reduced, it is time to analyze it. In particular, the physical phenomena responsible for motion must be elucidated. This is part of the effort planned for the FY 1988 effort. In addition, the net radial transport of entropy will be calculated from the data in order to quantify the effect the radial transport in this particular stage would have on engine performance. A general treatment of the subject is given below.

The Influence of Radial Loss Migration on Jet Engine Performance

While it has long been clear that the radial migration of loss (entropy) in a turbomachine is important for multistage matching, design verification, and therefore reduced development time, we are not aware of any examination of the effects of radial migration on jet engine performance itself. The question we are addressing here can be summarized as follows: If the fan designer offers the engine development team two different fans - both with the same overall average mass flow, pressure rise, and efficiency but with differing radial distribution of efficiency - which should be chosen?

We will suppose the same total entropy change along each fan streamline. The entropy generated along the streamlines can migrate radially but the radial migration does not change the local production of entropy. We will further assume that the entropy generated along the streamlines which enter the engine core can either enter the core ("no migration") or be moved outward so that this entropy flows through the bypass or fan stream ("with migration"). No additional entropy is assumed to be generated in the migration process.

A cycle analysis with losses was then performed to estimate the effect of this radial loss migration on thrust and specific impulse (the reciprocal of

specific fuel consumption). Since entropy appears primarily as a decrease in total pressure, we are in effect supercharging the core in this process. Thus, in an attempt to do an "apples to apples" comparison, two calculations were done in each case - one in which the overall compressor pressure ratio was kept constant and a second in which the core (or high) compressor pressure ratio was fixed. (The first case might correspond to an all-new design while the second to a reforming of an existing core.)

For an engine of fixed bypass ratio, the results are given in Table 1. We can see that the thrust is increased by 1/2 to 1% while the specific impulse is similarly reduced. These are changes of significant magnitude for a turbine engine. Their specific importance is extremely mission dependent however.

Table 1
Effect of Radial Fan Loss Migration on Engine Performance

	Transport Engine	Fighter Engine
Bypass Ratio	6	1.0
Turbine Inlet Temperature	2960°F (1900°K)	2600°F (1700°K)
Flight Mach No.	0.8	1.0
A. Fixed High Pressure Ratio		
High Compressor Pressure Ratio	18	8
Change in Thrust With Migration	0.6%	0
Change in Impulse With Migration	-0.3%	-0.7%
B. Fixed Overall Pressure Ratio		
Compressor Pressure Ratio	32	25
Change in Thrust With Migration	0.6%	0.9%
Change in Impulse With Migration	-0.8%	-0.7%

The sensitivity of these conclusions to bypass ratio is shown in Figs. 6 and 7. Figure 6 plots percent change in thrust against bypass ratio for the two cases of fixed overall pressure ratio and fixed high pressure compressor pressure ratio. For reasons of simplicity, the fan pressure ratio was chosen to set the core and bypass stream exhaust velocities equal without radial

entropy migration. The corresponding change in specific impulse can be seen in Fig. 7. The increase in thrust is quite dramatic, ∿2%, for the bypass ratio of 5-6 characteristics of modern transport aircraft. The change in specific impulse can be positive or negative but, in either case, is quite small in magnitude, on the order of 1/2% or less. The sensitivity of these results to turbine inlet temperature is shown in Figs. 8 and 9. The magnitude of this effect decreases with turbine inlet temperature (2000°K = 3141°F, a little above current inlet temperatures).

The conclusion from these calculations is that the radial migration can have a very significant effect on the performance of an aircraft gas turbine engine. Clearly, the actual magnitude of the effect in current designs must be assessed (work in progress) and information allowing the designer to optimize migration should be developed.

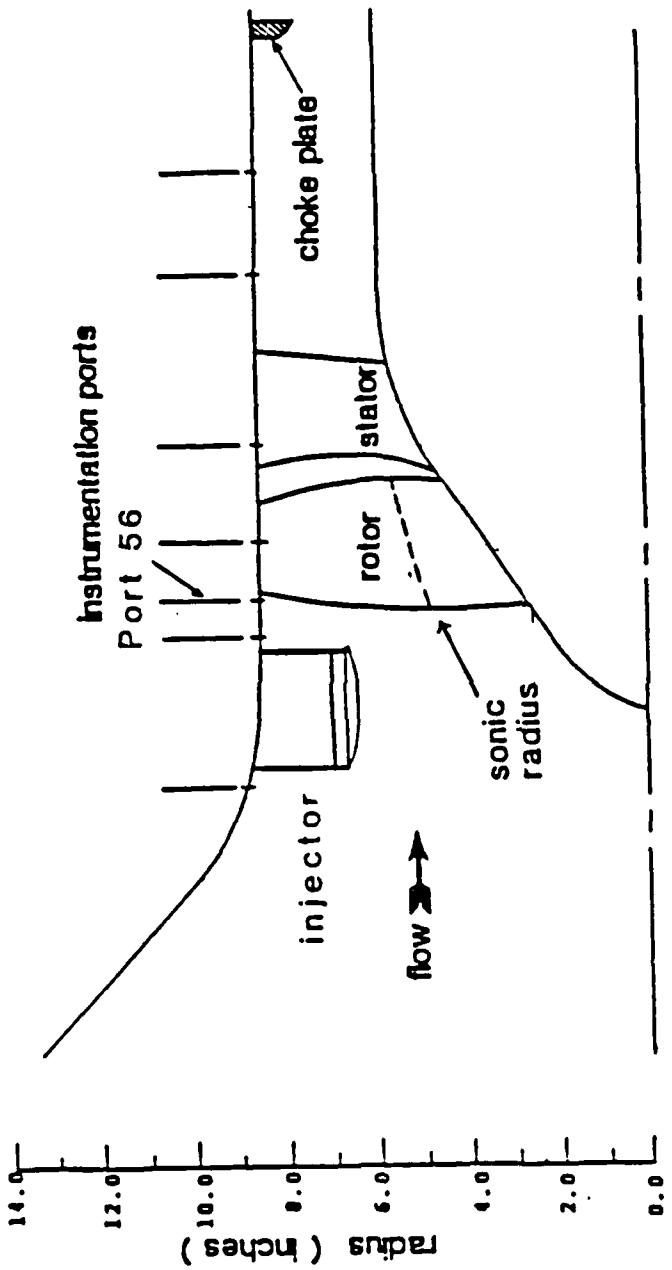

Figure 1: Scale drawing of the test section

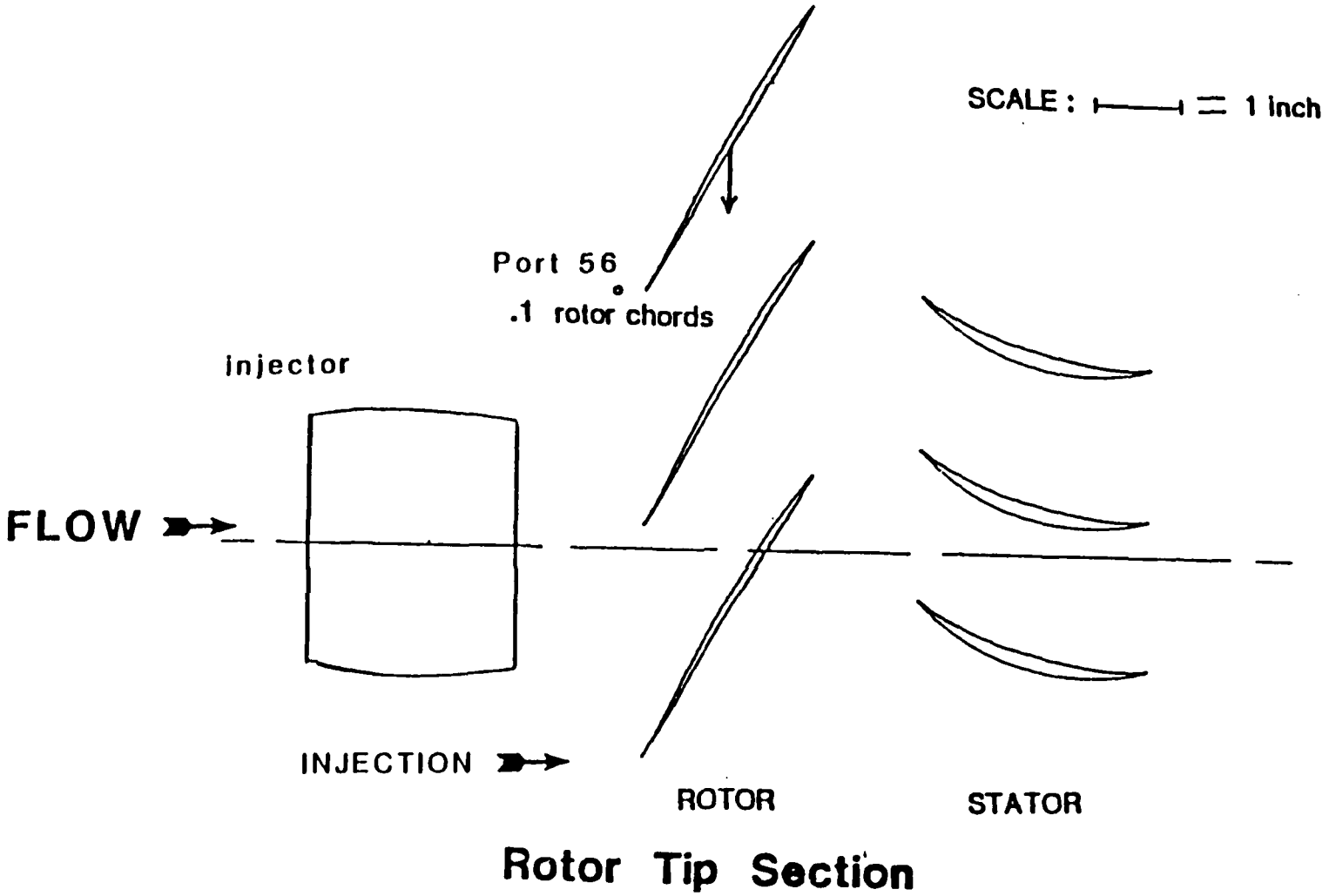

Figure 2: Top view of the experimental arrangement

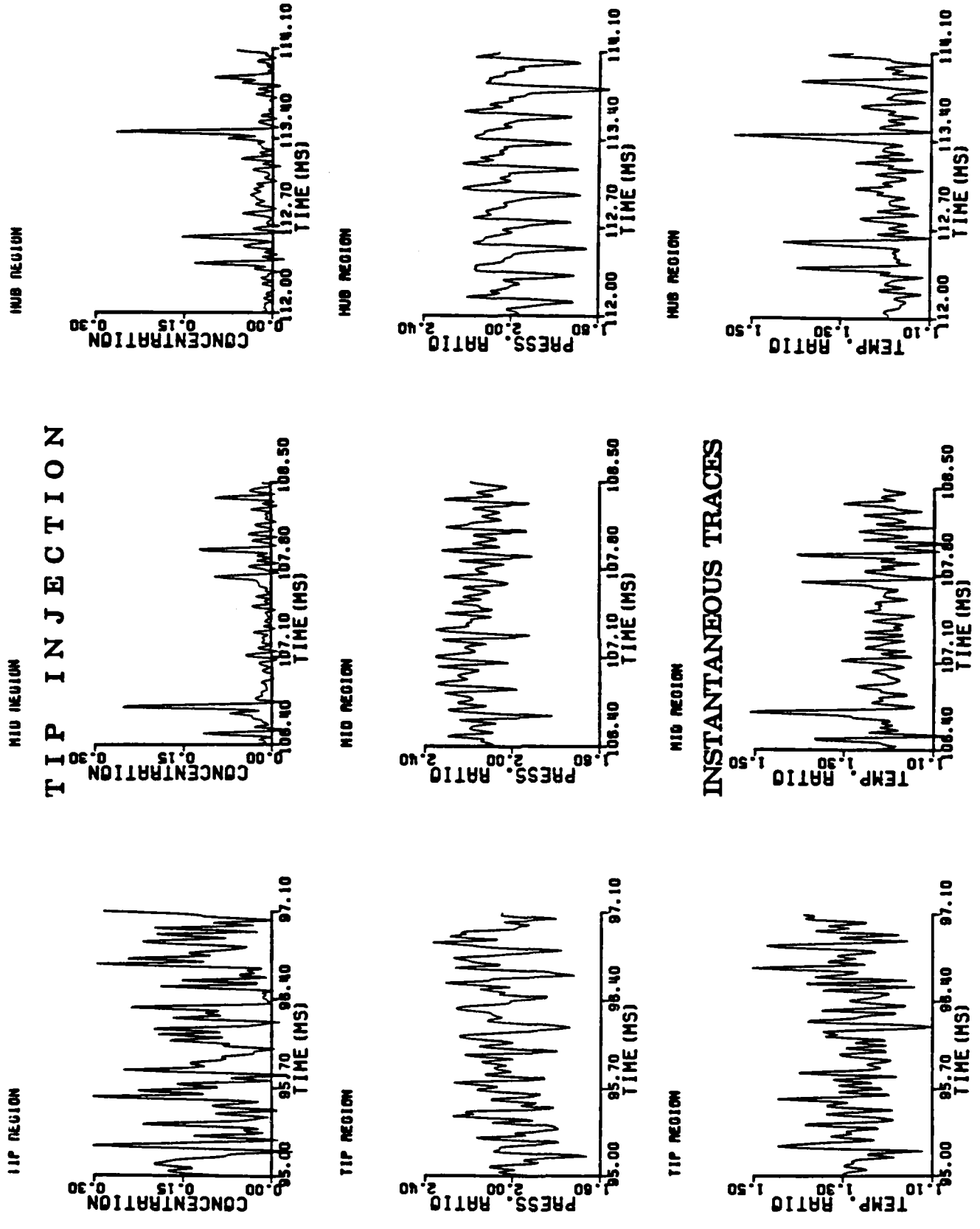

Fig. 3a: Instantaneous concentration, total temperature, and total pressure measured at rotor exit with tracer injected upstream of rotor near the compressor tip

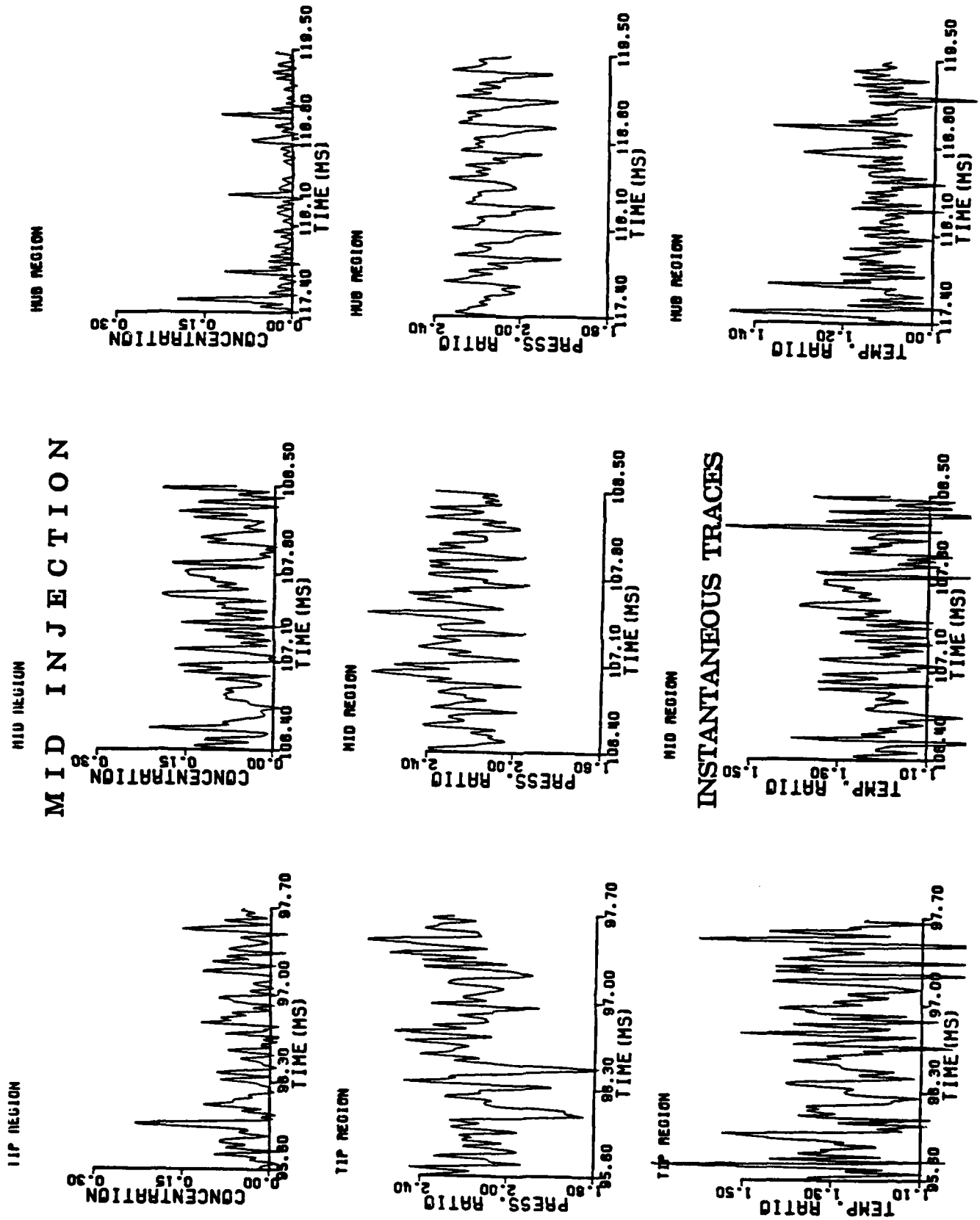

Fig. 3b: Instantaneous concentration, total temperature, and total pressure measured at rotor exit with tracer injected upstream of rotor near the compressor midspan

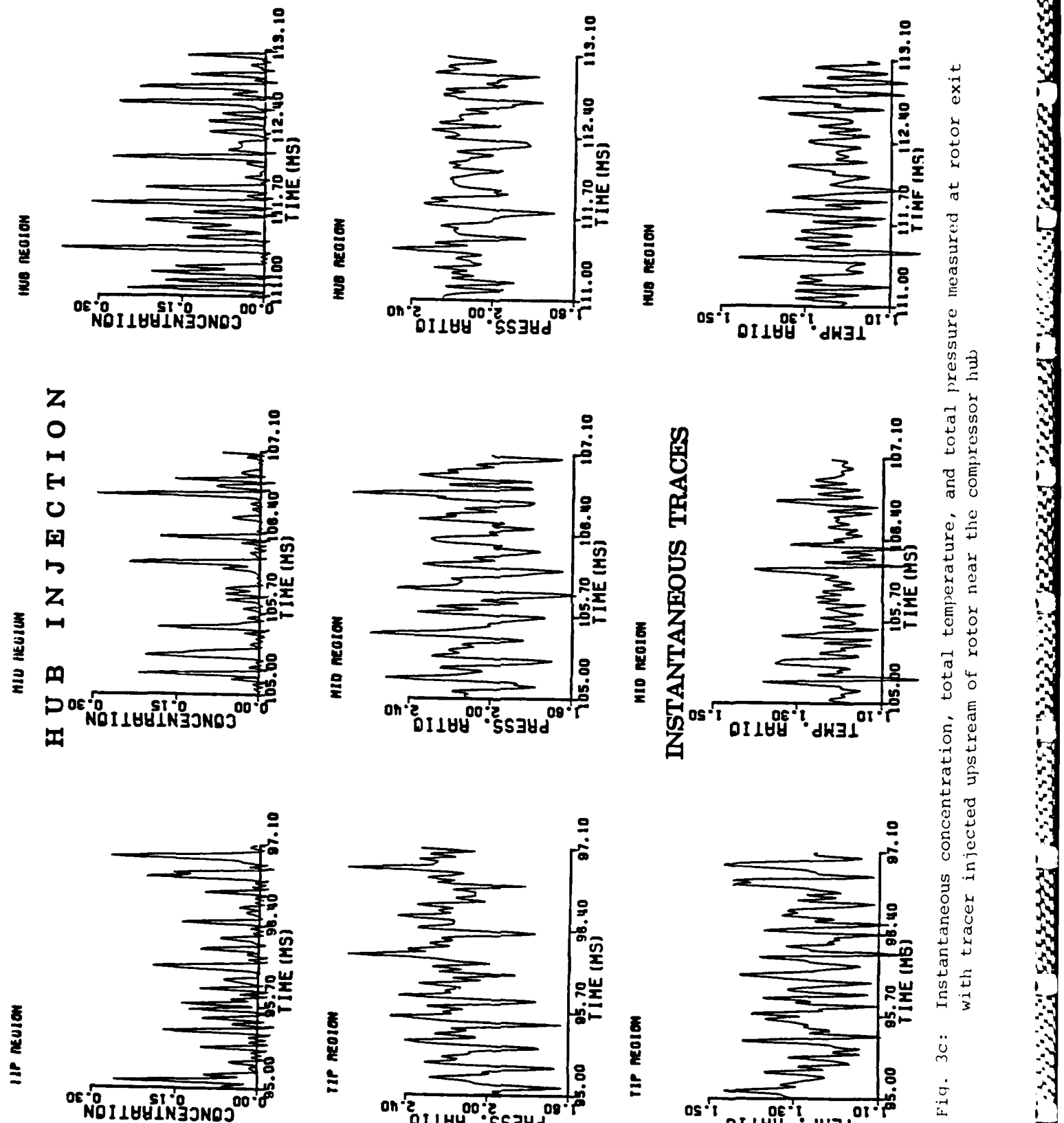

Fig. 3c: Instantaneous concentration, total temperature, and total pressure measured at rotor exit with tracer injected upstream of rotor near the compressor hub

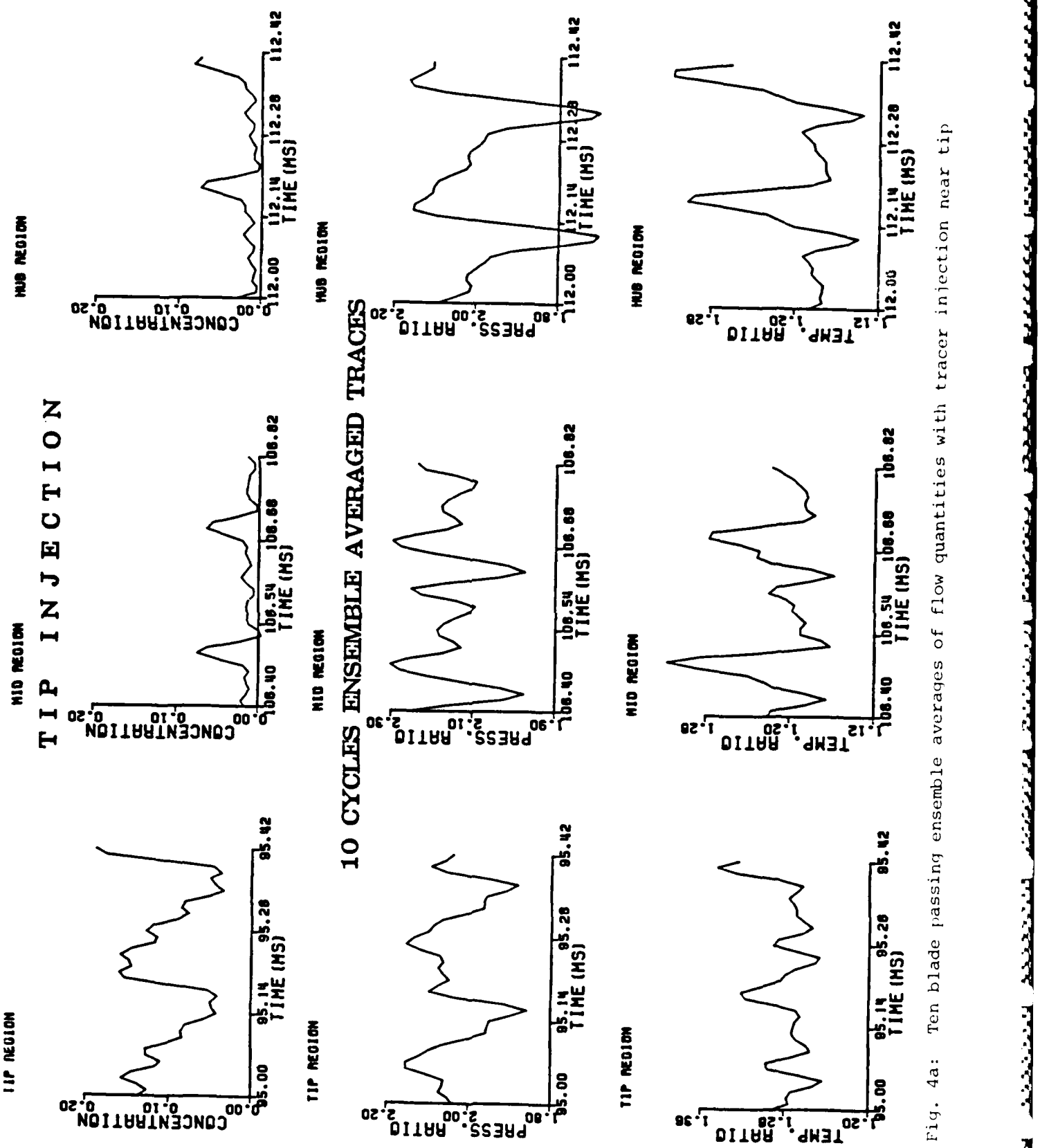

Fig. 4a: Ten blade passing ensemble averages of flow quantities with tracer injection near tip

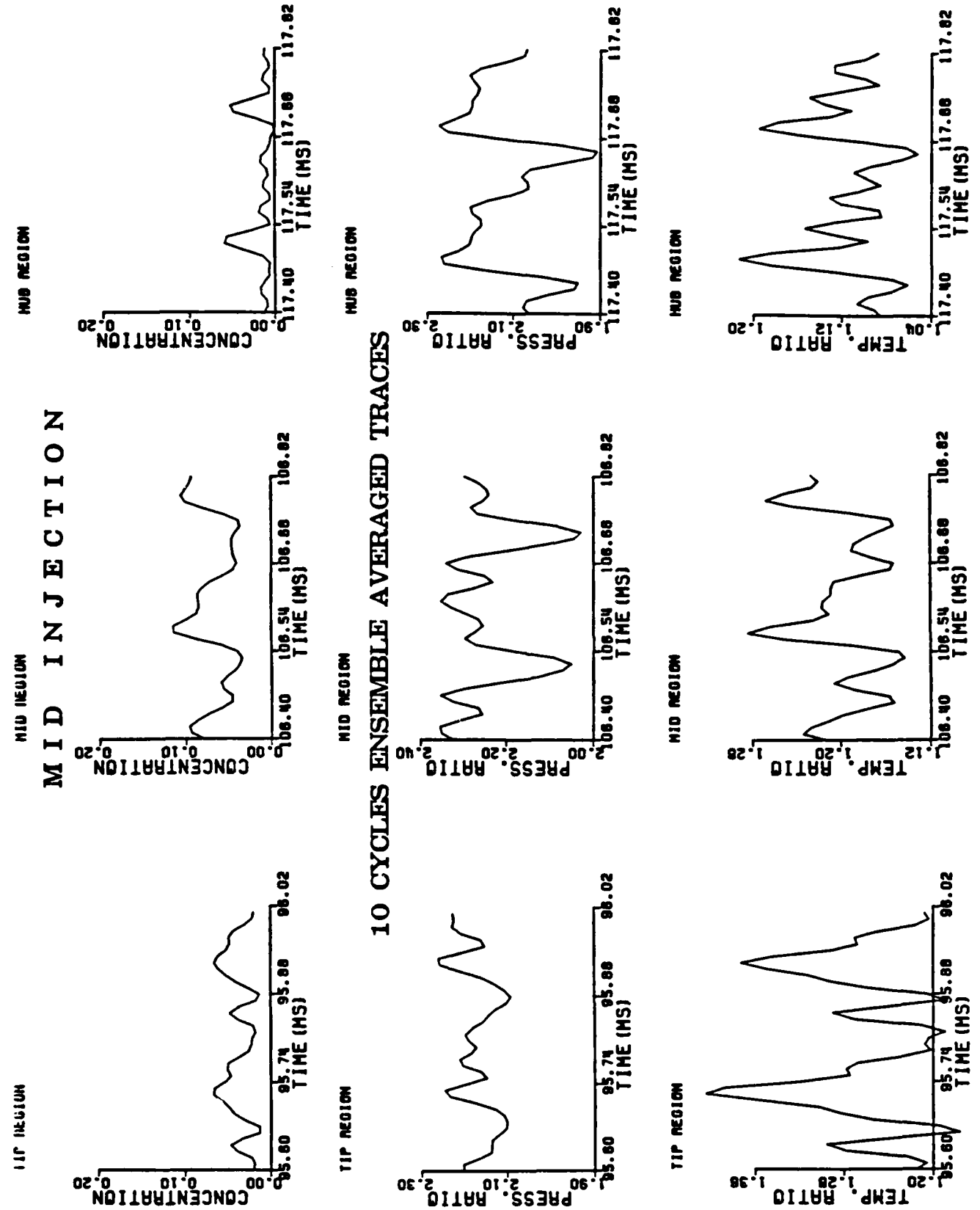

Fig. 4b: Ten blade passing ensemble averages of flow quantities with tracer injection near midspan

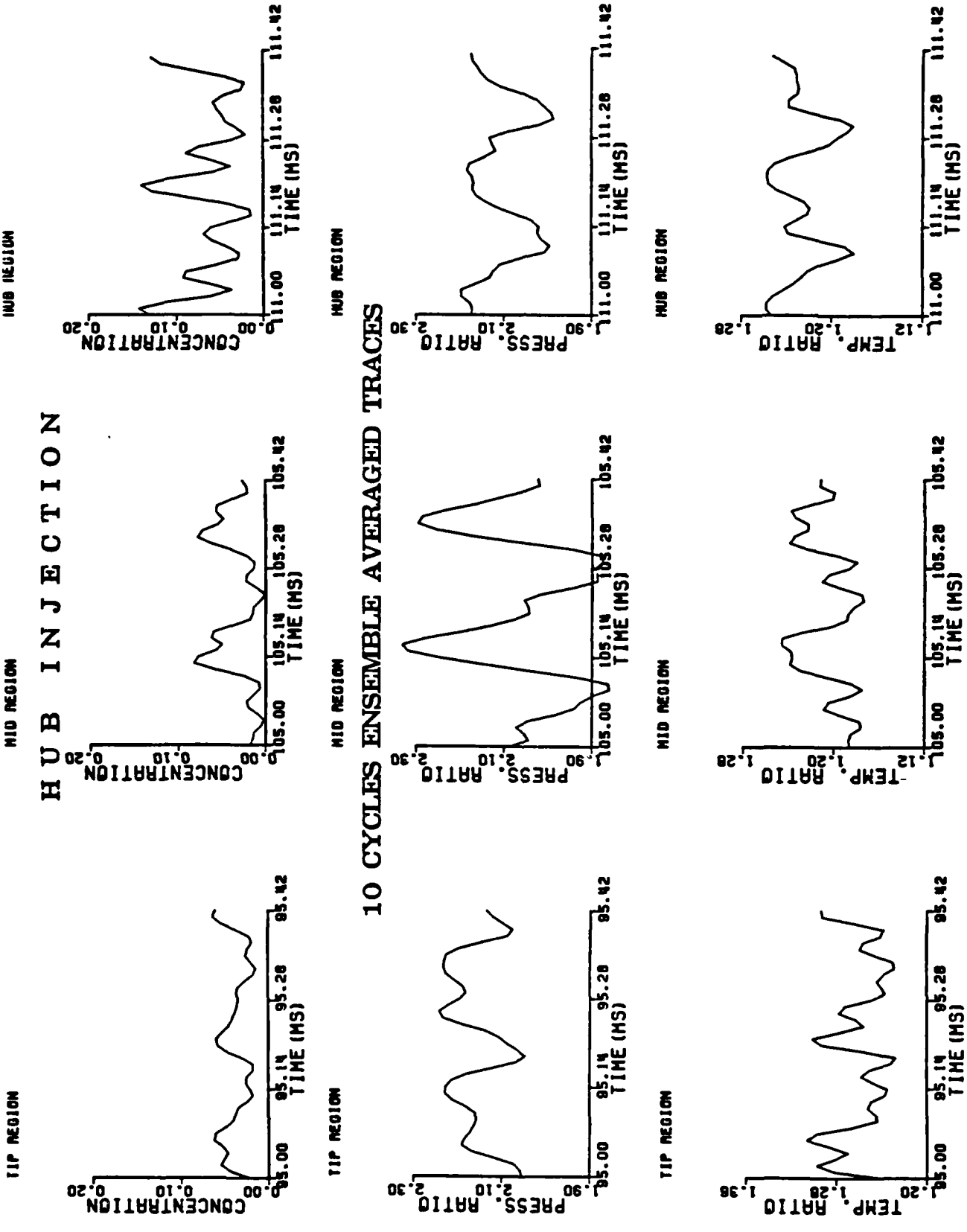

Fig. 4c: Ten blade passing ensemble averages of flow quantities with tracer injection near hub

TIP INJECTION

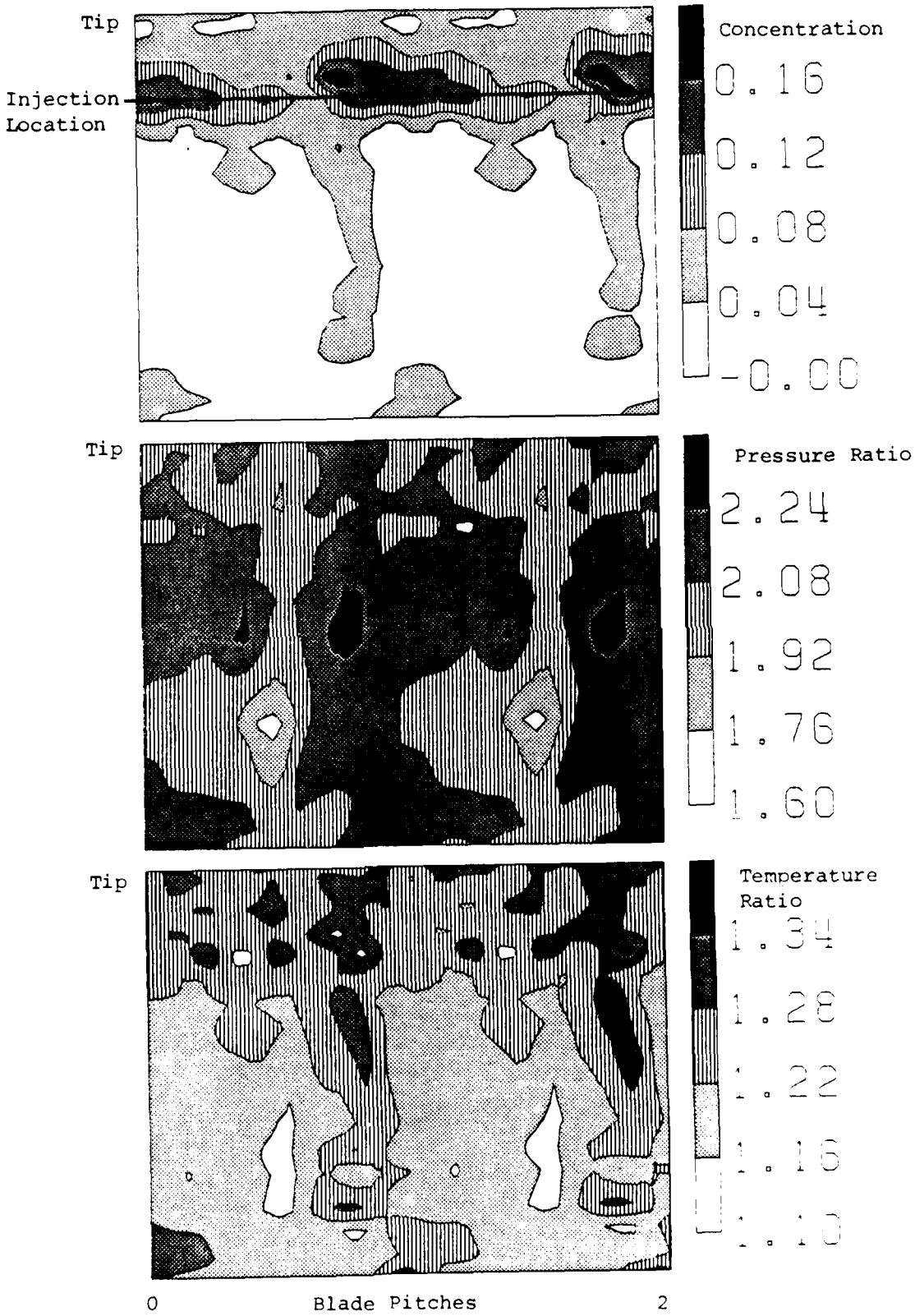

Fig. 5a: Contour maps constructed from the data in Fig. 4, tracer injection as indicated near tip

MIDSPAN INJECTION

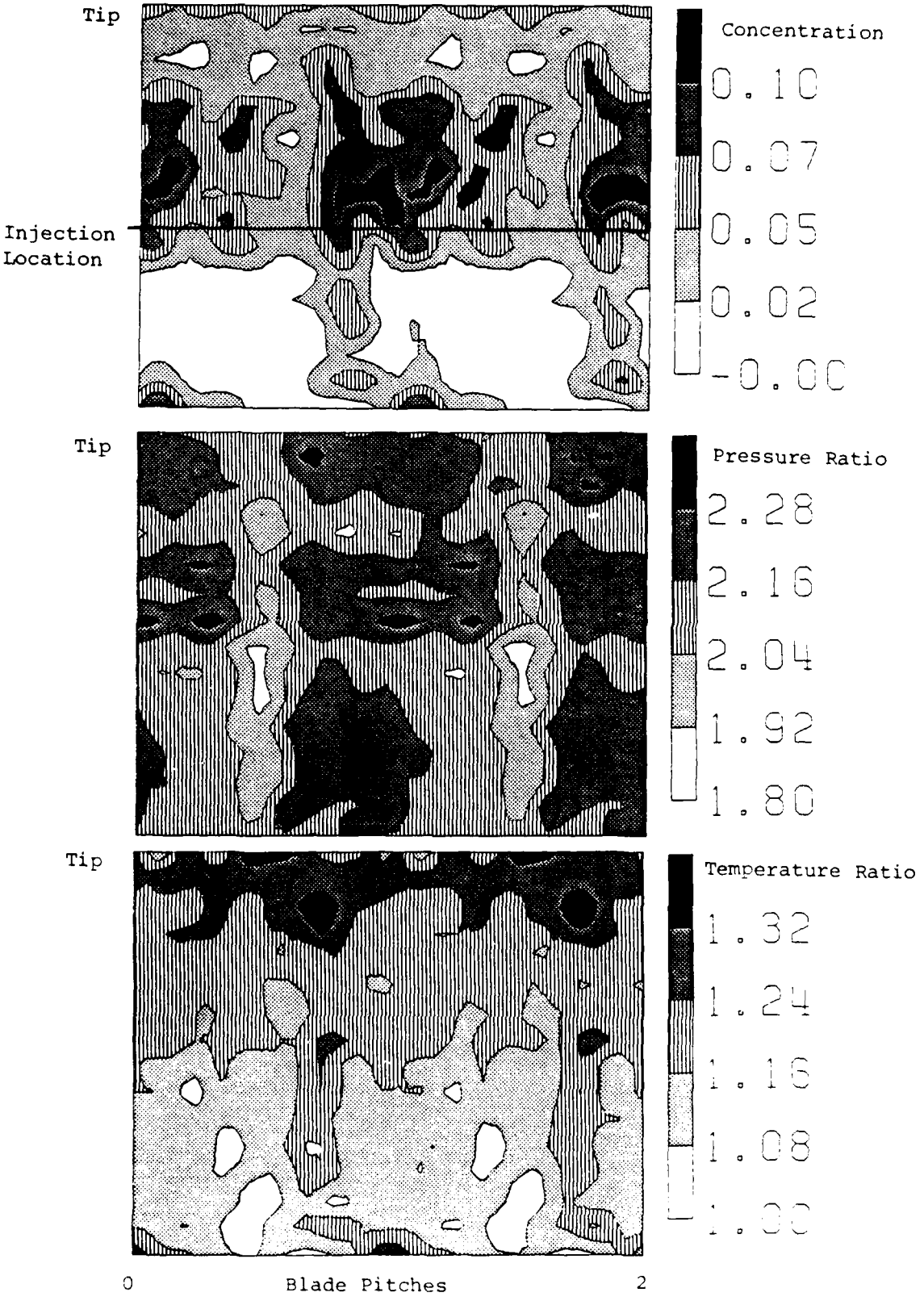

Fig. 5b: Contour maps constructed from the data in Fig. 4, tracer injection as indicated near midspan

HUB INJECTION

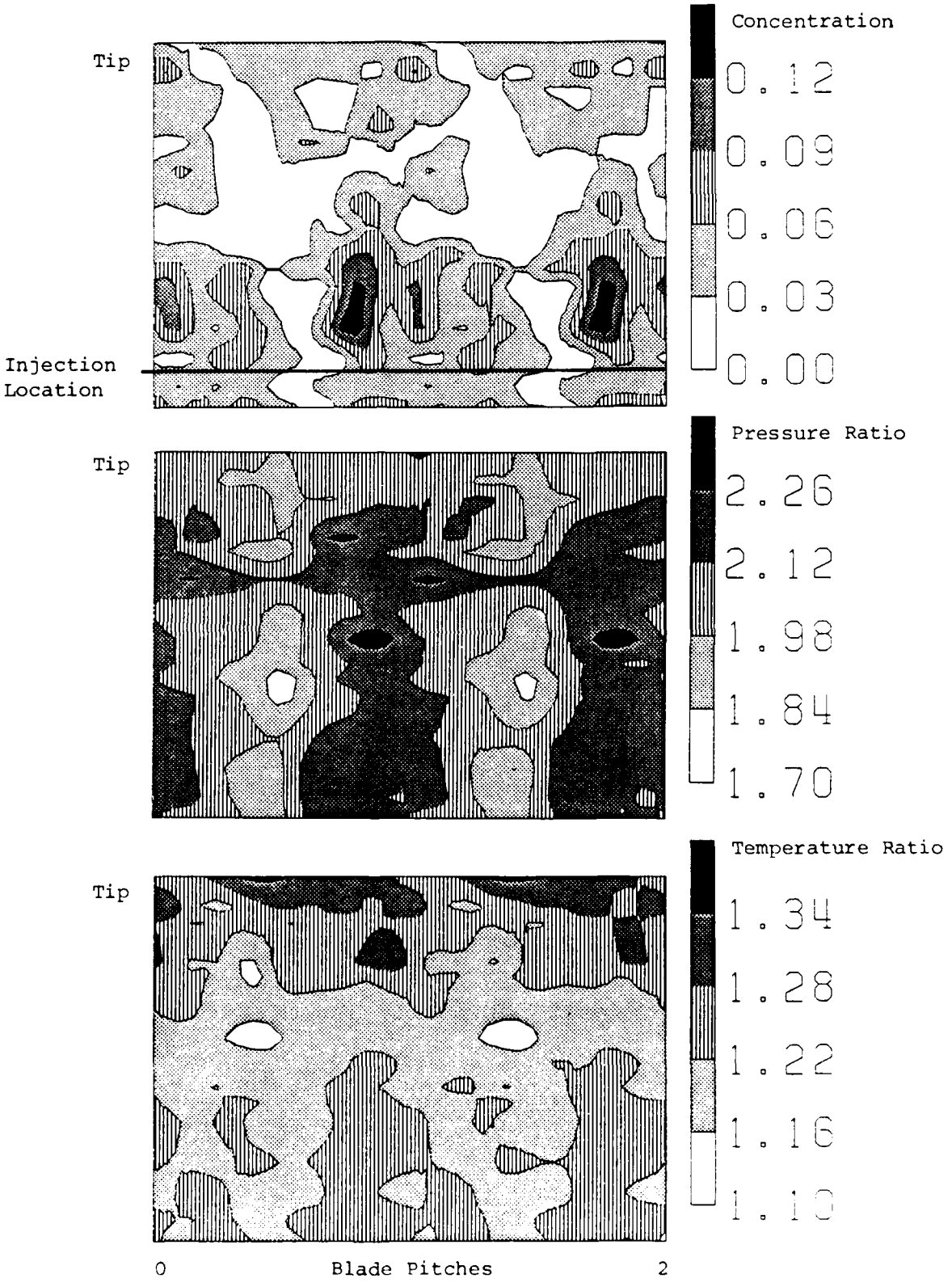

Fig. 5c: Contour maps constructed from the data in Fig. 4, tracer injection as indicated near hub

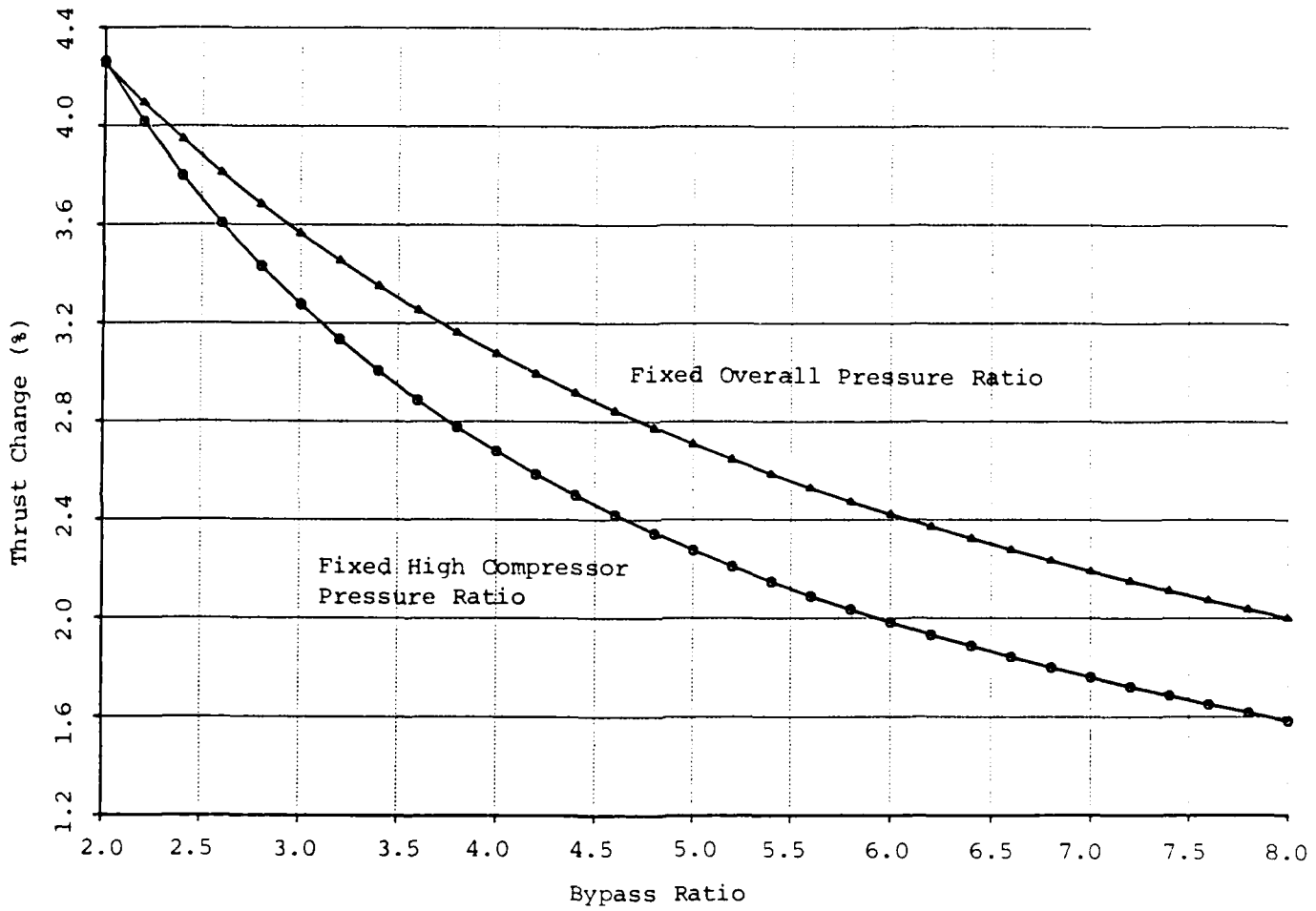

Fig. 6: Change in thrust due to isentropic movement of the core streamtube loss (entropy) to the bypass stream

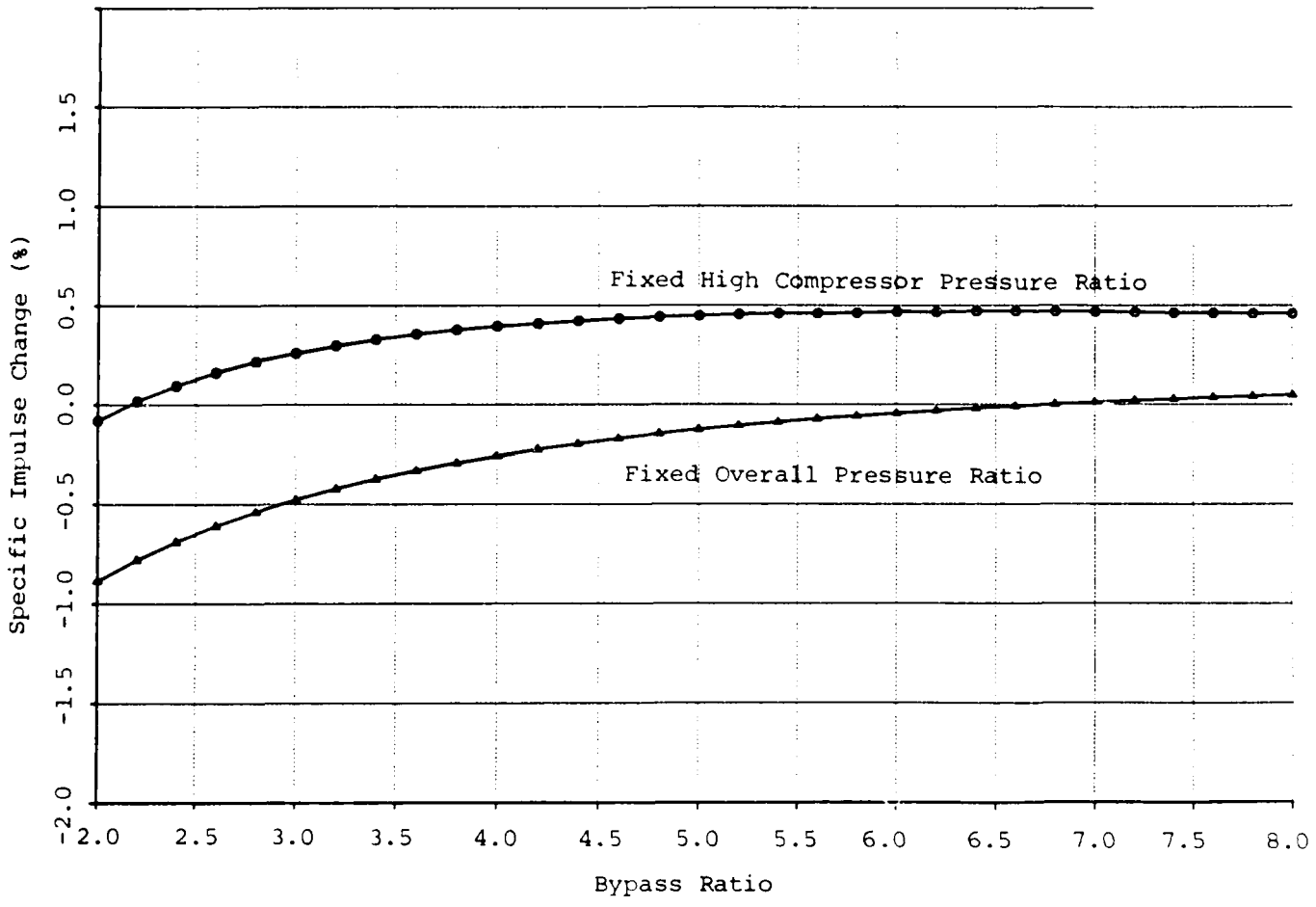

Fig. 7: Change in specific impulse due to isentropic movement of the core streamtube loss (entropy) to the bypass stream

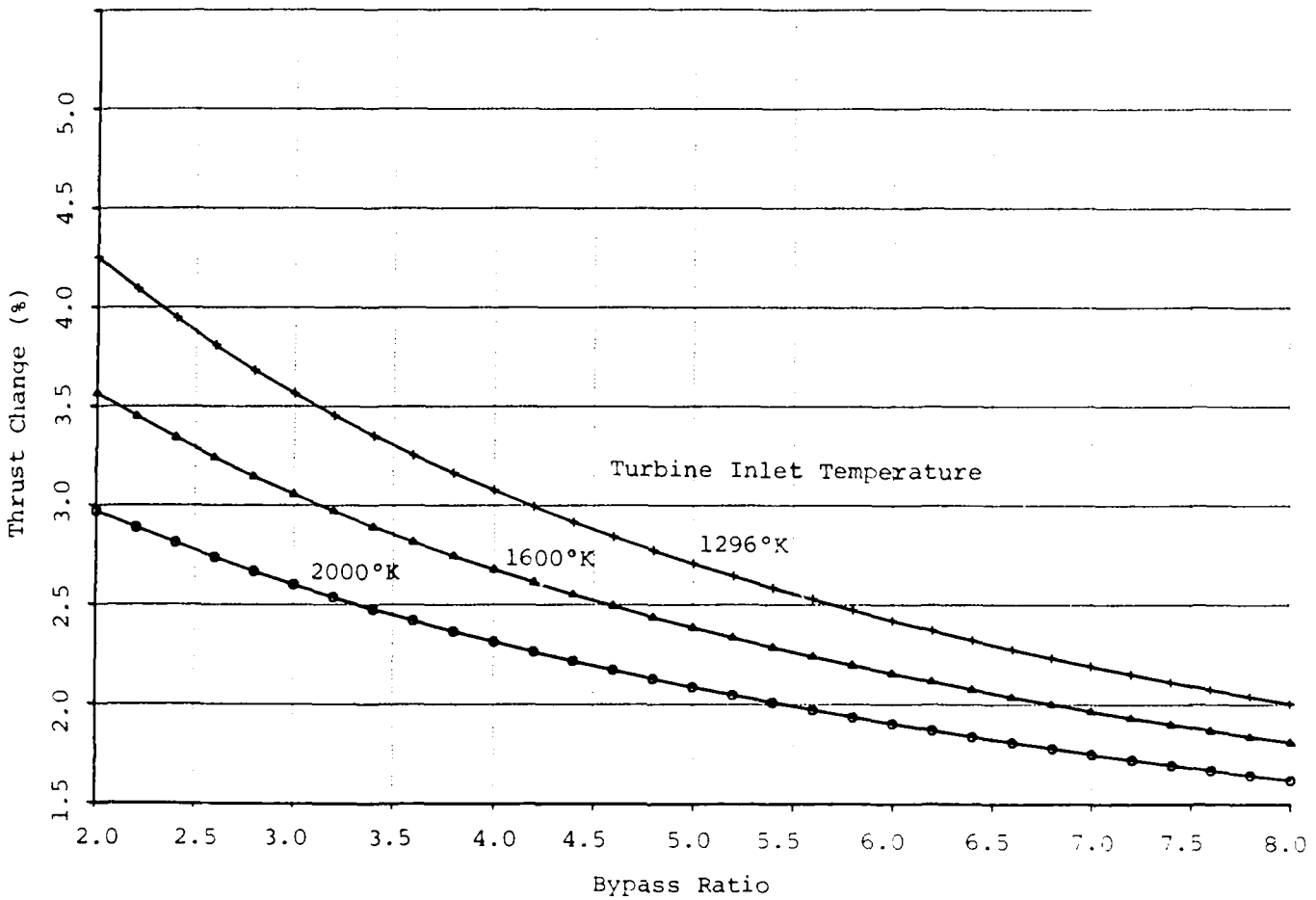

Fig. 8: Influence of turbine inlet temperature on thrust change due to radial entropy migration

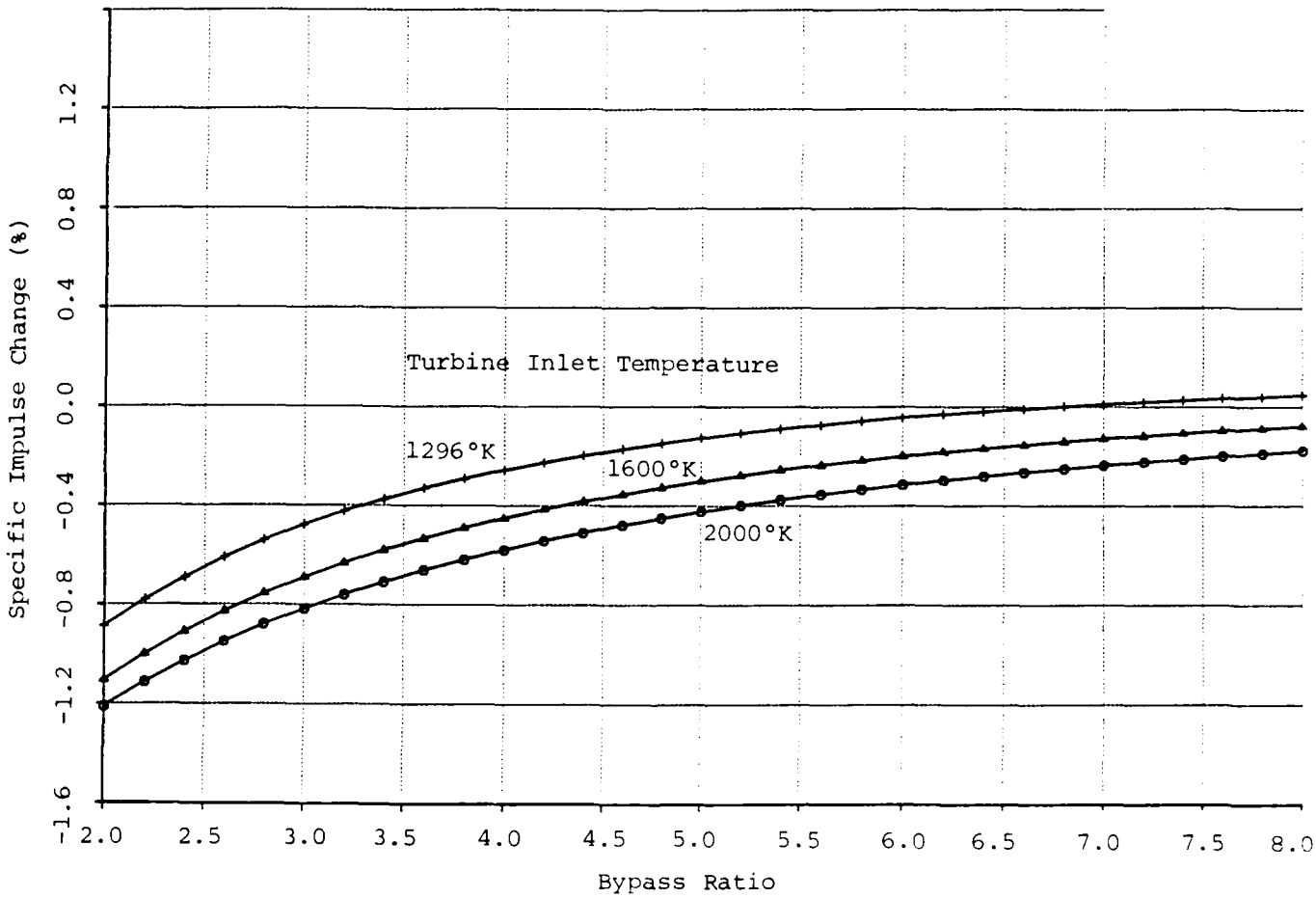

Fig. 9: Influence of turbine inlet temperature on specific impulse change due to radial entropy migration

TASK II: EXPERIMENTAL AND THEORETICAL STUDY OF FLOWS IN COMPRESSOR HUB/CASING TREATMENT
(Investigators: E.M. Greitzer, C.S. Tan, N. Lee)

Introduction

This project is a combined analytical/experimental investigation of the mechanism of compressor stability enhancement using casing/hub treatment. The program is focussed on detailed exploration of the mechanism of one slotted endwall (axial skewed slots) configuration that has worked extremely well in improving stable flow range. Two issues of interest are: (1) what is the mechanism by which the slots suppress the onset of rotating stall, and (2) what is the source of efficiency penalty associated with the slots. This work has been jointly supported by Allison Gas Turbine Division of General Motors.

To address the above points, we have carried out first-of-a-kind experiments using controlled hub slot suction and injection into the endwall layer [1], basic computations of the flow in the grooves, as well as measurements of the three-dimensional flow in the endwall region with a smooth wall and with a grooved configuration. The experiments during the past year centered around the acquisition and interpretation of detailed hot wire measurements of the three-dimensional velocity field in the endwall region with controlled blowing and suction.

Background to the Experimental Effort

From the data of previous investigators, as well as from our previous measurements of the three-dimensional flow in the endwall region, it is known that there is a significant flow into and out of a slotted wall over a compressor rotor tip or under a stator hub. This flow is driven by the overall pressure rise in the blade row, and its direction is into the slots at the rear (near the blade row trailing edge) and out of the slots at the front (near the blade row leading edge). It had previously been hypothesized that

it was this jet from the leading edge region that was the cause of the increase in aerodynamic stability of the blade row.

The experiments of Johnson [2], however, showed that this was too narrow a view and that the "suction" associated with the flow into the grooves near the trailing edge could also be important. The implication of Johnson's in-passage measurements were that the suction removed the blockage near the trailing edge, thus suppressing the tendency for rotating stall inception.

The experiments thus raised the basic question of which of the two mechanisms due to the flow through the grooves (the suction near the trailing edge or the injection near the leading edge) had the most crucial fluid dynamic role in suppressing stall. Associated with this are the more general questions of what the precise mechanism is by which the instability is suppressed, as well as what one means, in a basic fluid dynamic sense, by "compressor stall".

To resolve this question, in our view, it was necessary to provide an experimental configuration in which the suction and injection occurred separately so the influence of each could be assessed. As described in previous progress reports, this was accomplished by modifying our facility so that the slots on the hub communicated with a plenum through which a metered amount of flow could be either extracted or injected. The amount of flow that could be so utilized ranged from zero to a value that was substantially more than the value that occurred in either the jet or the suction regions of the actual treatment slot.

The experiments to determine the overall effect of the suction and injection rates on the blade row pressure rise were carried out during 1985-1986. These have been described in previous reports and will thus be only briefly summarized. An important aspect to note is that blading parameters were chosen so that the stator (rather than the rotor) stalled first, that stall

occurred at the stator hub, that the stall was wall stall, and that the flow at the stator hub did indeed model the flow over the tip of a rotor. A schematic of the modified test facility is shown in Fig. 2.1.

The overall results of the experiments can be summarized as follows. Four hubs were fabricated with 60 degree axial skewed slots, but varying axial length and location. The slots extended radially through the hubs, so that they were open to the distribution plenum. Two hubs were subsequently modified to yield three more configurations, so seven configurations were eventually tested, designated as:

Nomenclature	Nominal Extent of Slot (Referred to axial blade chord)
1. Full 90% slots	5% - 95%
2. 22.5% front	5% - 27.5%
3. 22.5% middle front	27.5% - 50%
4. 22.5% skewed middle front	27.5% - 50%
5. 22.5% rear	67.5% - 90%
6. 45% front	5% - 50%
7. 45% rear	50% - 95%

For reference, Fig. 2.2 shows locations of the slots in the stator passage. With the "full 90% slots", the slot covers the middle 90% of the axial chord of the stator, similar to the original treatment. The "22.5% rear" had slots, 22.5% of the axial chord in length, located at the rear part of the stator passage, etc. The "22.5% skewed middle front" were constructed so that the front and rear slot edges had a 45-degree angle. Relative flow at slot exit for these slots would then be inclined at 45 degrees to the axial direction, measured in the plane of the slots.

Individual speedlines showing performance for each configuration and net mass flow into, or out of, the annulus were given in the previous progress report, so these are not shown. Instead, a summary plot of all the stall onset data is presented in Figs. 2.3a and 2.3b. The first of these is the

percent increase in stall pressure rise in terms of $\Delta P/\frac{1}{2}\rho U^2$ (stator static pressure rise divided by dynamic pressure based on wheel speed). The second shows basically the same information but with the pressure rise normalized by the inlet dynamic pressure, $\frac{1}{2}\rho V_1^2$. The horizontal axis in the figures is the amount of mass flow injected or removed, in percent of the flow through the compressor annulus at the solid wall near stall point.

Work Done During the Previous Year

During the past year, attention has been focussed on studying the injection of the jet and its effects on the compressor endwall flowfield. One question, for example, is whether the injection (only) experiments had indeed simulated the flow that occurs in the actual situation correctly.

Figure 2.4 shows the velocity vector projected onto a radial plane at 2% span above the hub surface. The convention adopted is that a circle and a cross at the root of a velocity vector represent flow coming out of, and going into, the paper respectively. The jet can be seen to traverse across the blade passage, and impinge on the pressure side of blade 1. Figure 2.5, which is on an axial plane looking downstream at 8% axial chord, shows another view of this. Although the magnitude of the simulated jet is roughly only 3/4 of that in the original hub treatment [2], [3], the overall endwall flow pattern associated with the jet seen in [2] and [3] is reproduced.

One other feature is also seen in the present experiment. This is a large scale circulation at the rear of the stator passage, illustrated in Fig. 2.6, which shows an axial plane at 78% axial chord from the leading edge. Additional figures showing the endwall flowfield can be found in [1]. These also bear out the strong similarity between the flow in the front of the passage with hub treatment and the situation with injection from the hub.

Discussion of the Results

Performance With No Net Injection or Removal

The performance of the 90% slots is close to (5% lower than) the original hub treatment used in [2]. There is no hot wire data for the 90% slots, and the exact amount of slot flow (i.e., low momentum flow at the rear end of the stator passage being sucked into the slots and emerging at the front as a high momentum jet) in this build is not known. In view of the similar performance of the 90% slots and the treated hub, however, one would expect that slot flow in the former is close to the magnitude of 3.5% found in the latter.

With the 45% slots, the performance drops to half of the value reached by the 90% slots. Even so, the increase in stall margin implies that there is still some internal injection and removal, similar to the 90% slots. For the 22.5% slots, the speedlines are very similar to the smooth wall baseline, and one can infer that little internal injection or removal occurs in these slots.

Performance With Flow Removal

First consider flow removal at the rear. The success of the 22.5% and the 45% rear slots in suppressing stall supports Johnson's hypothesis regarding endwall flow removal [3]. The basic idea is that the removal of low momentum fluid at the rear of hub or casing treatment slot helps delay stall. It may thus be simply that the blockage as seen in the smooth hub prior to stall [3] is simply removed by the imposed suction. One would expect the amount of stall suppression to increase with suction rate, and this is in fact the case, as confirmed by the data for the 22.5% rear slot and for the 45% rear slot at high suction rates. (Behavior of the 45% rear slots at low suction rates will be addressed subsequently.)

Consider now local suction at the front half of the stator passage, through the 22.5% front and 22.5% middle front slots. Since the hot wire

measurements of [2] and [3] indicate that blockage does not appear at the front half of the passage, it is not appropriate to talk about the direct action of removal on the blockage. Rather, as in the case of suction not far from the leading edge of an airfoil, removal at the front half of the passage may alter substantially the initial development of the low total pressure flow. Both suction at the rear and at the front appear effective, as Figs. 2.3a,b show little difference of the stall pressure rise for the 22.5% front and rear slots over the whole suction regime.

Behavior of the 45% front and rear slots can be explained by supposing that with no suction they work like conventional hub treatments. As the suction increases, the flow pattern changes so that there is a change from circulating flow (at zero suction rate) to non-circulating (net outflow). The success of the 45% front slots at low suction rates is thought to be attributed to this.

At 3.6% suction, the approximate amount of circulating slot flow in the 90% slots, the stalling $DP/0.5\rho\overline{V}_{in}^2$ of all slots is 55% higher than that of the smooth wall build, but is less than the 70% level attained by the 90% slots. This implies that suction is not the sole cause of the increase in stall margin and that the jet is also responsible for the observed improvement.

Flow Injection

Endwall flow injection can also delay stall, but there is much more variation in effectiveness among the slots. With blowing, both the location of the jet, as well as its momentum, govern the amount of improvement. Injection through the 22.5% front and 22.5% middle front is much more effective than that through slots of the same size at the rear. (Comparison with the 22.5% skewed middle front is excluded for the present because of its different configuration.)

Figure 2.7 plots the performance of all of the 22.5% slots with injection as a function of the absolute injection momentum flux of injection. Data is the same as that of Fig. 2.3b for blowing except that the momentum flux is used rather than the mass flow rate. Performance of the 90% slots is represented as a solid bar in the figure.

The superior performance of the 22.5% middle front is again visible in Fig. 2.7. The 22.5% front achieves 15% less than the the 90% slots at 9% momentum flux, whereas the 22.5% middle front is slightly more effective than the baseline. Re-orienting the jet at the middle front location so that it is less aligned with the main flow (corresponding to injection through the 22.5% skewed middle front), however, results in poor performance. More specifically, the 22.5% skewed middle front, which was designed to have 40% less streamwise momentum flux than the 22.5% middle front (at 9% absolute momentum influx), had a 45% drop in performance at that amount of absolute momentum influx. This suggests, as one might expect, a correlation between streamwise momentum influx and stall-delaying potential.

In Fig. 2.8, the effect of the streamwise component of jet movement is brought out more explicitly. The abcissa in the figure is the component of momentum flux in the streamwise direction, based on the approximation that flow angle of the stator "free stream" flow decreases linearly from inlet to exit.

The 22.5% skewed middle front performance curve has poor performance at zero injection, but then a rapid increase, and at 5% streamwise momentum influx it performs nearly as well as the 22.5% middle front. It thus appears that the streamwise component of the jet momentum flux is linked to the stall suppression, although the reason underlying its success is still unresolved. One possible explanation is that the streamwise component of the jet helps

delay stall by actually "energizing" the endwall boundary layer. However, it is also possible that the jet has the effect of restricting the root leakage flow, and thereby suppressing stall. Without further investigation, however, the correct mechanism cannot be identified.

Pitch-Averaged Streamwise Velocity Profile

The hot wire measurements allow one to examine the flowfield in another manner, as in Fig. 2.9, which presents the evolution of the pitch-averaged streamwise velocity through the stator passage. The pitch-averaged streamwise velocity is normalized by the annulus-averaged streamwise velocity at that location. At inlet to the stator (0% axial chord), all three profiles, corresponding to the smooth hub, Johnson's hub treatment and 22.5% front slots with 2.8% injection, have roughly the same shape, with no significant reduction in velocities near the hub surface, although some traces of the jet are already visible.

At 8% axial chord, the jets from the hub treatment and from the injection appear, covering approximately the lowest 10% of the span. From 8% to 55% axial chord, the upward movement of the point of highest velocity is seen. This occurs because the jets travel towards the stator exit after being deflected by the pressure surface of the blade. The strong similarity between the injected flow and the hub treatment flow is clearly evident. Up to 55% axial chord, the smooth wall profile shows no marked reduction in velocities close to the hub surface; after this axial location, considerable reduction in streamwise velocities near the wall takes place. The reduction of streamwise velocities also occurs with the hub treatment and with the injection, although it is much less severe. At 100% axial chord, flow at 2% span in the case of the smooth hub leaves the passage with a streamwise velocity that is 40% of the mean flow, compared to 60% in the other two cases. This is consistent

with the existence of blockage in case (a) described previously.

Examination of Secondary Circulation in the Stator Passage

In Fig. 2.6, one sees downward velocities in the upper radial planes near the trailing edge. Around the contour shown, the circulation is equal to $0.45\ \bar{C}_x b_{ax}$, where b_{ax} is the stator axial chord. The flowfield associated with this amount of circulation is such that, at 6% span, flow near the suction side of the blade passage possesses velocities towards the hub while, near the pressure side, the flow is away from the hub. The flow transported downward through the radial plane at 6% span is found to be 1.4% of the mass flow rate of the main flow, equivalent to 1.2% normalized momentum flux. In contrast to the flow at 6% span, at 2% span the flow is parallel to the hub; from the previous paragraph, it is known that no blockage exists in this region.

The circulation also occurs with conventional hub treatment, but around a similar contour, the circulation is equal to $0.49\ \bar{C}_x b_{ax}$.

This passage circulation is directly due to the jet, because the circulation around the same contour in the case of the smooth hub has a value of $-0.10\ \bar{C}_x b_{ax}$, in the opposite sense. The positive circulation found with the treated slots thus originates from the jet (and not from other sources, such as upstream vorticity).

It is natural to ask if the mixing due to this circulation might energize the flow near the hub and thus help delay the stall. At 2.8% mass injection rate at the front, the normalized streamwise momentum influx at the location of blowing corresponds to 5.1%. This implies that momentum addition to the low total pressure flow due to mixing with the main flow is clearly not a dominant feature although its role should perhaps not be altogether ignored.

Summary of the Experimental Results

An experimental investigation has been carried out to examine the effects on stall margin of flow injection into and removal from the endwall of an axial compressor blade row. The goal was to identify the mechanism by which wall treatment suppresses stall in turbomachines.

Results showed that, even though both injection at the front and removal at the rear of the blade passage increased the stall margin, neither was as effective as the complete treatment. This implies that both the removal of high blockage flow from the rear of the slot and the high velocity injection at the front are causes of stall margin improvement in casing or hub treatment.

In regard to removal, the extent of stall enhancement did not depend heavily on the location of suction; in fact localized suction at the rear and front of the stator passage were equally effective. With the exception of improvement due to the pressure field generated slot flow which occurred at low suction rates only, for the 45% slots, the performance increased monotonically with the amount of removal. The overall trend suggests that endwall suction delayed stall either by directly removing low momentum flow, as in the case of rear-passage suction, or by delaying the formation of such a flow, as in the case of front-passage suction.

With endwall injection, both the amount of momentum injected and the location of the injection strongly affected the stall margin improvement. Injection through a location from 27.5% to 50% of the passage worked as well as the full treatment. Injection through a location from 5% to 27.5%, which corresponds most closely to the simulation of the jet in the full treatment, was less effective. Injection in the rear of the passage delayed stall by only a small amount. The streamwise momentum component was found to be important to the success of endwall injection. Stall suppression correlated with

the streamwise momentum influx. Detailed flowfield measurements also revealed the presence of a large scale vortical flow at the rear of the passage, when the jet was simulated at the front.

Based on these findings, it is hypothesized by Lee [1] that three aspects of the jet could contribute to stall enhancement. In the order in which Lee assesses their importance, these are: 1) direct streamwise momentum addition to the endwall boundary layer, 2) decrease in the tip (or root) leakage flow, and 3) (a distant third) mixing of the latter with main flow due to the rear passage vorticity.

Future Work on This Problem

We would regard the next step in this investigation to be a detailed examination of what the jet flow does. For example, does it "simply" provide a streamwise momentum injection into the endwall boundary layer, or is there some other mechanism such as the suppressing of the deleterious tip leakage flow, i.e., having the effect of effectively closing the clearance down.

These questions, however, really only scratch the surface of the more important problem which one might start on by asking what it is that tip leakage does that has such an adverse effect. The flow on the endwall has a very high dynamic pressure. The static pressure rise in the stator with a smooth wall is roughly ten percent of the dynamic pressure of the fluid on the endwall. Why should this fluid separate? Is it in fact the fluid on the endwall that separates? What are the controlling physical mechanisms? None of these questions has, as far as we can see, a good answer, even after forty years of axial compressor research.

Part of the difficulty is the complexity of the flow field. Enough has been written on the endwall to make it unnecessary to expand on this statement. Experiments up to now have shown mainly the manifestations of what goes on,

i.e., the conditions at the exit of the blade passage. What is really needed is the conditions inside the passage on a detailed level.

Some of these blade passage measurements have been made, but the scale of resolution is not enough. Further, in addition to the pointwise measurements, it appears to be very useful to obtain some idea of quantities such as the trajectories followed by the fluid particles in the layers near the wall. This would enable one to answer questions about where the fluid that contributes to the high blockage comes from.

Although one might be able to do all this experimentally, it seems that the present state of the art in computational fluid mechanics is such that one could do this investigation more efficiently, and perhaps even more effectively, by making use of a three-dimensional viscous computation. This will be carried out under Allison sponsorship during the coming year.

We propose to use an existing three-dimensional code to perform a numerical experiment on the passage flow. In other words, the code would be run not so much to obtain performance data, but to obtain information about the structure of the flow. For example, in terms of the features described above, the trajectory of leakage elements can be tracked computationally.

The computational procedure can also be used to simulate the effects of the casing treatment. The experimental results have parameterized the effects of jet momentum injection, and have shown that the jet and the suction can be studied separately. One could thus envision just simulating the jet, and examining what effects it has on the flow in the passage, including streamwise momentum injection, health of the endwall flow, and effect on leakage. The influence of leading edge suction could also be examined in the same manner.

REFERENCES

1. Lee, N., "The Effects of Compressor Endwall Suction and Blowing on Stability Enhancement," forthcoming MIT GTL Report, 1987.

2. Johnson, M.C., "The Effects of Hub Treatment on Compressor Endwall Flowfields," M.S. Thesis, Department of Aeronautics and Astronautics, MIT, January 1985.

3. Johnson, M.C. and Greitzer, E.M., "Effects of Slotted Hub and Casing Treatments on Compressor Endwall Flowfields," ASME J. Turbomachinery, Vol. 109, July 1987, pp. 380-388.

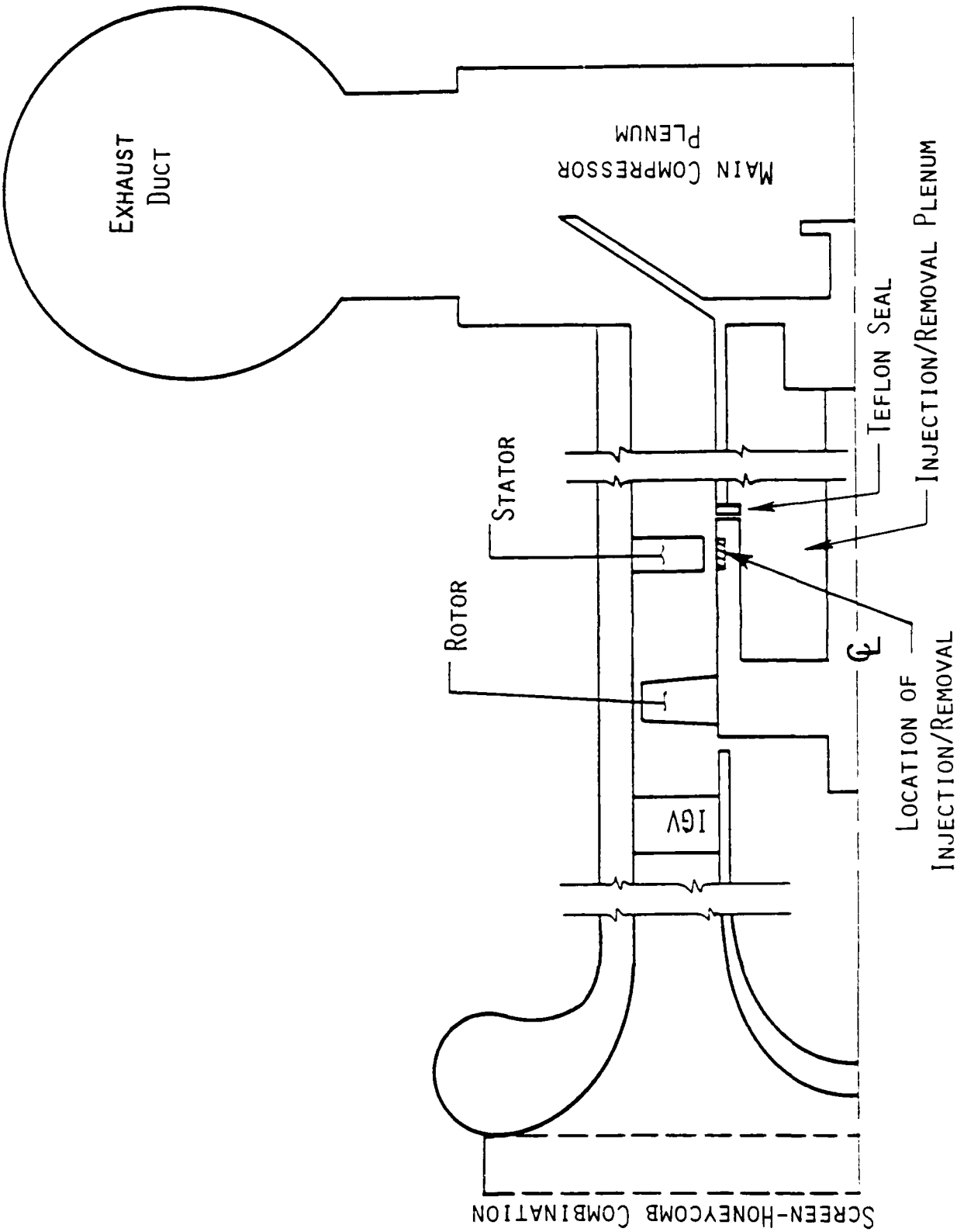

Fig. 2.1: Schematic drawing of compressor

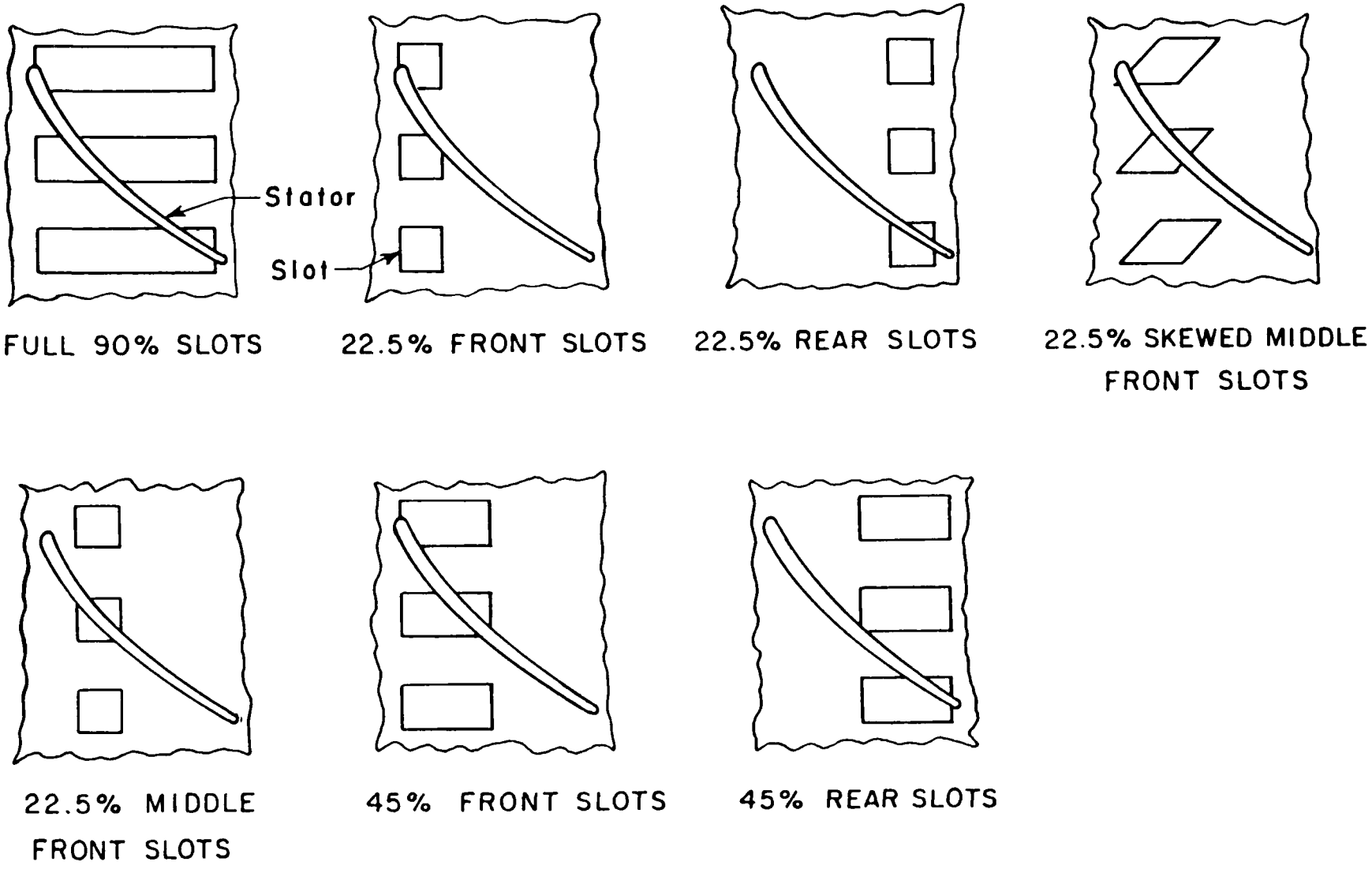

Fig. 2.2: Locations of slots

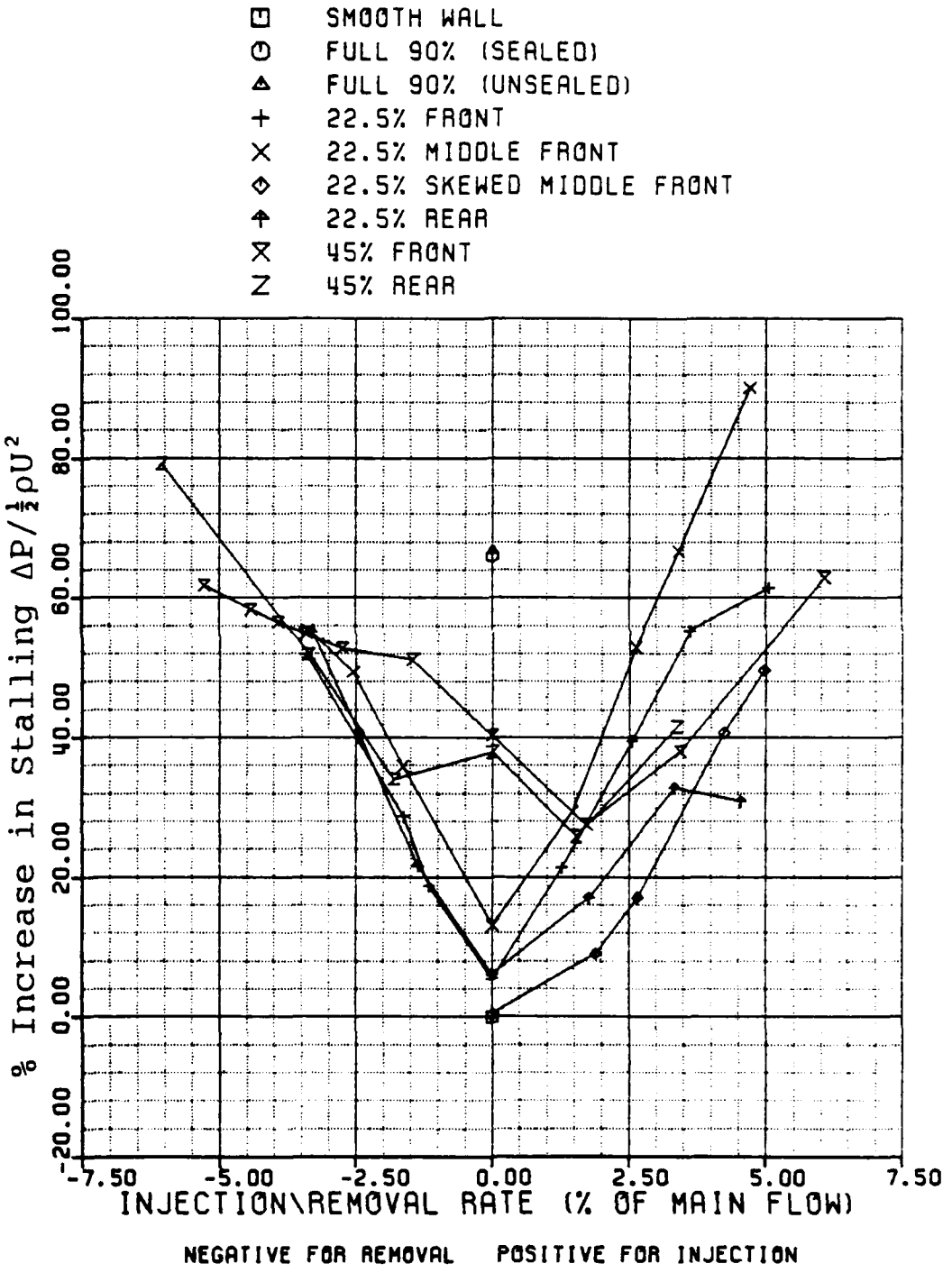

Fig. 2.3a: Percentage increase in performance of various slots over smooth wall

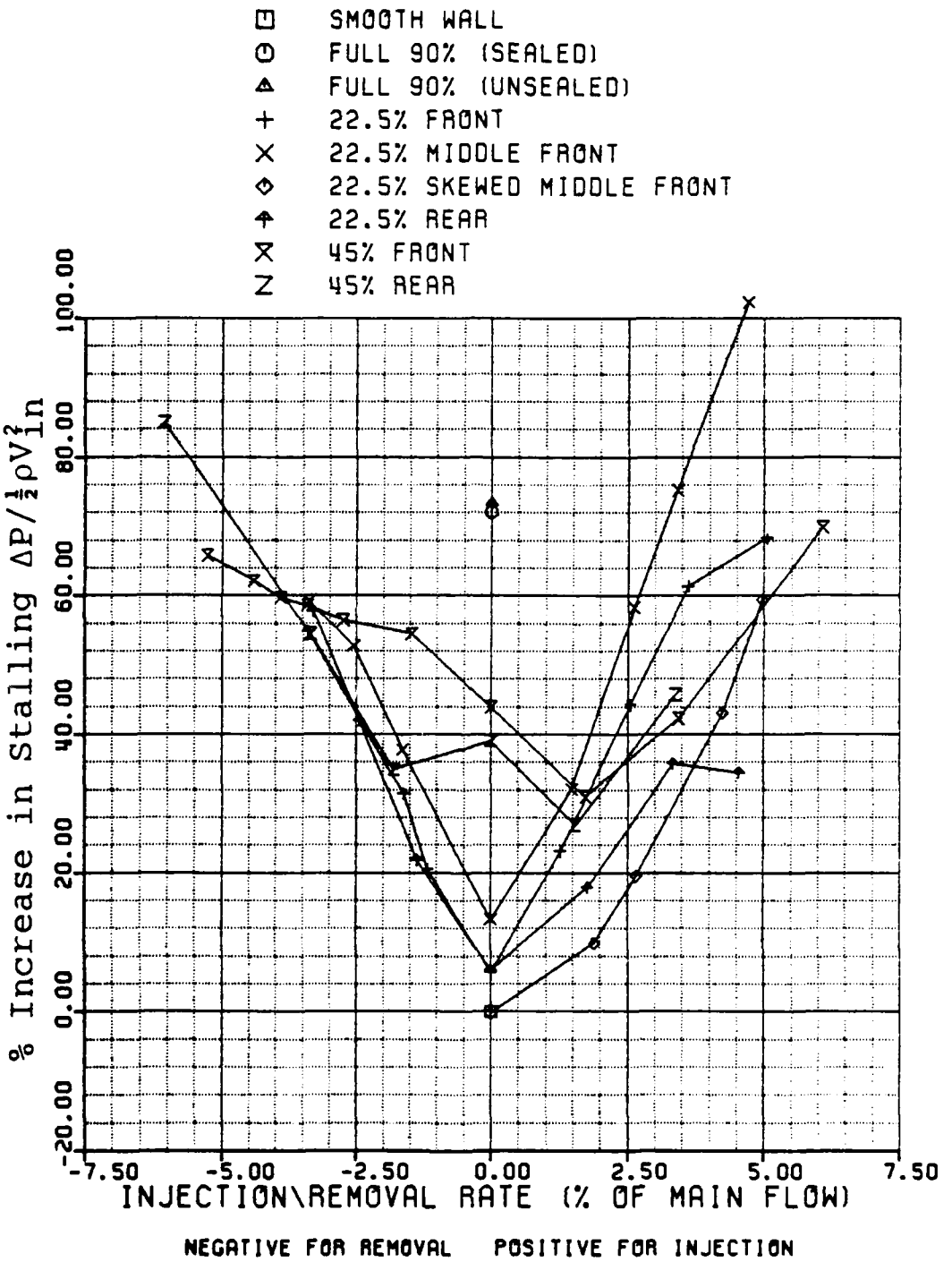

Fig. 2.3b: Percentage increase in performance of various slots over smooth wall

VELOCITY VECTORS

HUB TYPE	22.5% FRONT
SCALE (FT/S/IN)	150
TIME NO.	AVERAGE
BLOWING RATE (%)	2.82

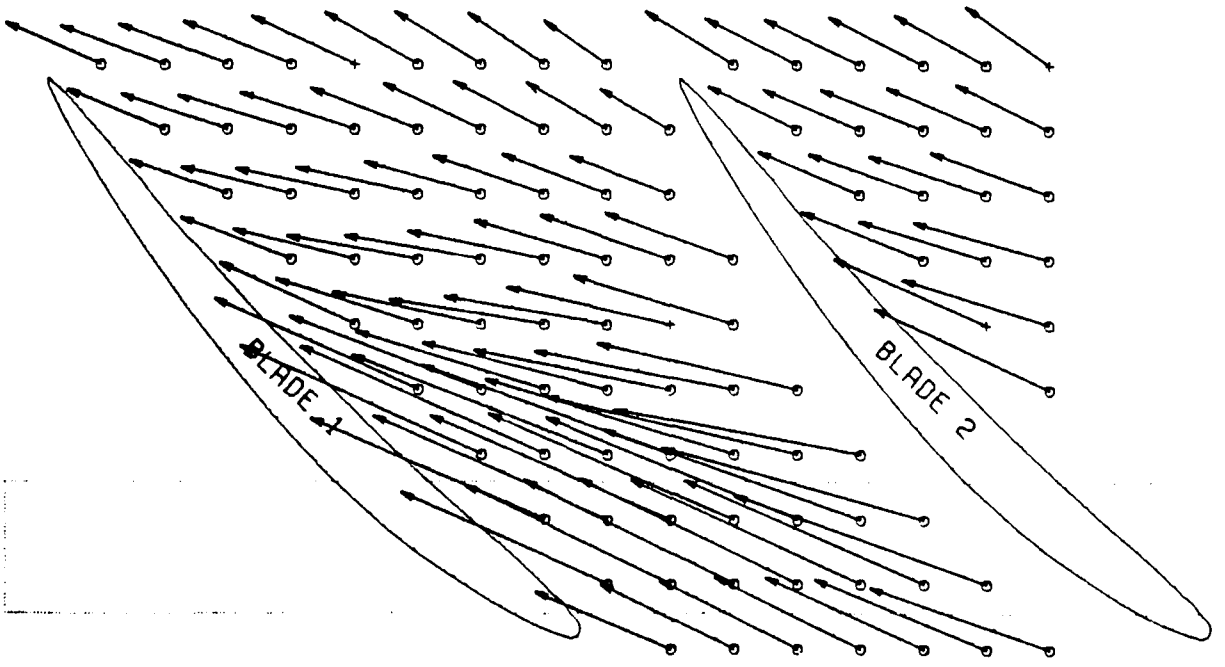

Fig. 2.4: Radial plane no. 1 at 2% span

VELOCITY VECTORS

HUB TYPE	22.5% FRONT
SCALE (FT/S/IN)	150
TIME NO.	AVERAGE
BLOWING RATE (%)	2.82

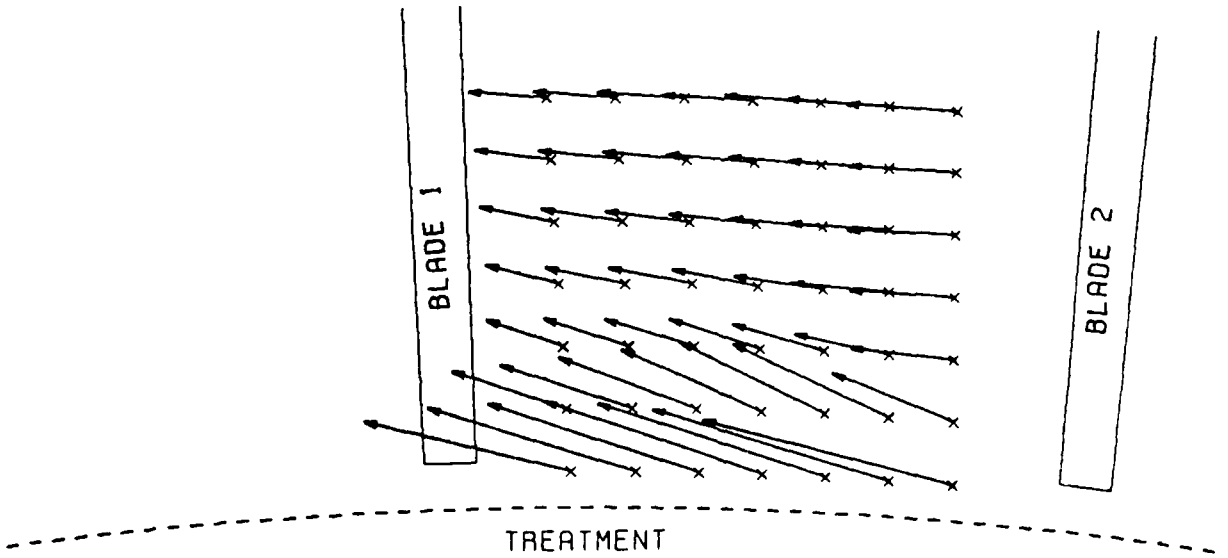

Fig. 2.5: Z plane no. 9 at 8% axial chord

VELOCITY VECTORS

HUB TYPE	22.5% FRONT
SCALE (FT/S/IN)	150
TIME NO.	AVERAGE
BLOWING RATE (%)	2.82

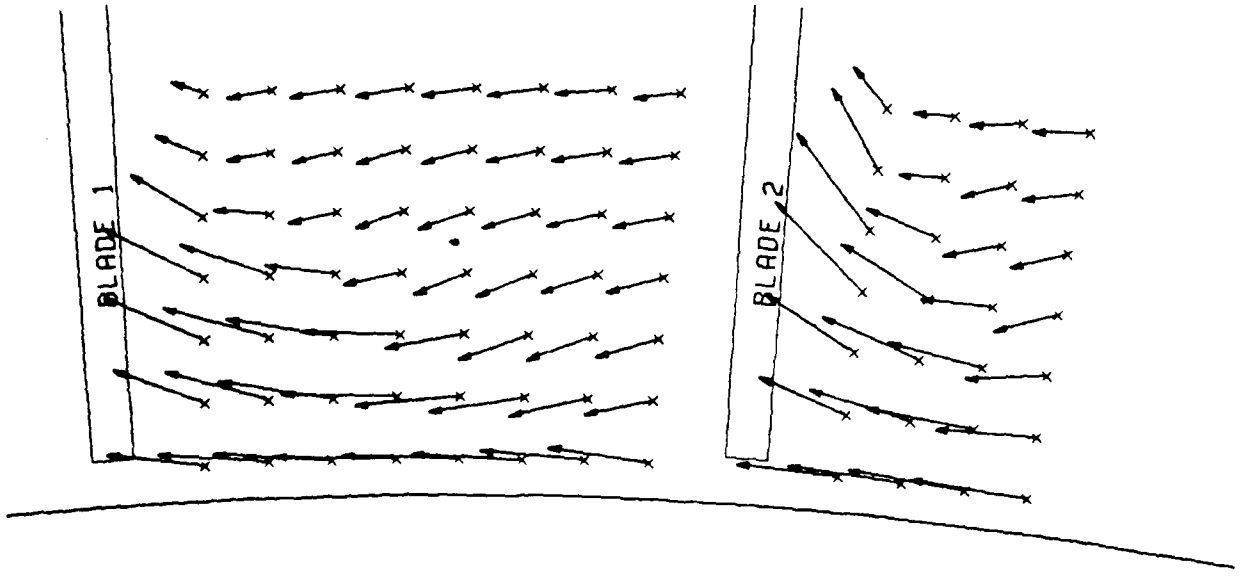

Fig. 2.6: Z plane no. 3 at 78% axial chord

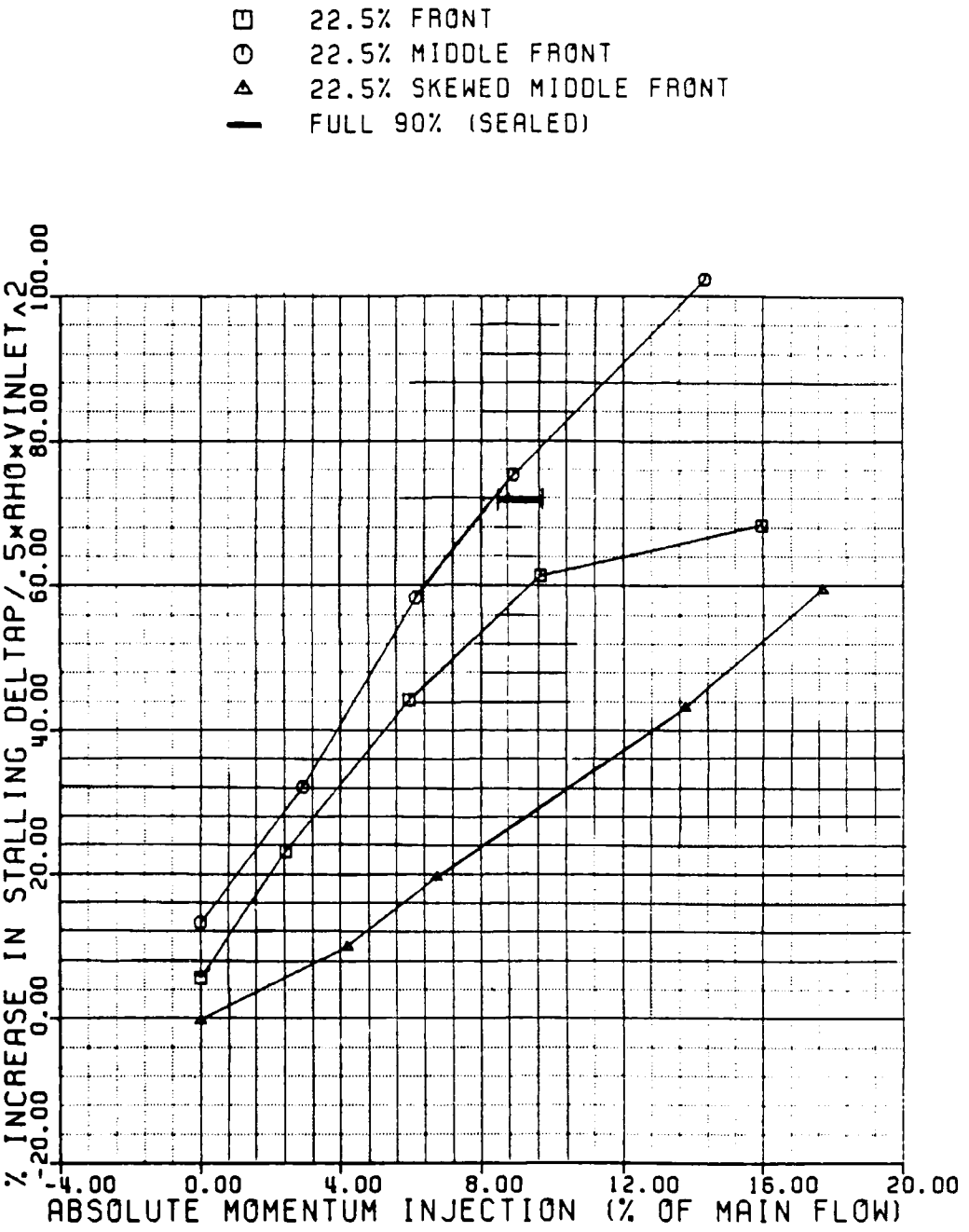

Fig. 2.7: Variation of performance with absolute momentum influx for the 22.5% slots

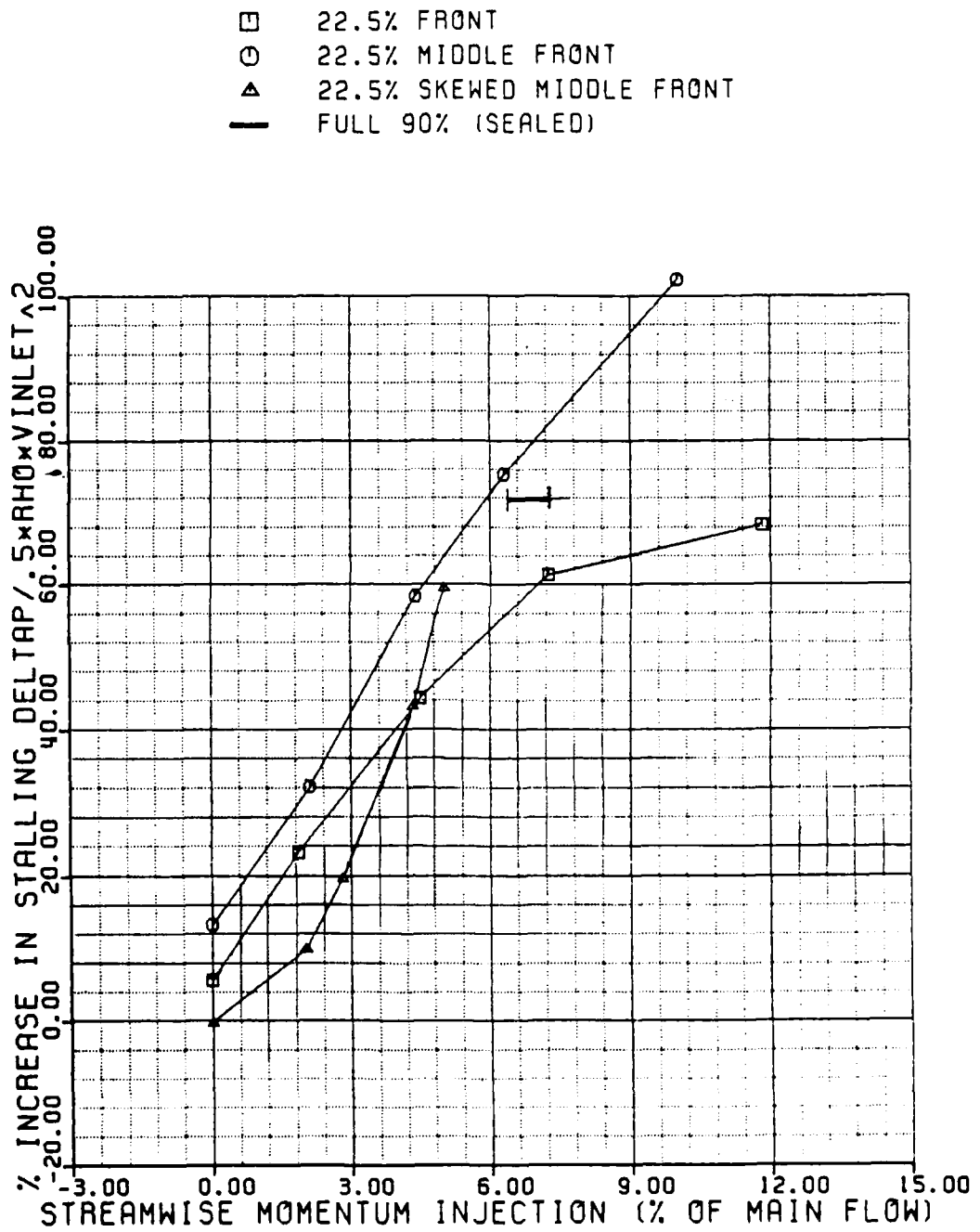

Fig. 2.8: Variation of performance with streamwise momentum influx for the 22.5% slots

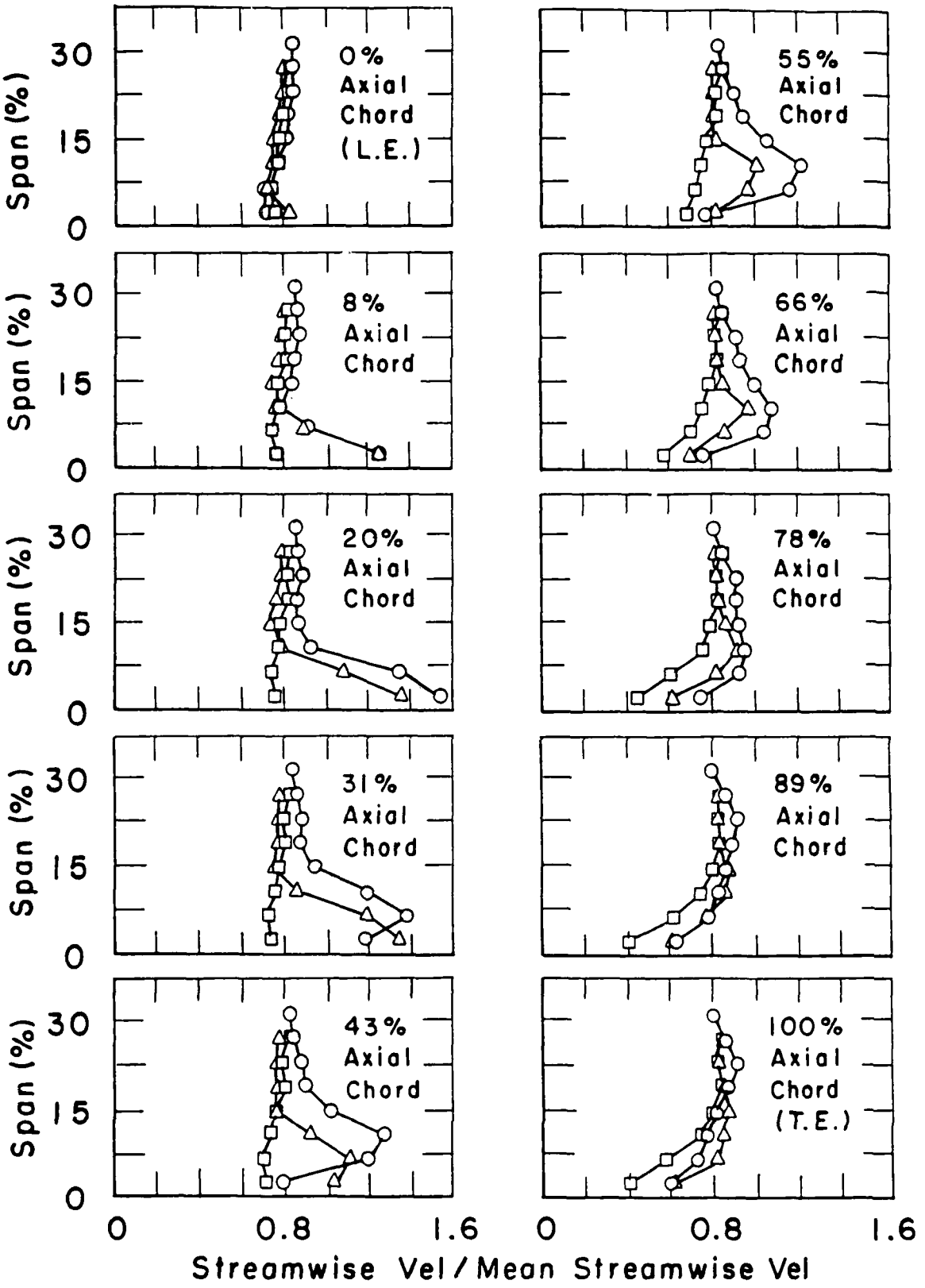

Fig. 2.9: Development of pitch-averaged streamwise velocity profile

TASK III: COMPUTATIONAL TECHNIQUES FOR TURBOMACHINES
(Investigators: M.B. Giles, M. Drela, S. Allmaras)

Second-Order Flux-Split Solution Scheme

Since the objective of this task is the calculation of unsteady flows due to shock/boundary-layer interactions, the first step was the development of an accurate, efficient method for calculating the outer inviscid flow with its moving shocks. Standard time-marching methods for solving the unsteady Euler equations capture the shock through the use of added numerical viscosity, which usually smears the shock over several grid cells, typically 5-8. In steady calculations, the effect of this smearing is minimized by using a very fine grid spacing in the shock region, and the use of a conservative numerical formulation guarantees the correct overall Rankine-Hugoniot shock jump relations. In unsteady calculations with moving shocks, it becomes very expensive if one must use a globally fine grid, and so instead one would like a method which captures the shock in just one or two grid cells. Even if such a method is slightly more expensive per grid cell, it would still be much cheaper in terms of cost/accuracy.

Following this reasoning, we decided to use a flux-split method developed by Van Leer. This captures shocks in at most two cells, but the accuracy in the smooth flow regions suffers because the method is only first-order accurate. There are variations of the Van Leer which are second-order accurate, but these require an extremely uniform grid to achieve this additional accuracy, and it is often not possible to generate a grid with the desired smoothness. Instead, we developed a new extension to the class of flux-split methods, which gives a method which is second-order accurate even on irregular grids. The details of the method are contained in a paper presented at the AIAA 8th Computational Fluid Dynamics Conference (a preprint

of this was included in a previous progress report). The central idea is that, in addition to the density, momentum and energy being unknown variables at the centers of quadrilateral cells, their gradients are also unknown variables. This allows an accurate, linear representation of the solution on each cell, and hence on each side of the interfaces between cells. These two values are used in the flux-splitting technique which determines the fluxes based on the information on the upwind side of the interface. Since we have additional variables, we require extra equations in addition to the usual unsteady flux-balance equations which are an approximation to the integral form of the unsteady, Euler equations. The extra equations are obtained by taking the moment of the Euler equations about the center of each cell, and then approximating the integral of these equations over the cell.

In the paper, results are shown for both a subsonic, two-dimensional duct, a one-dimensional transonic nozzle, and a two-dimensional transonic diffuser. The duct results are for a steady flow, and establish the second-order accuracy when the flow is smooth. The nozzle results are for an unsteady flow caused by an oscillating exit pressure. This causes a pressure wave which steepens into a shock wave and moves upstream. Comparison to an extremely fine grid solution shows the accuracy of the shock tracking on a relatively coarse grid. Finally, the diffuser results are also for a flow with unsteadiness due to an oscillating back pressure, and show the capability of the algorithm to handle two-dimensional flows with moving shocks.

Unsteady Coupled Boundary-Layer Method

The next step is the development of an unsteady boundary layer method to be coupled to the outer inviscid calculation. This algorithm will involve the solution of the thin-shear-layer Reynolds-averaged Navier-Stokes equations, with some appropriate turbulence model. Wall functions are being contemplated

to eliminate the necessity to have very fine grid resolution in the "law-of-the-wall" region. The algorithm will be implicit, coupling together all of the points across the boundary layer at each time step. This allows the use of time-steps similar to those allowed in the outer inviscid flow, whereas an explicit treatment would have required extremely small time-steps because of the CFL restriction. The calculation will be performed in using transformed coordinates (s,η), where s is the surface coordinate, and $\eta = n/\delta^*$ is the normal coordinate scaled by the boundary layer thickness. This scaling will automatically ensure that grid resolution is maintained in the correct place as the boundary layer thickness varies.

We considered the use of cubic or quartic splines to increase the accuracy and/or reduce the number of variables and computational cost. However, preliminary work with solving the Falkner-Skan equations showed that the higher-order schemes were more efficient only if the desired accuracy was greater than 99.9%. Since the turbulence modelling is probably responsible for a 5% error, we decided not to pursue the idea of using the cubic or quartic splines.

Non-Reflecting Boundary Conditions

A major research accomplishment of the last year is the derivation of improved non-reflecting boundary conditions for the Euler equations. Although the analytic problem is defined with an infinite far-field, the computational treatment truncates the domain and places the far-field boundaries less than one chord length upstream and downstream from the blade row. This raises the difficulty of constructing boundary conditions so that they do not cause non-physical reflections. In steady-state problems, this means that any oblique shock extending from the trailing edge of transonic turbines should pass cleanly through the outflow boundary, and not produce a reflected expansion or compression wave which would contaminate the solution at the blade.

For unsteady problems, this means that any outgoing pressure wave should not produce a reflected pressure wave. The standard method currently for dealing with these problems is to use one-dimensional characteristic theory. This approach neglects any variations in the pitchwise circumferential direction, and under this assumption it is possible to construct ideal non-reflecting boundary conditions. Unfortunately, if the outgoing wave does have a circumferential variation (as is almost always the case), then it does produce a reflected wave which can contaminate the solution.

The mathematical theory for constructing better boundary conditions is still an active research area. Most of the work is being performed for the scalar wave theory, and the main contribution of the present theory is the extension to general systems of partial differential equations, and particularly the Euler equations. The details are contained in a lengthy report which is now in its final draft form and is attached. The end result of these new boundary conditions is more accurate results for both steady and unsteady calculations, and increased efficiency because of the ability to place the far-field boundaries closer to the blades.

Non-Reflecting Boundary Conditions for the Euler Equations

by

Michael Giles

CFDL-TR-88- 1988

This research was supported by Air Force Office of Scientific Research contract F49620-85-C-0018, supervised by Dr. J. Wilson.

Contents

1 Introduction

1.1 Statement of problem

When calculating a numerical solution to an unsteady, hyperbolic, partial differential equation on an infinite domain, it is normal to perform the calculation on a truncated finite domain. This raises the problem of choosing appropriate boundary conditions for this far-field boundary. Ideally these should prevent any non-physical reflection of outgoing waves, and should be straightforward to implement numerically. Also they must produce a well-posed analytic problem since this is a basic requirement for the corresponding numerical approximation to be consistent and stable.

The motivation for this report lies in the author's research in the calculation of turbomachinery flows. In some respects these flows are much more complex than the flow past isoltaed airfoils. Whereas the far-field boundary for isolated airfoils can be taken to be many chords away from the airfoil, with turbomachinery the far-field boundary is typically less than one chord away from the blade. Consequently, whereas for isolated airfoils the steady-state far-field can be modelled as a vortex correction to the free-stream flow, in turbomachinery the far-field contains a significant component of several different spatial wavenumbers. This is particularly true for flows which are supersonic in the flow direction but subsonic in the axial direction, in which case shocks propagate indefinitely and can be reflected by improper boundary conditions. Thus one of the two aims of this report is the correct formulation of steady-state non-reflecting boundary conditions which will not produce artificial reflections of steady waves such as shock waves.

The other aim of the report is the formulation of accurate non-reflecting boundary conditions for unsteady waves. Here again isolated airfoils generally have fewer problems. The reason is that the primary concern for isolated airfoils is unsteady flow caused by either the airfoil's motion (airfoil flutter or aileron flutter) or a fluid-dynmaic instability (transonic buzz or stall). In either case the unsteadiness originates in the vicinity of the airfoil and radiates outward. Typically the grids on which such calculations are performed becoming progressively coarser as the waves move out towards the far-field boundary, until a radius is reached at which the wavelength of the unsteady wave is of the order of a few mesh cells. At this point the numerical viscosity will dissipate the wave and so the unsteadiness will not reach the far-field boundary and accurate non-reflecting boundary conditions are unnecessary. One of the main concerns in turbomachinery is the unsteadiness caused by incoming shock waves and wakes from upstream blade rows. The need to retain an accurate representation of these incoming

waves prevents the use of coarse grids in the far-field, and instead one must concentrate on accurate non-reflecting boundary conditions.

Unsteady flows can be split into two classes, nonlinear and linear, depending on the amplitude of the unsteadiness. If the amplitude is sufficiently small that the disturbances everywhere can be considered to be linear perturbations to a steady flow, then by the principle of superposition the solution can be decomposed into a sum of modes with different temporal frequencies. and different inter-blade phase angles. Each of these modes can then be analyzed separately and so the problem is reduced to finding the complex amplitude of the harmonic disturbance. This can be achieved by either a direct method or a pseudo-time-marching method. In either case there is the same need for accurate boundary conditions, and it is found that because there is only a single frequency it is possible to construct the exact non-reflecting boundary conditions. In nonlinear unsteady flows there are regions where the amplitude of the unsteadiness is great enough for second order effects to become extremely important. This produces a coupling between the different frequencies, and so they cannot be separated. In the far-field however it is again assumed that the unsteady amplitudes are small so that linear theory can be applied. It is no longer possible to construct exact non-reflecting boundary conditions which can be implemented numerically, but approximate boundary conditions can be derived instead.

Fortunately in some respects the turbomachinery problem is simpler than the isolated airfoil problem. There are separate inflow and outflow boundaries, each with a trivial geometry. In this report x denotes the axial coordinate and y denotes the circumferential coordinate. The inflow boundary is at $x=0$ and the outflow is at $x=1$. Periodicity in y allows one to decompose the solution into its Fourier components, and the uniform orientation of the boundary relative to the flow field allows one to perform the analysis by considering linear perturbations to a uniform flow. With isolated airfoils it is harder to perform an eigenmode decomposition of the far-field because the varying orientation of the boundary relative to the flow field; at some places it is an inflow boundary while at the others it is an outflow boundary and this varies as the solution develops.

1.2 History

The subject of non-reflecting boundary conditions for hyperbolic equations is less than twenty years old. The key paper which formed the firm, theoretical foundation for later research was a paper by Kreiss [1] in 1970 which examined the well-posedness of initial-boundary-value problmes for hyperbolic systems in multiple dimensions. Well-

posedness is the requirement that a solution exists, is unique, and is bounded in the sense that the magnitude of the solution (defined using some appropriate norm) divided by the magnitude of the initial and boundary data (defined using some other norm) is less than some function which depends on time but not on the initial and boundary data. Any hyperbolic system arising from a model of a physical problem ought to be well-posed and so it is critical that any far-field boundary conditions which are used to truncate the solution domain must give a well-posed problem. Higdon has written an excellent review [2] of the work of Kreiss and others and in particular gives a physical interpretation of the theory in terms of wave propagation which is used in this report.

In solving the Euler equations for unsteady flows it was quickly realized that for one-dimensional flow the correct non-reflecting boundary conditions could be established using hyperbolic characteristic theory. For example, in 1977 Hedstrom [3] derived both the linear and the nonlinear form of these boundary equations for the Euler equations, using an eigenvector approach which will be used in this report. The boundary conditions were also used in two and three-dimensional flow calculations by doing a local analysis normal to the far-field boundary and ignoring all tangential derivatives. This approach (referred to as the quasi-one-dimensional or normal one-dimensional boundary conditions or the method of characteristics) remains the most commonly used boundary condition in unsteady calculations.

Also in 1977, Engquist and Majda wrote an important paper [4] deriving a hierarchy of approximate non-reflecting boundary conditions for multi-dimensional problems, with the first order approximation being the one-dimensional approximation. Unfortunately, like the Kreiss paper, this paper was written for mathematicians specializing in the analysis of partial differential equations, assuming a familarity with concepts, definitions and background literature which is not possessed by more applied mathematicians and engineers who are working in the area of computational fluid dynamics. Consequentially, over the last decade the important contributions of this paper have not been fully appreciated and implemented by the CFD community, and the higher order boundary conditions have only been implemented for acoustic and elastic wave propagation [4] and the scalar, unsteady potential equation [5]. A related approach to constructing approximate non-reflecting boundary conditions has been derived for the Euler equations by Gustafsson [6] in 1987.

When calculating linearized, harmonic unsteady flows, exact non-reflecting boundary conditions can be constructed. For the potential equation this was first done by Verdon *et al* [7] in 1975, and it is now the standard technique used by unsteady harmonic potential methods. Because the harmonic equations are solved directly (usually

by a finite element method) the issue of well-posedness does not arise. In 1987 Hall [8] extended the technique for the Euler equations, again using a finite element method to solve the harmonic linearized, Euler equations.

Early methods for calculating the steady-state solution to the two-dimensional Euler equations for isolated airfoils used the free-stream conditions at the far-field boundary, and it was found that the boundary had to be placed 50-100 chord lengths away from airfoil to obtain the correct lift. Later methods found that the inclusion of a vortex correction due to the lift on the airfoil enabled the far-field boundary to be brought in to about 25 chords away. In 1986 Giles and Drela [9] showed that by including both the source effect due to the drag and the next order doublet terms the far-field radius could be further reduced to about 5 chords (suitably scaled by the Prandtl-Glauert factor for transonic flows). The same result was also achieved by Ferm [10] using an approach based upon the zero-frequency limit of the ideal non-reflecting boundary conditions. It is this viewpoint which links together the construction of boundary conditions for steady-state, single-frequency and general, unsteady flows, and it forms this basis for this report's unified approach to non-reflecting boundary conditions for the Euler equations.

1.3 Present paper

This report is intended for CFD researchers, who wish to implement accurate non-reflecting boundary conditions, and wish to understand the underlying theory. Most of the boundary conditions which will be derived have been implemented by the author in a program for the calculation of steady and unsteady flows in turbomachinery. The precise numerical details are presented in a separate report [11] but this report contains the full details of the analytic boundary conditions from which others can derive implementations which are appropriate to their numerical algorithms.

The first half presents a unified treatment of the construction of non-reflecting boundary conditions for hyperbolic systems. Four different types are derived; quasi-one-dimensional b.c.'s, exact single-frequency unsteady non-reflecting b.c.'s, exact steady-state non-reflecting b.c.'s, and approximate unsteady non-reflecting b.c.'s. It should be remembered that the term 'exact' refers to the solution of the linear problem. Since the linear problem is itself an approximation to the nonlinear problem there will be errors which are proportional to the square of the amplitude of the unsteadiness at the far-field boundaries. The theory section is essentially a condensed restatement of the previous work described in the last section. The one significant original contribution lies in the analysis of well-posedness. Kreiss [1] and subsequent investigators assumed for simplicity that there is no degeneracy in the eigenvalues of the hyperbolic system.

Unfortunately the Euler equations have a multiple root with distinct eigenvectors, and at a particular complex frequency there is an eigenvalue/eigenvector coalescence. The extensions to the well-posedness analysis which are necessary to treat these problems are presented, but lack the mathematical rigor of Kreiss' work.

The second half presents the application of the theory to the Euler equations. First the dispersion relation and the eigenvalues and eigenvectors are found. Then the quasi-one-dimensional, single-frequency, steady-state and second-order non-reflecting boundary conditions are formed. The well-posedness of the quasi-one-dimensional b.c.'s is assured due to a general energy analysis performed in the theory section. The well-posedness of the steady-state and single-frequency b.c.'s depends on the numerical method being used. If a direct solution method is used then the question does not arise. If a time-marching method is used then the analysis of the associated initial-boundary-value problem becomes too complicated to perform. Much of the second half is concerned with the well-posedness of the second-order, approximate b.c.'s derived from the general Engquist-Majda theory. An unexpected result is that the outflow b.c. is well-posed but the inlet b.c.'s are ill-posed. Modified inflow boundary conditions which are well-posed are then derived by an *ad hoc* method. A calculation of the reflection coefficients shows that the modified inflow boundary conditions are fourth order and the outflow boundary condition is second order. A corresponding modified outflow boundary condition is shown to give first order reflections for outgoing vorticity waves but fourth order reflections for outgoing pressure waves, and so might be a useful boundary condition in applications or regions where it is known that there are no outgoing vorticity waves. Finally a reference section lists all of the boundary conditions in a dimensional form suitable for implementation.

2 General analysis

2.1 Fourier analysis

Consider the following general unsteady, two-dimensional, hyperbolic partial differential equation.

$$\frac{\partial U}{\partial t} + A\frac{\partial U}{\partial x} + B\frac{\partial U}{\partial y} = 0 \tag{1}$$

U is a N-component vector and A and B are constant $N \times N$ matrices, which are symmetric under a suitable change of variables. Fourier analysis assumes wave-like solutions of the form

$$U(x,y,t) = ue^{i(kx+ly-\omega t)}. \tag{2}$$

Substituting this into the differential equation gives

$$(-\omega I + kA + lB)u = 0. \tag{3}$$

$$\Longrightarrow \quad \det(-\omega I + kA + lB) = 0 \tag{4}$$

This equation is called the dispersion relation, and is a polynomial equation of degree N in each of ω, k, and l. Let $k_n(\omega,l)$ be the N roots for a particular choice of ω and l, and let u_n^R be the corresponding right eigenvector defined by

$$(-\omega I + k_n A + lB)u_n^R = 0. \tag{5}$$

A critical step in the construction and analysis of boundary conditions is to separate the waves into incoming and outgoing modes. If ω is complex with $Im(\omega) > 0$ (giving an exponential growth in time) then the incoming waves are those for which $Im(k_n) > 0$, because as shown in Fig. 1 these modes 'grow into' the domain. If ω and k_n are real then a standard result in the analysis of dispersive wave propagation [12] is that the velocity of energy propagation is the group velocity defined by

$$\vec{c}_g = \begin{pmatrix} \frac{\partial \omega}{\partial k_n} \\ \\ \frac{\partial \omega}{\partial l} \end{pmatrix} \tag{6}$$

Hence for real ω the incoming waves are those which either have $Im(k_n) > 0$, or have real k_n and $\frac{\partial \omega}{\partial k_n} > 0$. Fig. 1 also illustrates both of these types of waves.

Figure 1: Different incoming waves

2.2 Non-reflecting b.c.'s for a single Fourier mode

Suppose that the differential equation is to be solved in the domain $x > 0$, and one wants to construct non-reflecting boundary conditions at $x = 0$ to minimize or ideally prevent the reflection of outgoing waves. At the boundary at $x = 0$, U can be decomposed into a sum of Fourier modes with different values of ω and l, so the analysis begins by considering just one particular choice of ω and l. In this case this most general form for U is

$$U(x,y,t) = \left[\sum_{n=1}^{N} a_n u_n^R e^{ik_n x}\right] e^{i(ly-\omega t)}. \tag{7}$$

Note that it is because the boundary is a $y-t$ plane that we considered k_n as a function of ω, l rather than ω_n as a function of k, l (which might seem more natural).

The ideal non-reflecting boundary condition would be to specify that $a_n = 0$ for each n that corresponds to an incoming wave. Equivalent to this is the equation

$$v_n^L U = 0 \tag{8}$$

for a suitable choice of vector v_n^L such that

$$v_n^L u_m^R = 0 \quad \text{if} \quad m \neq n. \tag{9}$$

v_n^L can be constructed in two ways. Firstly, it can be chosen to be the left eigenvector of $(-\omega A^{-1} + k_n I + l A^{-1} B)$. Thus,

$$v_n^L(-\omega A^{-1} + k_n I + l A^{-1} B) = 0 \tag{10}$$

$$\Longrightarrow \quad v_n^L(\omega A^{-1} - l A^{-1} B)\, u_m^R = k_n v_n^L u_m^R \tag{11}$$

and also

$$\begin{aligned} v_n^L(\omega A^{-1} - l A^{-1} B) u_m^R &= v_n^L A^{-1}(\omega I - l B) u_m^R \\ &= v_n^L A^{-1} k_m A u_m^R \\ &= k_m v_n^L u_m^R \end{aligned} \tag{12}$$

Combining the last two equations gives

$$\Longrightarrow \quad (k_n - k_m)\, v_n^L u_m^R = 0 \tag{13}$$

$$\Longrightarrow \quad v_n^L u_m^R = 0 \quad \text{if} \quad k_m \neq k_n \tag{14}$$

If there are no multiple eigenvalues this completes the proof. If there are multiple eigenvalues then provided there is a complete set of N eigenvectors, v_n^L and u_m^R can still be constructed, using the Gram-Schmidt orthogonalization method [13], so that $v_n^L u_m^R = 0$ if $m \neq n$.

The second way to construct v_n^L is to note that

$$\left(v_n^L A^{-1}\right)(-\omega I + k_n A + l B) = 0 \tag{15}$$

so $v_n^L A^{-1}$ is a multiple of u_n^L, the left eigenvector of $(-\omega I + k_n A + l B)$.

By choice let the constant of proportionality be $\left.\frac{k_n}{\omega}\right|_{l=0}$ so that

$$v_n^L = \left.\frac{k_n}{\omega}\right|_{l=0} u_n^L A \tag{16}$$

$$= u_n^L \quad \text{if} \quad l = 0 \tag{17}$$

The second approach, finding u_n^L first and then calculating v_n^L, will often be simpler because it avoids the necessity of calculating A^{-1} and $A^{-1}B$.

In principle these exact boundary conditions can be implemented in a numerical method. The problem is that v_n^L depends on ω and l and so the implementation would involve a Fourier transform in y and a Laplace transform in t. Computationally this is both difficult and expensive to implement and so instead we will consider four simpler variations which use different assumptions and approximations. One final observation is that by dividing the dispersion relation by ω it is clear that k_n/ω, u_n^R, u_n^L and v_n^L are all functions of l/ω. Thus the variable $\lambda = l/\omega$ will play a key role in constructing all of the boundary conditions.

2.3 One-dimensional, unsteady b.c.'s

The one-dimensional, non-reflecting boundary conditions are obtained by ignoring all variations in the y-direction and setting $\lambda = 0$. The corresponding right and left eigenvectors are important in defining and implementing the other boundary conditions, and so we label them $\boldsymbol{w}$.

$$\boldsymbol{w}_n^R = \boldsymbol{u}_n^R\Big|_{\lambda=0} \tag{18}$$

$$\boldsymbol{w}_n^L = \boldsymbol{u}_n^L\Big|_{\lambda=0} = \boldsymbol{v}_n^L\Big|_{\lambda=0} \tag{19}$$

The boundary condition, expressed in terms of the primitive variables, is

$$\boldsymbol{w}_n^L U = 0 \tag{20}$$

for all n corresponding to incoming waves.

If the right and left eigenvectors are normalized so that

$$\boldsymbol{w}_m^L \boldsymbol{w}_n^R = \delta_{mn} \equiv \begin{cases} 1 & , \; m = n \\ 0 & , \; m \neq n \end{cases} \tag{21}$$

then they can be used to define a transformation between the primitive variables and the one-dimensional characteristic variables.

$$U = \sum_{n=1}^{N} c_n \boldsymbol{w}_n^R, \tag{22}$$

where

$$c_n = \boldsymbol{w}_n^L U. \tag{23}$$

Expressed in terms of the characteristic variables, the boundary condition is simply

$$c_n = 0 \tag{24}$$

for all n corresponding to incoming waves.

Numerical implementations of these boundary conditions usually extrapolate the outgoing characteristic variables, in addition to setting the incoming characteristic variables to zero, and then reconstruct the solution on the boundary using Eq. (22).

An observation, which will be needed later in the section on well-posedness, is that

$$(\omega \boldsymbol{I} + k_n \boldsymbol{A})\, \boldsymbol{w}_n^R = 0, \tag{25}$$

so

$$\boldsymbol{A} \boldsymbol{w}_n^R = \frac{\omega}{k_n} \boldsymbol{w}_n^R. \tag{26}$$

Thus w_n^R is an eigenvector of A with eigenvalue $\alpha_n = \frac{\omega}{k_n}$. Furthermore,

$$\omega = \alpha_n k_n \quad \Rightarrow \quad \vec{c}_g = \begin{pmatrix} \alpha_n \\ 0 \end{pmatrix}, \tag{27}$$

so the incoming waves are those for which $\alpha_n > 0$.

2.4 Exact, two-dimensional, single-frequency b.c.'s

In the introduction it was pointed out that if the interior differential equation is linear then by the principle of linear superposition it is possible to split a general solution into a sum of different frequencies, and calculate them independently, each with its own forcing terms and boundary conditions. In this case it is possible to construct the exact non-reflecting boundary conditions for simple geometries in which the far-field boundary is at $x=0$ and the solution is periodic in y, with period 2π This is achieved by performing a Fourier transform in y along the boundary to decompose the solution into a sum of Fourier modes, and then using the exact non-reflecting boundary conditions for each Fourier mode.

The Fourier decomposition of U at the boundary can be written as

$$U(0,y,t) = \sum_{-\infty}^{\infty} \hat{U}_l(t) e^{ily}, \tag{28}$$

where

$$\hat{U}_l(t) = \frac{1}{2\pi} \int_0^{2\pi} U(0,y,t) e^{-ily}\, dy. \tag{29}$$

The boundary condition is then

$$v_n^L(l/\omega)\hat{U}_l = 0 \tag{30}$$

for each Fourier mode l and incoming wave n. Since ω and l are both known for each Fourier mode, this is simply an algebraic equation in the Fourier domain. Because the numerical implementation of these conditions is very dependent on the numerical algorithm being used for the interior equations, further discussion conditions will be postponed to a later section which discusses the application to the Euler equations and turbomachinery problems in particular. One general comment however is that one of the principal difficulties is determining which waves are incoming and which are outgoing.

2.5 Exact, two-dimensional, steady b.c.'s

The exact, two-dimensional steady boundary conditions may be considered to be the limit of the single-frequency boundary conditions as $\omega \to 0$. Performing the same

Fourier decomposition as in the last section, the boundary conditions for $l \neq 0$ are

$$s_n^L \hat{U}_l = 0 \tag{31}$$

for each incoming wave n, where

$$s_n^L = \lim_{\lambda \to \infty} v_n^L(\lambda). \tag{32}$$

The boundary condition for the $l = 0$ mode, which is the solution average at the boundary, is

$$\begin{aligned} & v_n^L(0)\hat{U}_0 = 0 \\ \Rightarrow \quad & w_n^L \hat{U}_0 = 0 \end{aligned} \tag{33}$$

for each incoming wave n. The right-hand-side of Eq. (33) can be modified by the user to specify the value of the incoming average characteristics. For example, in fluid flow calculations this is how the average inlet flow angle, stagnation enthalpy and entropy can be specified. The right-hand-side of Eq. (31) could also be modified, but in most applications the solution at $x = -\infty$ is assumed to be uniform and so the zero right-hand-side is correct.

Again, discussion of the numerical implementation of these boundary conditions will be postponed to a later section dealing with the application to the Euler equations and turbomachinery flows. Also, one of the principal difficulties is again determining which waves are incoming and which are outgoing.

2.6 Approximate, two-dimensional, unsteady b.c.'s

By dividing the dispersion relation by ω it is clear that $k_n/\omega, u_n^R, u_n^L, v_n^L$ are all functions of l/ω. Thus a sequence of approximations can be obtained by expanding v_n^L in a Taylor series as a function of $\lambda = l/\omega$.

$$v_n^L(\lambda) = v_n^L\Big|_{\lambda=0} + \lambda \left.\frac{dv_n^L}{d\lambda}\right|_{\lambda=0} + \tfrac{1}{2}\lambda^2 \left.\frac{d^2 v_n^L}{d\lambda^2}\right|_{\lambda=0} + \cdots \tag{34}$$

The first order approximation obtained by just keeping the leading term just gives the one-dimensional boundary conditions which have already been discussed. The second order approximation is

$$\begin{aligned} \bar{v}_n^L(\lambda) &= v_n^L\Big|_{\lambda=0} + \frac{l}{\omega}\left.\frac{dv_n^L}{d\lambda}\right|_{\lambda=0} \\ &= u_n^L\Big|_{\lambda=0} + \frac{l}{\omega}\left.\left[\frac{k_n}{\omega}\frac{du_n^L}{d\lambda}\boldsymbol{A}\right]\right|_{\lambda=0} \end{aligned} \tag{35}$$

The overbar denotes the fact that $\bar{v}$ is an approximation to v. This produces the boundary condition

$$\left(u_n^L\Big|_{\lambda=0} + \frac{l}{\omega}\left[\frac{k_n}{\omega}\frac{du_n^L}{d\lambda}A\right]\Big|_{\lambda=0}\right) U = 0. \tag{36}$$

Multiplying by ω, and replacing ω and l by $i\frac{\partial}{\partial t}$ and $-i\frac{\partial}{\partial y}$ respectively gives,

$$u_n^L\Big|_{\lambda=0}\frac{\partial U}{\partial t} - \left[\frac{k_n}{\omega}\frac{du_n^L}{d\lambda}A\right]\Big|_{\lambda=0}\frac{\partial U}{\partial y} = 0 \tag{37}$$

This is a local boundary condition (meaning that it does not involve any global decomposition into Fourier modes) and so can be implemented without difficulty. As the equation is similar in nature to the original differential equation (i.e. it has first order derivatives in both y and t) the numerical algorithm used for the interior equations can probably also be used for the boundary conditions.

2.7 Analysis of well-posedness

2.7.1 One-dimensional b.c.'s

It is relatively easy to prove that the one-dimensional b.c.'s are always well-posed, by using an energy analysis method. A key step in the proof is that because the system is hyperbolic there exists a transformation of variables under which the transformed A and B matrices are symmetric, and so without loss of generality we can assume that A and B are symmetric.

The 'energy' is defined by

$$E(t) = \int_{-\infty}^{\infty}\int_{0}^{\infty} |u|^2 \, dx \, dy \tag{38}$$

The rate of change of the energy is given by

$$\begin{aligned}
\frac{dE}{dt} &= 2\int_{-\infty}^{\infty}\int_{0}^{\infty} u^T \frac{\partial u}{\partial t} \, dx \, dy \\
&= -2\int_{-\infty}^{\infty}\int_{0}^{\infty} u^T \left(A\frac{\partial u}{\partial x} + B\frac{\partial u}{\partial y} \right) dx \, dy \\
&= -\int_{-\infty}^{\infty}\int_{0}^{\infty} \frac{\partial}{\partial x}(u^T A u) + \frac{\partial}{\partial y}(u^T B u) \, dx \, dy \\
&= \int_{-\infty}^{\infty} u^T A u \, dy
\end{aligned} \tag{39}$$

The next step is to note that

$$\begin{aligned}
u^T A u &= \left(\sum_{n=1}^{N} c_n w_n^R \right)^T A \left(\sum_{n=1}^{N} c_n w_n^R \right) \\
&= \sum_{n=1}^{N} \alpha_n c_n^2
\end{aligned} \tag{40}$$

where, as defined earlier, α_n is the n^{th} eigenvalue of A, w_n^R is the corresponding right eigenvector which is also the transpose of the left eigenvector w_n^L since A is symmetric, and $c_n = w_n^L u$).

The final step is to note that the one-dimensional b.c. states that $c_n = 0$ for incoming waves, which are those for which $\alpha_n \geq 0$. Thus each term in the above sum is either zero or negative, and hence $u^T A u$ is non-positive and the energy is non-increasing, proving that the initial-boundary-value problem is well-posed.

2.7.2 Approximate, two-dimensional b.c.'s

To analyze the well-posedness of the approximate, two-dimensional boundary conditions, one must use the theory developed by Kreiss [1]. As explained by Trefethen

[14] and Higdon [2], the aim is to verify that there is no incoming mode which exactly satisfies the boundary condition.

As explained earlier, an incoming mode is a solution of the interior differential equation which *either* is growing exponentially in time but decaying exponentially in space away fron the boundary, *or* has a real frequency and a group velocity which is incoming. If this incoming mode also satisfies the boundary condition then in the first case there is an exponentially growing energy and in the second case there is a linear growth as the incoming mode moves into the interior.

If there are N' incoming waves then the generalized incoming mode may be written as

$$U(x,y,t) = \left[\sum_{n=1}^{N'} a_n u_n^R e^{ik_n x}\right] e^{i(ly-\omega t)}, \tag{41}$$

with $Im(\omega) \geq 0$. Substituting this into the N' non-reflecting boundary conditions produces a matrix equation of the form

$$C \begin{pmatrix} a_1 \\ \vdots \\ a_{N'} \end{pmatrix} = 0 \tag{42}$$

where C is a $N' \times N'$ matrix whose elements are the products of the approximate left eigenvectors and the exact right eigenvectors.

$$C_{mn} = \overline{v}_m^L u_n^R \tag{43}$$

Provided that the right eigenvectors are linearly independent, the requirement that there is no non-trivial incoming mode satisfying the boundary conditions is equivalent to the statement that there in no non-trivial solution to the above matrix equation. Thus the initial-boundary-value problem is well-posed if it can be proved that the determinant of C is non-zero for all real l and complex ω with $Im(\omega) \geq 0$.

If the right eigenvectors are linearly dependent then the theory needs to be modified. Suppose for simplicity that there are just two incoming waves and that $k_1 = k_2$ and $u_1^R = u_2^R$ at $\omega = \omega_{crit}$. A general incoming mode may be written as the sum of two incoming modes with amplitudes a_1', a_2'.

$$U(x,y,t) = \left[a_1' u_1^R e^{ik_1 x} + a_2' \frac{1}{\omega - \omega_{crit}} \left(u_1^R e^{ik_1 x} - u_2^R e^{ik_2 x}\right)\right] e^{i(ly-\omega t)} \tag{44}$$

By construction the second mode is finite in the limit $\omega \to \omega_{crit}$, and so if the limit is defined to be the value at $\omega = \omega_{crit}$ then this expression is the correct general solution

to the eigenvalue problem

$$\omega U = A\frac{\partial U}{\partial x} + lBU \tag{45}$$

subject to the condition $U \to 0$ as $x \to \infty$.

The amplitudes $a_{1,2}$ and $a'_{1,2}$ are related by

$$\begin{pmatrix} a_1 \\ a_2 \end{pmatrix} = T \begin{pmatrix} a'_1 \\ a'_2 \end{pmatrix}, \tag{46}$$

where

$$T = \begin{pmatrix} 1 & 1/(\omega-\omega_{crit}) \\ 0 & -1/(\omega-\omega_{crit}) \end{pmatrix}. \tag{47}$$

Substituting this into the boundary conditions gives

$$CT \begin{pmatrix} a'_1 \\ a'_2 \end{pmatrix} = 0. \tag{48}$$

By continuity, the requirement for well-posedness is that $\det(CT) = \det(C)\det(T) \not\to 0$ as $\omega \to \omega_{crit}$. Since $\det(T) = O(\omega-\omega_{crit})^{-1}$, this requires that $\det(C) = O(\omega-\omega_{crit})$, or equivalently that

$$\frac{\partial}{\partial\omega}\det(C)\Big|_{\omega_{crit}} \neq 0. \tag{49}$$

More generally, we conjecture that if the N' right eigenvectors collapse to N'' linearly independent eigenvectors at some ω_{crit} then the requirement for well-posedness is that $\det(C) = O(\omega-\omega_{crit})^{N'-N''}$, or equivalently that

$$\frac{\partial^{N'-N''}}{\partial\omega^{N'-N''}}\det(C)\Big|_{\omega_{crit}} \neq 0. \tag{50}$$

Engquist and Majda conjectured that the second order approximation is always well-posed, but we will see in the next section that this is not true for the Euler equations. Trefethen and Halpern have proved that the boundary conditions for the scalar wave equation which come from the second and higher order Taylor series expansions in l^2/ω^2 are ill-posed [14]. Thus it seems likely that for the differential system of equations which we are considering the higher order Taylor series approximations may be ill-posed.

2.8 Reflection coefficients

The calculation of reflection coefficients is very similar to the well-posedness analysis. A general solution with a given frequency ω and wavenumber l can be written as a sum of incoming and outgoing modes.

$$U(x,y,t) = \left[\sum_{n=1}^{N'} a_n u_n^R e^{ik_n x} + \sum_{n=N'+1}^{N} a_n u_n^R e^{ik_n x}\right] e^{i(ly-\omega t)} \tag{51}$$

Substituting this into the approximate non-reflecting boundary conditions gives

$$C\begin{pmatrix} a_1 \\ \vdots \\ a_{N'} \end{pmatrix} + D\begin{pmatrix} a'_N+1 \\ \vdots \\ a_N \end{pmatrix} = 0 \tag{52}$$

where C is the same matrix as in the well-posednes analysis and D is defined by

$$D_{mn} = \overline{v}_m^L u_{N+n}^R. \tag{53}$$

If the initial-boundary-value problem is well-posed C is non-singular and so Eq. (52) can be solved to obtain

$$\begin{pmatrix} a_1 \\ \vdots \\ a_{N'} \end{pmatrix} = -C^{-1}D\begin{pmatrix} a_{N+1} \\ \vdots \\ a_N \end{pmatrix}. \tag{54}$$

This equation relates the amplitudes of the incoming waves to the amplitude of the outgoing waves, so $-C^{-1}D$ is the matrix of reflection coefficients.

Since $v_m^L u_n^R = 0$ if $m \neq n$, the off-diagonal elements of C and the elements of D can be re-expressed as

$$C_{mn} = (\overline{v}_m^L - v_m^L)u_n^R, \quad m \neq n \tag{55}$$

$$D_{mn} = (\overline{v}_m^L - v_m^L)u_{N+n}^R. \tag{56}$$

Because the elements on the diagonal of C are $O(1)$, C^{-1} is $O(1)$ and hence the order of magnitude of the reflection coefficents for $l/\omega \ll 1$ depends solely on the order of magnitude of D. Using the one-dimensional approximation $w_m^L - v_m^L = O(l/\omega)$. Hence $D = O(l/\omega)$ in general and the reflection coefficients will be $O(l/\omega)$. Similarly, using the approximate two-dimensional boundary condition gives reflection coefficients which are $O(l/\omega)^2$.

3 Application to Euler Equations

3.1 Dispersion relation

When the linearized, unsteady, two-dimensional Euler equations are expressed in primitive form, meaning that U, the vector of independent variables, is defined by

$$U = \begin{pmatrix} \rho \\ u \\ v \\ p \end{pmatrix}, \tag{57}$$

then the coefficient matrices A and B are as follows.

$$A = \begin{pmatrix} u & \rho & 0 & 0 \\ 0 & u & 0 & \frac{1}{\rho} \\ 0 & 0 & u & 0 \\ 0 & \gamma p & 0 & u \end{pmatrix}, \quad B = \begin{pmatrix} v & 0 & \rho & 0 \\ 0 & v & 0 & 0 \\ 0 & 0 & v & \frac{1}{\rho} \\ 0 & 0 & \gamma p & v \end{pmatrix} \tag{58}$$

The analysis is greatly simplified if the unsteady perturbations and the steady variables in A and B are all non-dimensionalized using the steady density and speed of sound. With this choice of non-dimensionalization the matrices A and B become

$$A = \begin{pmatrix} u & 1 & 0 & 0 \\ 0 & u & 0 & 1 \\ 0 & 0 & u & 0 \\ 0 & 1 & 0 & u \end{pmatrix}, \quad B = \begin{pmatrix} v & 0 & 1 & 0 \\ 0 & v & 0 & 0 \\ 0 & 0 & v & 1 \\ 0 & 0 & 1 & v \end{pmatrix}. \tag{59}$$

The variables u and v in the above matrices are now the Mach numbers in the x and y directions.

Following the analytic theory described earlier, we first obtain the dispersion relation.

$$\begin{aligned} \det(-\omega I + kA + lB) &= \det \begin{pmatrix} uk+vl-\omega & k & l & 0 \\ 0 & uk+vl-\omega & 0 & k \\ 0 & 0 & uk+vl-\omega & l \\ 0 & k & l & uk+vl-\omega \end{pmatrix} \\ &= (uk+vl-\omega)^2 \left((uk+vl-\omega)^2 - k^2 - l^2 \right) \\ &= 0 \end{aligned} \tag{60}$$

The first two roots are clearly identical.

$$k_{1,2} = \frac{\omega - vl}{u} \tag{61}$$

Let us assume that $u > 0$ and we are concerned with defining boundary conditions for an inflow boundary at $x = 0$ and an outflow boundary at $x = 1$. If $Im(\omega) > 0$ then $Im(k_{1,2}) > 0$, and if $Im(\omega) = 0$ then $\frac{\partial \omega}{\partial k} = u > 0$. In either case these satisfy the conditions for right-travelling waves, which are incoming waves at the inflow boundary and outgoing waves at the outflow boundary.

The other two roots are given by

$$\left(1 - u^2\right) k^2 - 2u(vl - \omega)k - (vl - \omega)^2 + l^2 = 0 \tag{62}$$

$$\begin{aligned} \Longrightarrow \quad k_{3,4} &= \frac{u(vl-\omega) \pm \sqrt{u^2(vl-\omega)^2 + (1-u^2)(vl-\omega)^2 - l^2(1-u^2)}}{1-u^2} \\ &= \frac{1}{1-u^2}\left(-u(\omega - vl) \pm \sqrt{(\omega - vl)^2 - (1-u^2)l^2}\right) \\ &= \frac{(\omega - vl)(-u \pm S)}{1-u^2} \end{aligned} \tag{63}$$

where

$$S = \sqrt{1 - (1-u^2)l^2/(\omega - vl)^2} \tag{64}$$

Hence the third and fourth roots are defined by,

$$k_3 = \frac{(\omega - vl)(-u + S)}{1-u^2} \tag{65}$$

$$k_4 = \frac{(\omega - vl)(-u - S)}{1-u^2} \tag{66}$$

Now we must be extremely careful with which branch of the complex square root function is used in defining S. If ω is real and S^2 is real and positive, then after some straightforward algebra we obtain

$$\frac{\partial k_3}{\partial \omega} = \frac{-u + 1/S}{1-u^2} \quad \Longrightarrow \quad \frac{\partial \omega}{\partial k_3} = \frac{1-u^2}{-u + 1/S} \tag{67}$$

$$\frac{\partial k_4}{\partial \omega} = \frac{-u - 1/S}{1-u^2} \quad \Longrightarrow \quad \frac{\partial \omega}{\partial k_4} = \frac{1-u^2}{-u - 1/S} \tag{68}$$

If $u > 1$ then $S^2 > 1$, and hence it follows that both $\frac{\partial \omega}{\partial k_3}$ and $\frac{\partial \omega}{\partial k_4}$ are positive and so both waves are right-running which is what one expects for supersonic flow. However

there are very few turbomachines with axially supersonic flow and so henceforth we will assume that $0 < u < 1$.

If $u < 1$ and we take the positive real branch for S, then $0 < S < 1$ and hence $\frac{\partial \omega}{\partial k_3}$ is positive but $\frac{\partial \omega}{\partial k_4}$ is negative. Thus the third wave is a right-running wave, but the fourth is left-running. It can be proved that if ω and/or S^2 are complex then one of the two roots for k has positive imaginary part, while the other has a negative imaginary part. To be consistent with the results when S^2 is real and positive, k_3 is defined to be the root with positive imaginary component so that it corresponds to a complex right-running wave, and k_4 remains a left-running wave.

3.2 Eigenvalues and eigenvectors

3.2.1 Root 1: entropy wave

$$k_1 = \frac{\omega - vl}{u}, \qquad \omega = uk_1 + vl \tag{69}$$

Substituting for ω gives

$$-\omega I + k_1 A + lB = \begin{pmatrix} 0 & k_1 & l & 0 \\ 0 & 0 & 0 & k_1 \\ 0 & 0 & 0 & l \\ 0 & k_1 & l & 0 \end{pmatrix} \tag{70}$$

and by observation one obtains a right eigenvector

$$u_1^R = \begin{pmatrix} -1 \\ 0 \\ 0 \\ 0 \end{pmatrix}, \tag{71}$$

and a corresponding left eigenvector

$$u_1^L = \begin{pmatrix} -1 & 0 & 0 & 1 \end{pmatrix}. \tag{72}$$

The vector v_1^L, which is needed to construct the non-relecting boundary conditions, is calculated following the procedure given in the theory section.

$$\begin{aligned} v_1^L &= \frac{1}{u} u_1^L A \\ &= \begin{pmatrix} -1 & 0 & 0 & 1 \end{pmatrix} \end{aligned} \tag{73}$$

This choice of eigenvectors corresponds to the entropy wave. This can be verified by noting that the only non-zero term in the right eigenvector is the density, so that the wave has varying entropy, no vorticity and constant pressure. Also, the left eigenvector 'measures' entropy in the sense that $u_1^L U$ is equal to the linearized entropy, $\delta p - \delta \rho$ (remembering that $c = 1$ because of the non-dimensionalization).

The eigenvectors are only determined to within an arbitrary factor; i.e. they may be multplied by an arbitary constant or function of λ and they would still be eigenvectors. In the case of both this root and the other roots the arbitary factor was chosen to give the simplest possible form for the eigenvectors subject to the one restriction that at $\lambda = 0$, $u^L u^R = 1$. This restriction gives the orthonormal form for the vectors w which was assumed in the theory section, Eq. (21).

3.2.2 Root 2: vorticity wave

$$k_2 = \frac{\omega - vl}{u}, \qquad \omega = uk_2 + vl \tag{74}$$

By inspection, a second set of right and left eigenvectors for the multiple root is given by

$$u_2^R = \begin{pmatrix} 0 \\ -ul/\omega \\ uk_2/\omega \\ 0 \end{pmatrix} = \begin{pmatrix} 0 \\ -u\lambda \\ 1-v\lambda \\ 0 \end{pmatrix}, \tag{75}$$

and

$$\begin{aligned} u_2^L &= \begin{pmatrix} 0 & -ul/\omega & uk_2/\omega & 0 \end{pmatrix} \\ &= \begin{pmatrix} 0 & -u\lambda & 1-v\lambda & 0 \end{pmatrix} \end{aligned} \tag{76}$$

Hence,

$$\begin{aligned} v_2^L &= \frac{1}{u} u_2^L A \\ &= \begin{pmatrix} 0 & -u\lambda & 1-v\lambda & -\lambda \end{pmatrix} \end{aligned} \tag{77}$$

This root corresponds to the vorticity wave, which can be verified by noting that the right eigenvector gives a wave with vorticity, but uniform entropy and pressure. Since the first two roots are a multiple root we must check that the chosen right and left eigenvectors satisfy the necessary orthogonality relations.

$$v_1^L u_2^R = 0 \tag{78}$$

$$v_2^L u_1^R = 0 \tag{79}$$

It is easily verified that these are correct.

3.2.3 Root 3: downstream running pressure wave

$$k_3 = \frac{(\omega - vl)(S-u)}{1-u^2} \tag{80}$$

The eigenvectors are derived by the usual method.

$$-\omega I + k_3 A + lB = \begin{pmatrix} uk_3+vl-\omega & k_3 & l & 0 \\ 0 & uk_3+vl-\omega & 0 & k_3 \\ 0 & 0 & uk_3+vl-\omega & l \\ 0 & k_3 & l & uk_3+vl-\omega \end{pmatrix} \tag{81}$$

$$u_3^R = \frac{1+u}{2\omega}\begin{pmatrix} \omega-uk_3-vl \\ k_3 \\ l \\ \omega-uk_3-vl \end{pmatrix} = \frac{1}{2(1-u)}\begin{pmatrix} 1-(1-v\lambda)uS \\ (1-v\lambda)(S-u) \\ (1-u^2)\lambda \\ 1-(1-v\lambda)uS \end{pmatrix} \tag{82}$$

$$\begin{aligned} u_3^L &= \frac{1+u}{\omega}\begin{pmatrix} 0 & k_3 & l & \omega-uk_3-vl \end{pmatrix} \\ &= \frac{1}{1-u}\begin{pmatrix} 0 & (1-v\lambda)(S-u) & (1-u^2)\lambda & 1-(1-v\lambda)uS \end{pmatrix} \end{aligned} \tag{83}$$

$$\begin{aligned} v_3^L &= \frac{1}{1+u}u_3^L A \\ &= \frac{1}{\omega}\begin{pmatrix} 0 & \omega-vl & ul & u(\omega-vl)+(1-u^2)k_3 \end{pmatrix} \\ &= \begin{pmatrix} 0 & (1-v\lambda) & u\lambda & (1-v\lambda)S \end{pmatrix} \end{aligned} \tag{84}$$

This root corresponds to an isentropic, irrotational pressure wave, travelling downstream provided $u > -1$.

3.2.4 Root 4: upstream running pressure wave

$$k_4 = -\frac{(\omega - vl)(S+u)}{1-u^2} \tag{85}$$

The eigenvectors are derived by the usual method.

$$-\omega I + k_4 A + l B = \begin{pmatrix} uk_4+vl-\omega & k_4 & l & 0 \\ 0 & uk_4+vl-\omega & 0 & k_4 \\ 0 & 0 & uk_4+vl-\omega & l \\ 0 & k_4 & l & uk_4+vl-\omega \end{pmatrix} \tag{86}$$

$$u_4^R = \frac{1-u}{2\omega}\begin{pmatrix} \omega-uk_4-vl \\ k_4 \\ l \\ \omega-uk_4-vl \end{pmatrix} = \frac{1}{2(1+u)}\begin{pmatrix} 1+(1-v\lambda)uS \\ -(1-v\lambda)(S+u) \\ (1-u^2)\lambda \\ 1+(1-v\lambda)uS \end{pmatrix} \tag{87}$$

$$\begin{aligned} u_4^L &= \frac{1-u}{\omega}\begin{pmatrix} 0 & k_4 & l & \omega-uk_4-vl \end{pmatrix} \\ &= \frac{1}{1+u}\begin{pmatrix} 0 & -(1-v\lambda)(S+u) & (1-u^2)\lambda & 1+(1-v\lambda)uS \end{pmatrix} \end{aligned} \tag{88}$$

$$\begin{aligned} v_4^L &= -\frac{1}{1-u}u_4^L A \\ &= -\frac{1}{\omega}\begin{pmatrix} 0 & \omega-vl & ul & u(\omega-vl)+(1-u^2)k_4 \end{pmatrix} \\ &= \begin{pmatrix} 0 & -(1-v\lambda) & -u\lambda & (1-v\lambda)S \end{pmatrix} \end{aligned} \tag{89}$$

This root corresponds to an isentropic, irrotational pressure wave, travelling upstream provided $u<1$.

3.3 One-dimensional, unsteady b.c.'s

If the computational domain is $0<x<1$, and $0<u<1$, then the boundary at $x=0$ is an inflow boundary with incoming waves corresponding to the first three roots, and the boundary at $x=1$ is an outflow boundary with just one incoming wave due to the fourth root.

When $\lambda=0$, $S=1$, and so the right eigenvectors w^R are

$$w_1^R = \begin{pmatrix} -1 \\ 0 \\ 0 \\ 0 \end{pmatrix}, \quad w_2^R = \begin{pmatrix} 0 \\ 0 \\ 1 \\ 0 \end{pmatrix}, \quad w_3^R = \begin{pmatrix} \frac{1}{2} \\ \frac{1}{2} \\ 0 \\ \frac{1}{2} \end{pmatrix}, \quad w_4^R = \begin{pmatrix} \frac{1}{2} \\ -\frac{1}{2} \\ 0 \\ \frac{1}{2} \end{pmatrix}, \tag{90}$$

and the left eigenvectors w^L are

$$\begin{aligned} w_1^L &= (-1 \quad 0 \quad 0 \quad 1) \\ w_2^L &= (0 \quad 0 \quad 1 \quad 0) \\ w_3^L &= (0 \quad 1 \quad 0 \quad 1) \\ w_4^L &= (0 \quad -1 \quad 0 \quad 1). \end{aligned} \tag{91}$$

Hence the transformation to, and from, 1-D characteristic variables is given by the following two matrix equations.

$$\begin{pmatrix} c_1 \\ c_2 \\ c_3 \\ c_4 \end{pmatrix} = \begin{pmatrix} -1 & 0 & 0 & 1 \\ 0 & 0 & 1 & 0 \\ 0 & 1 & 0 & 1 \\ 0 & -1 & 0 & 1 \end{pmatrix} \begin{pmatrix} \delta\rho \\ \delta u \\ \delta v \\ \delta p \end{pmatrix} \tag{92}$$

$$\begin{pmatrix} \delta\rho \\ \delta u \\ \delta v \\ \delta p \end{pmatrix} = \begin{pmatrix} -1 & 0 & \frac{1}{2} & \frac{1}{2} \\ 0 & 0 & \frac{1}{2} & -\frac{1}{2} \\ 0 & 1 & 0 & 0 \\ 0 & 0 & \frac{1}{2} & \frac{1}{2} \end{pmatrix} \begin{pmatrix} c_1 \\ c_2 \\ c_3 \\ c_4 \end{pmatrix} \tag{93}$$

$\delta\rho, \delta u, \delta v$ and δp are the perturbations from the uniform flow about which the Euler equations were linearized, and c_1, c_2, c_3 and c_4 are the amplitudes of the four characteristic waves. At the inflow boundary the correct unsteady, non-reflecting, boundary conditions are

$$\begin{pmatrix} c_1 \\ c_2 \\ c_3 \end{pmatrix} = 0, \tag{94}$$

while at the outflow boundary the correct non-reflecting boundary condition is

$$c_4 = 0 \tag{95}$$

The standard numerical method for implementing these is to calculate or extrapolate the outgoing characteristic values from the interior domain, and then use Eq. (93) to reconstruct the solution on the boundary.

3.4 Exact, two-dimensional, single-frequency b.c.'s

The construction of the exact, non-reflecting boundary conditions for a linear, two-dimensional, single-frequency solution begins by performing a Fourier decomposition of the flow field at the boundary. Whereas before we assumed that the field was periodic with period 2π, we will now be more specifically concerned with turbomachinery applications, and will consider a problem in which the pitch is P and the inter-blade phase angle is σ. In this case the Fourier decomposition of U at the boundary can be written as

$$U(0,y,t) = \sum_{-\infty}^{\infty} \hat{U}_m(t) e^{il_m y}, \tag{96}$$

where

$$\hat{U}_m(t) = \frac{1}{P} \int_0^P U(0,y,t) e^{-il_m y}\, dy, \tag{97}$$

and

$$l_m = \frac{2\pi m + \sigma}{P}. \tag{98}$$

Using the expressions for v^L derived earlier, the exact, two-dimensional, single-frequency, non-reflecting boundary conditions at the inflow are

$$\begin{pmatrix} -1 & 0 & 0 & 1 \\ 0 & -u\lambda & 1-v\lambda & -\lambda \\ 0 & 1-v\lambda & u\lambda & (1-v\lambda)S \end{pmatrix} \hat{U}_m = 0, \tag{99}$$

and at the outflow the boundary condition is

$$\begin{pmatrix} 0 & -(1-v\lambda) & -u\lambda & (1-v\lambda)S \end{pmatrix} \hat{U}_m = 0. \tag{100}$$

λ and hence S are functions of l_m/ω and so depend on the mode number m.

How these conditions are implemented depends greatly on the numerical method being used to solve the linear, differential equations in the interior. The most efficient methods begin by expressing the flow field as the real part of a complex amplitude multiplying a complex oscillation in time.

$$U(x,y,t) = U e^{-i\omega t} \tag{101}$$

The direct class of methods now treat the amplitude U as a function of x and y only, and substitutes this definition into the equations of mtoion to obtain a spatial, partial differential equation for U. This is then spatially discretized in some manner and solved by an iterative or direct matrix solution method. Following this approach the exact, non-reflecting boundary conditions can be introduced and solved directly.

This was done by Hall, and the full details and some results are presented in his thesis [15] and a recent paper [8].

An alternative approach is to still treat the complex amplitude U as time-varying. In this way one obtains an unsteady, partial differential equation for U which can be solved by a time-marching method and integrated in time until U converges to a steady-state giving the correct complex amplitudes. This approach was developed by Ni for the isentropic, linearized Euler equations [16]. The exact, non-reflecting boundary conditions can still be used, but now one must be concerned with implementing them in a manner that gives the correct result in the converged steady-state but is also stable during the pseudo-time-evolution process. This requires that the associated initial-boundary-value problem be well-posed. To achieve this let us first express the non-reflecting boundary conditions in terms of the spatial Fourier transforms of the one-dimensional characteristic variables.

$$\hat{U}_m = \begin{pmatrix} -1 & 0 & \frac{1}{2} & \frac{1}{2} \\ 0 & 0 & \frac{1}{2} & -\frac{1}{2} \\ 0 & 1 & 0 & 0 \\ 0 & 0 & \frac{1}{2} & \frac{1}{2} \end{pmatrix} \begin{pmatrix} \hat{c}_1 \\ \hat{c}_2 \\ \hat{c}_3 \\ \hat{c}_4 \end{pmatrix} \tag{102}$$

Hence the inflow boundary condition is

$$\begin{pmatrix} 1 & 0 & 0 & 0 \\ 0 & 1-v\lambda & -\frac{1}{2}\lambda(u+1) & \frac{1}{2}\lambda(u-1) \\ 0 & u\lambda & \frac{1}{2}(1-v\lambda)(1+S) & -\frac{1}{2}(1-v\lambda)(1-S) \end{pmatrix} \begin{pmatrix} \hat{c}_1 \\ \hat{c}_2 \\ \hat{c}_3 \\ \hat{c}_4 \end{pmatrix} = 0, \tag{103}$$

and the outflow equation is

$$\begin{pmatrix} 0 & -u\lambda & -\frac{1}{2}(1-v\lambda)(1-S) & \frac{1}{2}(1-v\lambda)(1+S) \end{pmatrix} \begin{pmatrix} \hat{c}_1 \\ \hat{c}_2 \\ \hat{c}_3 \\ \hat{c}_4 \end{pmatrix} = 0, \tag{104}$$

These equations can now be solved to obtain the incoming characteristics as a function of the outgoing ones.

$$\begin{pmatrix} \hat{c}_1 \\ \hat{c}_2 \\ \hat{c}_3 \end{pmatrix} = \begin{pmatrix} 0 \\ \dfrac{(1-u)\lambda}{(1+S)(1-v\lambda)}\hat{c}_4 \\ \dfrac{(1-u)^2\lambda^2}{(1+S)^2(1-v\lambda)^2}\hat{c}_4 \end{pmatrix} \tag{105}$$

$$\hat{c}_4 = \frac{2u\lambda}{(1-v\lambda)(1+S)}\hat{c}_2 + \frac{1-S}{1+S}\hat{c}_3 \tag{106}$$

In inverting the inflow matrix the following identity was used to eliminate $\lambda^2(1 \pm u)$.

$$(1-u^2)\lambda^2 = (1-v\lambda)^2(1+S)(1-S) \tag{107}$$

Note that in the resulting inflow equation $(1+S)(1-v\lambda)$ remains finite as $(1-v\lambda) \to 0$, and so the reflection coefficient is never infinite.

It has already been proved that if the incoming one-dimensional characteristics are set to zero then the initial-boundary-value problam is well-posed. This suggests that the evolutionary process for this problem will be well-posed if we lag the updating of the incoming characteristics.

$$\frac{\partial}{\partial t}\begin{pmatrix} \hat{c}_1 \\ \hat{c}_2 \\ \hat{c}_3 \end{pmatrix} = \alpha \begin{pmatrix} -\hat{c}_1 \\ \dfrac{(1-u)\lambda}{(1+S)(1-v\lambda)}\hat{c}_4 - \hat{c}_2 \\ \dfrac{(1-u)^2\lambda^2}{(1+S)^2(1-v\lambda)^2}\hat{c}_4 - \hat{c}_3 \end{pmatrix} \tag{108}$$

$$\frac{\partial \hat{c}_4}{\partial t} = \alpha\left(\frac{2u\lambda}{(1-v\lambda)(1+S)}\hat{c}_2 + \left(\frac{1-S}{1+S}\right)\hat{c}_3 - \hat{c}_4\right) \tag{109}$$

This is the one numerical boundary condition in this report which the author has not yet implemented, and so the correct value for α is not clear. Choosing too large a value for α may lead to ill-posedness and numerical instability. Choosing too small a value will lead to a poor convergence rate. Some numerical experimentation may be needed to obtain the best value for α. As before, the outgoing characteristics can be obtained by extrapolation or calculation from the interior solution, and then the solution on the boundary can be reconstructed by first converting back to the Fourier-transformed primitive variables, and finally back to the primitive variables in the physical domain.

3.5 Exact, two-dimensional, steady b.c.'s

The exact, two-dimensional steady boundary conditions are essentially the exact, two-dimensional single-frequency boundary conditions in the limit $\omega \to 0$. Again one begins by Fourier transforming the solution along the boundary, and then constructing boundary conditions for each Fourier mode. If the mode number m is non-zero, then

$$\begin{aligned} \lim_{\lambda \to 0} S(\lambda) &= \sqrt{1 - \frac{1-u^2}{v^2}} \\ &= -\frac{\beta}{v} \end{aligned} \tag{110}$$

where

$$\beta = \begin{cases} i\,\mathrm{sign}(l)\sqrt{1-u^2-v^2}\,, & u^2+v^2 < 1 \\ -\mathrm{sign}(v)\sqrt{u^2+v^2-1}\,, & u^2+v^2 > 1 \end{cases} \tag{111}$$

The reason for the choice of sign functions in the definition of β, is that for supersonic flow S must be positive, as discussed when S was first defined, and for subsonic flow S must be consistent with $Im(k_3) > 0$. To check that we have satisfied this latter condition, the steady-state values of the four wavenumbers are

$$\begin{aligned} k_1 &= -\frac{vl}{u} \\ k_2 &= -\frac{vl}{u} \\ k_3 &= -\frac{vl(-u+S)}{1-u^2} = \frac{uvl+\beta l}{1-u^2} \\ k_4 &= -\frac{vl(-u-S)}{1-u^2} = \frac{uvl-\beta l}{1-u^2}. \end{aligned} \tag{112}$$

If $u^2+v^2 < 1$ then

$$Im(k_3) = \frac{|l|\sqrt{1-u^2-v^2}}{1-u^2} > 0 \tag{113}$$

and so the condition is indeed satisfied.

It should be remembered that in discussing the supersonic flow condition we are still assuming that the flow is axially subsonic, $u < 1$, and so there are three incoming characteristics at the inflow boundary and one incoming characteristic at the outflow boundary.

The next step is to construct the steady-state left eigenvectors s^L. Since it is permissible to multiply the eigenvectors by any function of λ, we will slightly modify the

definition given in the theory section in order to keep the limits finite as $\lambda \to 0$.

$$\begin{aligned} s_1^L &= \lim_{\lambda\to 0} v_1^L &&= (\,-1 \quad 0 \quad 0 \quad 1\,) \\ s_2^L &= \lim_{\lambda\to 0} \tfrac{1}{\lambda} v_2^L &&= (\,0 \quad -u \quad -v \quad -1\,) \\ s_3^L &= \lim_{\lambda\to 0} \tfrac{1}{\lambda} v_3^L &&= (\,0 \quad -v \quad u \quad \beta\,) \\ s_4^L &= \lim_{\lambda\to 0} \tfrac{1}{\lambda} v_4^L &&= (\,0 \quad v \quad -u \quad \beta\,) \end{aligned} \tag{114}$$

Using these vectors, the exact, two-dimensional, steady-state, non-reflecting boundary conditions at the inflow are

$$\begin{pmatrix} -1 & 0 & 0 & 1 \\ 0 & -u & -v & -1 \\ 0 & -v & u & \beta \end{pmatrix} \hat{U}_m = 0, \tag{115}$$

and at the outflow the boundary condition is

$$\begin{pmatrix} 0 & v & -u & \beta \end{pmatrix} \hat{U}_m = 0. \tag{116}$$

For subsonic flow, β depends on l and hence the mode number m. For supersonic flow, β does not depend on l and so the boundary conditions are the same for each Fourier mode other than $m=0$.

As with the single-frequency boundary conditions we now transform from primitive variables into characteristic variables. The inflow boundary condition becomes

$$\begin{pmatrix} 1 & 0 & 0 & 0 \\ 0 & -v & -\frac{1}{2}(1+u) & -\frac{1}{2}(1-u) \\ 0 & u & \frac{1}{2}(\beta-v) & \frac{1}{2}(\beta+v) \end{pmatrix} \begin{pmatrix} \hat{c}_1 \\ \hat{c}_2 \\ \hat{c}_3 \\ \hat{c}_4 \end{pmatrix} = 0, \tag{117}$$

and the outflow equation becomes

$$\begin{pmatrix} 0 & -u & \frac{1}{2}(\beta+v) & \frac{1}{2}(\beta-v) \end{pmatrix} \begin{pmatrix} \hat{c}_1 \\ \hat{c}_2 \\ \hat{c}_3 \\ \hat{c}_4 \end{pmatrix} = 0, \tag{118}$$

Solving to obtain the incoming characteristics as a function of the outgoing ones gives

$$\begin{pmatrix} \hat{c}_1 \\ \hat{c}_2 \\ \hat{c}_3 \end{pmatrix} = \begin{pmatrix} 0 \\ -\left(\frac{\beta+v}{1+u}\right)\hat{c}_4 \\ \left(\frac{\beta+v}{1+u}\right)^2 \hat{c}_4 \end{pmatrix}, \tag{119}$$

and

$$\hat{c}_4 = \left(\frac{2u}{\beta - v}\right)\hat{c}_2 - \left(\frac{\beta + v}{\beta - v}\right)\hat{c}_3. \tag{120}$$

In inverting the inflow matrix we twice used the following identity.

$$(1+u)(1-u) = -(\beta+v)(\beta-v) \tag{121}$$

To ensure the well-posedness of the evolutionary process, these equations are again lagged.

$$\frac{\partial}{\partial t}\begin{pmatrix} \hat{c}_1 \\ \hat{c}_2 \\ \hat{c}_3 \end{pmatrix} = \alpha \begin{pmatrix} -\hat{c}_1 \\ -\left(\frac{\beta+v}{1+u}\right)\hat{c}_4 - \hat{c}_2 \\ \left(\frac{\beta+v}{1+u}\right)^2 \hat{c}_4 - \hat{c}_3 \end{pmatrix} \tag{122}$$

$$\frac{\partial \hat{c}_4}{\partial t} = \alpha\left(\left(\frac{2u}{\beta - v}\right)\hat{c}_2 - \left(\frac{\beta + v}{\beta - v}\right)\hat{c}_3 - \hat{c}_4\right) \tag{123}$$

Numerical experience indicates that a suitable choice for α is $1/P$. This completes the formulation of the boundary conditions for all of the Fourier modes except $m = 0$, which corresponds to $l = 0$ which is the average mode. For this mode the user specifies the changes in the incoming one-dimensional characteristics in order to achieved certain average flow conditions. For example at the inflow the three incoming characteristics can be determined by specifiying the average entropy, flow angle and stagnation enthalpy, and at the outflow boundary the one incoming characteristic can be determined by specifying the average exit pressure. Full details of this numerical procedure are given in a separate report [11], which also illustrates the effectiveness of these steady-state nonreflecting boundary conditions. It also tackles the problems caused by the fact that because we have used a linear theory we can get second-order non-uniformities in entropy and stagnation enthalpy across the inflow boundary. These are undesirable, and can be avoided by modifying one of the inflow boundary conditions, and replacing another be the constraint of uniform stagnation enthalpy. The report also shows how the same boundary condition approach can be used to match together two stator and rotor calculations, so that the interface is treated in a average, conservative manner.

3.6 Approximate, two-dimensional, unsteady b.c.'s

3.6.1 Second-order b.c.'s

Following the theory presented earlier, the second order non-reflecting boundary conditions are obtained by taking the second-order approximation to the left eigenvectors v^L in the limit $\lambda \approx 0$. In this limit $S \approx 1$ and so one obtains the following approximate eigenvectors.

$$\begin{aligned} \overline{v}_1^L &= (-1 \quad 0 \quad 0 \quad 1) \\ \overline{v}_2^L &= (0 \quad -u\lambda \quad 1-v\lambda \quad -\lambda) \\ \overline{v}_3^L &= (0 \quad 1-v\lambda \quad u\lambda \quad 1-v\lambda) \\ \overline{v}_4^L &= (0 \quad -(1-v\lambda) \quad -u\lambda \quad 1-v\lambda) \end{aligned} \tag{124}$$

The second step is to multiply by ω and replace ω by $-\frac{\partial}{\partial t}$ and l by $\frac{\partial}{\partial y}$. This gives the inflow boundary condition

$$\begin{pmatrix} -1 & 0 & 0 & 1 \\ 0 & 0 & 1 & 0 \\ 0 & 1 & 0 & 1 \end{pmatrix} \frac{\partial U}{\partial t} + \begin{pmatrix} 0 & 0 & 0 & 0 \\ 0 & u & v & 1 \\ 0 & v & -u & v \end{pmatrix} \frac{\partial U}{\partial y} = 0, \tag{125}$$

and the outflow boundary condition

$$\begin{pmatrix} 0 & -1 & 0 & 1 \end{pmatrix} \frac{\partial U}{\partial t} + \begin{pmatrix} 0 & -v & u & v \end{pmatrix} \frac{\partial U}{\partial y} = 0. \tag{126}$$

For implementation purposes it is preferable to rewrite these equations using one-dimensional characteristics.

$$\frac{\partial}{\partial t} \begin{pmatrix} c_1 \\ c_2 \\ c_3 \end{pmatrix} + \begin{pmatrix} 0 & 0 & 0 & 0 \\ 0 & v & \frac{1}{2}(1+u) & \frac{1}{2}(1-u) \\ 0 & -u & v & 0 \end{pmatrix} \frac{\partial}{\partial y} \begin{pmatrix} c_1 \\ c_2 \\ c_3 \\ c_4 \end{pmatrix} = 0 \tag{127}$$

$$\frac{\partial c_4}{\partial t} + \begin{pmatrix} 0 & u & 0 & v \end{pmatrix} \frac{\partial}{\partial y} \begin{pmatrix} c_1 \\ c_2 \\ c_3 \\ c_4 \end{pmatrix} = 0. \tag{128}$$

The outgoing characteristics can be extrapolated or calculated from the interior, and the incoming characteristics can be calculated by integrating these equations in

time using an appropriate method, which in many cases could probably be the same as is used for the interior, partial differential equations. Before using these conditions however, we must check whether or not they form a well-posed initial-boundary-value problem. If they do not then no matter how they are implemented they will produce a divergent solution on a sufficiently fine grid.

3.6.2 Analysis of well-posedness

The well-posedness of the second approximation non-reflecting boundary conditions can be analyzed using the theory discussed earlier. To simplify the analysis we shift to a frame of reference which is moving with speed v in the y-direction. The transformed equations of motion and boundary conditions then correspond to $v=0$ which simplifies the algebra, and well-posedness in this frame of reference is clearly both necessary and sufficient for well-posedness in the original frame of reference.

At the inflow boundary there are three incoming waves and the generalized incoming mode is

$$U(x,y,t) = \left[\sum_{n=1}^{3} a_n u_n^R e^{ik_n x}\right] e^{i(ly-\omega t)} \tag{129}$$

with $Im(\omega) \geq 0$. Using the assumption that $v=0$ the wave numbers are given by

$$k_1 = k_2 = \frac{\omega}{u} \tag{130}$$

$$k_3 = \frac{\omega(S-u)}{1-u^2} \tag{131}$$

where

$$S = \sqrt{1-(1-u^2)\lambda^2} \tag{132}$$

with the correct square root being taken in the definition of S to ensure that if ω and S are both real then S is positive, and if ω or S is complex then $Im(k_3)>0$. Following the procedure presented in the theory section, we obtain the critical matrix C.

$$C = \begin{pmatrix} 1 & 0 & 0 \\ 0 & 1+u^2\lambda^2 & 0 \\ 0 & 0 & \frac{1}{2}(S+1+u(1+u)\lambda^2) \end{pmatrix} \tag{133}$$

If $\omega = +iu|l|$ (satisfying the condition that $Im(\omega)\geq 0$), then $\lambda^2 = -u^2$ and $S = 1/u$ (with the correct branch of the square root being taken to ensure that $Im(k_3)\geq 0$). Hence, for this value of ω,

$$C = \begin{pmatrix} 1 & 0 & 0 \\ 0 & 0 & 0 \\ 0 & 0 & 0 \end{pmatrix} \tag{134}$$

so there is clearly a non-trivial incoming mode, $U(x,y,t) = a_2 u_2^R e^{i(k_2 x + ly - \omega t)}$, and the inflow boundary conditions are ill-posed.

It may appear that there is a second incoming mode, $U(x,y,t) = a_3 u_3^R e^{i(k_3 x + ly - \omega t)}$, but this is actually a multiple of the first, because when $\omega = iu|l|$, $k_3 = k_2$ and u_3^R is a multiple of u_2^R. This degenerate situation was discussed in the theory section, and in this case it is easily verified that in the neighborhood of $\omega_{crit} = iu|l|$, $\det(C) = O(\omega - \omega_{crit})^2$ and the initial-boundary-value problem is ill-posed with just one ill-posed mode.

At the outflow the generalized incoming mode is

$$U(x,y,t) = u_4^R e^{ik_4 x} e^{i(ly - \omega t)} \tag{135}$$

with $Im(\omega) \geq 0$. Since $v = 0$ the wave number is given by

$$k_4 = -\frac{\omega(S+u)}{1-u^2} \tag{136}$$

Again the correct square root must be taken in the definition of S to ensure that if ω and S are both real then S is positive, and if ω or S is complex then $Im(k_4) < 0$. Since there is now only one incoming mode, the matrix C is simply a scalar.

$$C = \frac{1}{2}(S + 1 - u(1-u)\lambda^2) \tag{137}$$

The outflow boundary conditions are ill-posed *if* there is a solution to

$$S = -1 + u(1-u)\lambda^2 \tag{138}$$

Squaring this equation gives

$$1 - (1-u^2)\lambda^2 = 1 - 2u(1-u)\lambda^2 + u^2(1-u)^2\lambda^4 \tag{139}$$

Solving for λ gives $\lambda^2 = -1/u^2$. This implies that $\omega = +iu|l|$ and $S = 1/u$, as with the inflow analysis. However, when these values are substituted back into Eq. (138) we obtain

$$\frac{1}{u} = -1 - \frac{1-u}{u} = -\frac{1}{u} \tag{140}$$

This inconsistent equation contradicts the supposition that there is a incoming mode which satisfies the boundary conditions, and so we conclude that the outflow boundary condition is well-posed.

3.6.3 Modified boundary conditions

To overcome the ill-posedness of the inflow boundary conditions we modify the third inflow boundary condition. To do this we note that we have been overly restrictive in

requiring v_3^L to be orthogonal to u_1^R and u_2^R. Since the first two inflow boundary conditions already require that $a_1 = a_2 = 0$, we only really require that v_3^L is orthogonal to u_4^R. Thus we propose a new definition of $\overline{v}_3^L$ which is equal to $(\overline{v}_3^L)_{old}$ plus λ times some multiple of the leading order term in $\overline{v}_2^L$.

$$\overline{v}_3^L = (\ 0 \quad 1 \quad u\lambda \quad 1\ ) + \lambda m\ 0 \quad 0 \quad 1 \quad 0\ ) \tag{141}$$

The variable m will be chosen to minimize $\overline{v}_3^L u_4^R$, which controls the magnitude of the reflection coefficient, and at the same time will produce a well-posed boundary condition. The motivation for this approach is that the second approximation to the scalar wave equation is well-posed and produces fourth order reflections [4].

Substituting definitions gives

$$\overline{v}_3^L u_4^R = \frac{1}{2}\left(\frac{1-u}{1+u}\right)\left(-S + 1 + (1+u)(m+u)\lambda^2\right). \tag{142}$$

Now $S(\lambda) = 1 - \frac{1}{2}(1-u^2)\lambda^2 + O(\lambda^4)$, so the reflection coefficient is fourth order if m is chosen such that $m+u = -\frac{1}{2}(1-u)$. Thus the new form for $\overline{v}_3^L$ is

$$\overline{v}_3^L = (\ 0 \quad 1 \quad -\tfrac{1}{2}\lambda \quad 1\ ) \tag{143}$$

To prove the well-posedness of this new boundary condition we examine the new C matrix which is obtained.

$$C = \begin{pmatrix} 1 & 0 & 0 \\ 0 & 1+u^2\lambda^2 & 0 \\ 0 & -\frac{1}{2}(1+u)\lambda & \frac{1}{2}(S+1-\frac{1}{2}(1-u^2)\lambda^2) \end{pmatrix} \tag{144}$$

$\det(C) = 0$ implies that either

$$-S = 1 + \frac{1}{2}(1-u^2)\lambda^2, \tag{145}$$

or

$$\lambda^2 = -1/u^2. \tag{146}$$

Examining the first possibility, squaring both sides gives

$$1 - (1-u^2)\lambda^2 = 1 - (1-u^2)\lambda^2 + \tfrac{1}{4}(1-u^2)^2\lambda^4, \tag{147}$$

which implies that $\lambda = 0$. In this case $S = 1$ and so Eq. (145) becomes $-1 = 1$ which is inconsistent. Thus the first possibility does not lead to an ill-posed mode.

The second possibility corresponds to $\omega = iu|l|$. At this frequency the second and third eigenvectors become degenerate and so we must apply the extended theory again.

$$\det(C) = (1+iu\lambda)(1-iu\lambda)(S+1-\frac{1}{2}(1-u^2)\lambda^2) \tag{148}$$

$$\Longrightarrow \quad \frac{\partial}{\partial\omega}\det(C)\Big|_{\omega_{crit}} = \frac{(1+u)^2}{u^2\omega_{crit}} \neq 0 \tag{149}$$

Thus the problem is well-posed at the critical degenerate frequency, and this concludes the proof of well-posedness.

Transforming back into the original frame of reference in which $v \neq 0$, the modified inflow boundary conditions are

$$\begin{pmatrix} -1 & 0 & 0 & 1 \\ 0 & 0 & 1 & 0 \\ 0 & 1 & 0 & 1 \end{pmatrix} \frac{\partial U}{\partial t} + \begin{pmatrix} -v & 0 & 0 & v \\ 0 & u & v & 1 \\ 0 & v & \frac{1}{2}(1-u) & v \end{pmatrix} \frac{\partial U}{\partial y} = 0. \tag{150}$$

There is also a corresponding modified outflow boundary condition which is

$$\begin{pmatrix} 0 & -1 & 0 & 1 \end{pmatrix} \frac{\partial U}{\partial t} + \begin{pmatrix} 0 & -v & \frac{1}{2}(1+u) & v \end{pmatrix} \frac{\partial U}{\partial y} = 0. \tag{151}$$

It is easily proved that this boundary condition gives a well-posed problem. The properties of this condition, and why one might wish to use it instead of the second order approximation, are discussed in the next section.

Finally, it is helpful to express these boundary conditions in their one-dimensional characteristic form.

$$\frac{\partial}{\partial t}\begin{pmatrix} c_1 \\ c_2 \\ c_3 \end{pmatrix} + \begin{pmatrix} v & 0 & 0 & 0 \\ 0 & v & \frac{1}{2}(1+u) & \frac{1}{2}(1-u) \\ 0 & \frac{1}{2}(1-u) & v & 0 \end{pmatrix} \frac{\partial}{\partial y}\begin{pmatrix} c_1 \\ c_2 \\ c_3 \\ c_4 \end{pmatrix} = 0 \tag{152}$$

$$\frac{\partial c_4}{\partial t} + \begin{pmatrix} 0 & \frac{1}{2}(1+u) & 0 & v \end{pmatrix} \frac{\partial}{\partial y}\begin{pmatrix} c_1 \\ c_2 \\ c_3 \\ c_4 \end{pmatrix} = 0. \tag{153}$$

3.6.4 Reflection coefficients

The reflection matrix for the modified inflow boundary conditions is

$$-C^{-1}D \tag{154}$$

$$= -\begin{pmatrix} 1 & 0 & 0 \\ 0 & 1+u^2\lambda^2 & 0 \\ 0 & -\frac{1}{2}(1+u)\lambda & \frac{1}{2}(S+1-\frac{1}{2}(1-u^2)\lambda^2) \end{pmatrix}^{-1} \begin{pmatrix} 0 \\ 0 \\ \frac{1}{2}\left(\frac{1-u}{1+u}\right)\left(-S+1-\frac{1}{2}(1-u^2)\lambda^2\right) \end{pmatrix}$$

$$= \begin{pmatrix} 0 \\ 0 \\ \left(\frac{1-u}{1+u}\right)\frac{S-1+\frac{1}{2}(1-u^2)\lambda^2}{S+1-\frac{1}{2}(1-u^2)\lambda^2} \end{pmatrix} \tag{155}$$

There are three things to note in the above result. Firstly, the outgoing pressure wave produces no reflected entropy or vorticity waves. Secondly, the reflected pressure wave has an amplitude which is $O(l/\omega)^4$. Lastly, at the cutoff frequency, at which $\lambda^2 = 1/(1-u^2)$ and the x-component of the group velocity is zero, the pressure wave reflection coefficient is $-\frac{1-u}{1+u}$.

The reflection coefficient matrix for the second order outflow boundary condition is

$$-C^{-1}D = -\frac{2}{(-S-1+u(1-u)\lambda^2)}\begin{pmatrix} 0 & 0 & \frac{1}{2}\left(\frac{1+u}{1-u}\right)(S-1+u(1-u)\lambda^2) \end{pmatrix}$$

$$= \begin{pmatrix} 0 & 0 & \left(\frac{1+u}{1-u}\right)\frac{S-1+u(1-u)\lambda^2}{S+1-u(1-u)\lambda^2} \end{pmatrix} \tag{156}$$

Again there are three things to note. The outgoing entropy and vorticity waves produce no reflections, the outgoing pressure wave produces a second order reflection, and at the cutoff frequency the reflection coefficient is $-\frac{1+u}{1-u}$. The product of the pressure wave reflection coefficients at the cutoff frequency is 1, which is to be expected because at the cutoff frequency both pressure waves have zero group velocity in the x-direction and so it is impossible to discriminate between them.

The reflection coefficient matrix for the modified outflow boundary condition is

$$-C^{-1}D = -\frac{2}{(-S-1+\frac{1}{2}(1-u^2)\lambda^2)}\begin{pmatrix} 0 & \frac{1}{2}(1-u)\lambda & \frac{1}{2}\left(\frac{1+u}{1-u}\right)(S-1+\frac{1}{2}(1-u^2)\lambda^2) \end{pmatrix}$$

$$= \begin{pmatrix} 0 & \frac{\frac{1}{2}(1-u)\lambda}{S+1-\frac{1}{2}(1-u^2)\lambda^2} & \left(\frac{1+u}{1-u}\right)\frac{S-1+\frac{1}{2}(1-u^2)\lambda^2}{S+1-\frac{1}{2}(1-u^2)\lambda^2} \end{pmatrix} \tag{157}$$

This differs from the second order outflow condition in that now the outgoing pressure wave produces a fourth order reflection, but the outgoing vorticity wave produces a first order reflection. Thus this boundary condition is preferable only in situations where it is known that there is no outgoing vorticity wave. As an example, in the far-field of an oscillating transonic airfoil there will be an outgoing vorticity wave only at the outflow boundary directly behind the airfoil because the only vorticity generation mechanisms are a shock and the unsteady Kutta condition. Thus one might use the second order boundary condition directly behind the airfoil, and the modified boundary condition on the remainder of the outflow far-field boundary.

3.7 Dimensional boundary conditions

For convenience, this section lists all of the boundary conditions in the original dimensional variables.

a) Transformation to, and from, one-dimensional characteristic variables.

$$\begin{pmatrix} c_1 \\ c_2 \\ c_3 \\ c_4 \end{pmatrix} = \begin{pmatrix} -c^2 & 0 & 0 & 1 \\ 0 & 0 & \rho c & 0 \\ 0 & \rho c & 0 & 1 \\ 0 & -\rho c & 0 & 1 \end{pmatrix} \begin{pmatrix} \delta\rho \\ \delta u \\ \delta v \\ \delta p \end{pmatrix} \tag{158}$$

$$\begin{pmatrix} \delta\rho \\ \delta u \\ \delta v \\ \delta p \end{pmatrix} = \begin{pmatrix} -\frac{1}{c^2} & 0 & \frac{1}{2\rho c} & \frac{1}{2} \\ 0 & 0 & \frac{1}{2\rho c} & -\frac{1}{2} \\ 0 & \frac{1}{\rho c} & 0 & 0 \\ 0 & 0 & \frac{1}{2\rho c} & \frac{1}{2} \end{pmatrix} \begin{pmatrix} c_1 \\ c_2 \\ c_3 \\ c_4 \end{pmatrix} \tag{159}$$

b) One-dimensional, unsteady b.c.'s.

Inflow:

$$\begin{pmatrix} c_1 \\ c_2 \\ c_3 \end{pmatrix} = 0 \tag{160}$$

Outflow:

$$c_4 = 0 \tag{161}$$

c) Exact, two-dimensional, single-frequency b.c.'s.

Inflow:

$$\frac{\partial}{\partial t}\begin{pmatrix} \hat{c}_1 \\ \hat{c}_2 \\ \hat{c}_3 \end{pmatrix} = \alpha \begin{pmatrix} -\hat{c}_1 \\ \frac{(c-u)\lambda}{(1+S)(c-v\lambda)}\hat{c}_4 - \hat{c}_2 \\ \frac{(c-u)^2\lambda^2}{(1+S)^2(c-v\lambda)^2}\hat{c}_4 - \hat{c}_3 \end{pmatrix} \tag{162}$$

Outflow:

$$\frac{\partial \hat{c}_4}{\partial t} = \alpha\left(\frac{2u\lambda}{(c-v\lambda)(1+S)}\hat{c}_2 + \left(\frac{1-S}{1+S}\right)\hat{c}_3 - \hat{c}_4\right) \tag{163}$$

where

$$\lambda = \frac{cl}{\omega}, \tag{164}$$

and

$$S = \sqrt{1 - \frac{(c^2-u^2)\lambda^2}{(c-v\lambda)^2}}. \tag{165}$$

d) Exact, two-dimensional, steady b.c.'s.

Inflow:

$$\frac{\partial}{\partial t}\begin{pmatrix}\hat{c}_1\\ \hat{c}_2\\ \hat{c}_3\end{pmatrix} = \alpha\begin{pmatrix} -\hat{c}_1 \\ -\left(\frac{c\beta+v}{c+u}\right)\hat{c}_4 - \hat{c}_2 \\ \left(\frac{c\beta+v}{c+u}\right)^2\hat{c}_4 - \hat{c}_3\end{pmatrix} \tag{166}$$

Outflow:

$$\frac{\partial \hat{c}_4}{\partial t} = \alpha\left(\left(\frac{2u}{c\beta-v}\right)\hat{c}_2 - \left(\frac{c\beta+v}{c\beta-v}\right)\hat{c}_3 - \hat{c}_4\right) \tag{167}$$

where

$$\beta = \begin{cases} i\,\mathrm{sign}(l)\sqrt{1-M^2}\,, & M<1 \\ -\mathrm{sign}(v)\sqrt{M^2-1}\,, & M>1 \end{cases} \tag{168}$$

e) Fourth order, two-dimensional, unsteady, inflow b.c.

$$\frac{\partial}{\partial t}\begin{pmatrix}c_1\\ c_2\\ c_3\end{pmatrix} + \begin{pmatrix} v & 0 & 0 & 0 \\ 0 & v & \frac{1}{2}(c+u) & \frac{1}{2}(c-u) \\ 0 & \frac{1}{2}(c-u) & v & 0\end{pmatrix}\frac{\partial}{\partial y}\begin{pmatrix}c_1\\ c_2\\ c_3\\ c_4\end{pmatrix} = 0 \tag{169}$$

f) Second order, two-dimensional, unsteady, outflow b.c.

$$\frac{\partial c_4}{\partial t} + \begin{pmatrix} 0 & u & 0 & v\end{pmatrix}\frac{\partial}{\partial y}\begin{pmatrix}c_1\\ c_2\\ c_3\\ c_4\end{pmatrix} = 0. \tag{170}$$

g) First/fourth order, two-dimensional, unsteady, outflow b.c.

$$\frac{\partial c_4}{\partial t} + \begin{pmatrix} 0 & \frac{1}{2}(c+u) & 0 & v\end{pmatrix}\frac{\partial}{\partial y}\begin{pmatrix}c_1\\ c_2\\ c_3\\ c_4\end{pmatrix} = 0. \tag{171}$$

AD-A192 073 FLUID DYNAMICS OF HIGH PERFORMANCE TURBOMACHINES(U) 2/2
MASSACHUSETTS INST OF TECH CAMBRIDGE DEPT OF
AERONAUTICS AND ASTRONAUTICS E M GREITZER ET AL.
UNCLASSIFIED DEC 87 AFOSR-TR-88-0183 F49620-85-C-0010 F/G 20/4 NL

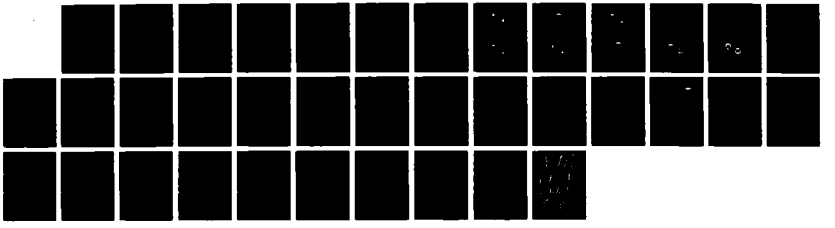

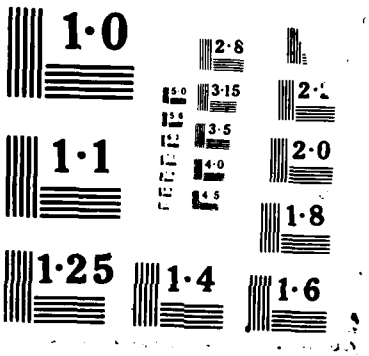
1·0
1·1
1·25
1·4
1·6
1·8
2·0
2·8
3·15
3·5
4·0

References

[1] Kreiss H.-O. Initial Boundary Value Problems for Hyperbolic Systems. *Communications on Pure and Applied Mathematics*, 23:277–298, 1970.

[2] R. L. Higdon. Initial-Boundary Value Problems for Linear Hyperbolic Systems. *SIAM Review*, 28:177–217, 1986.

[3] G. W. Hedstrom. Nonreflecting Boundary Conditions for Nonlinear Hyperbolic Systems. *Journal of Computational Physics*, 30:222–237, 1979.

[4] B. Engquist and A. Majda. Absorbing Boundary Conditions for the Numerical Simulation of Waves. *Mathematics of Computation*, 31:629–651, July 1977.

[5] D. Kwak. Nonreflecting Far-Field Boundary Conditions for Unsteady Transonic Flow Computation. *AIAA Journal*, 19:1401–1407, 1981.

[6] B. Gustafsson. *Far Field Boundary Conditions for Time-Dependent Hyperbolic Systems.* Center for Large Scale Scientific Computation CLaSSiC-87-16, Stanford University, Feb 1987.

[7] J. M. Verdon. *Linearized Unsteady Aerodynamic Theory.* Technical Report R85-151774-1, UTRC, Nov 1985.

[8] K. C. Hall and E. F. Crawley. *Calculation of Unsteady Flows in Turbomachinery Using the Linearized Euler Equations.* proceedings of Fourth Symposium on Unsteady Aerodynamics and Aeroelasticity of Turbomachines and Propellers, Sept 1987.

[9] M. B. Giles, M. Drela, and W. T. Thompkins. *Newton Solution of Direct and Inverse Transonic Euler Equations.* AIAA Paper 85-1530, July 1985.

[10] L. Ferm. *Open Boundary Conditions for Exterval Flow Problmes.* Dept. of Computing Science Report 108, Uppsala University, Feb 1987.

[11] M. B. Giles. *UNSFLO: A Numerical Method for Calculating Unsteady Stator/Rotor Interaction.* Technical Report TR-86-6, MIT Computational Fluid Dynamics Laboratory, 1986.

[12] G. B. Whitham. *Linear and Nonlinear Waves.* John Wiley & Sons, 1974.

[13] J. Mathews and R. L. Walker. *Mathematical Methods of Physics.* W. A. Benjamin, Inc., 1970.

[14] L. N. Trefethen and L. Halpern. Well-Posedness of One-Way Wave Equations and Absorbing Boundary Conditions. *Mathematics of Computation*, 47:421–435, 1986.

[15] K. C. Hall. *A Linearized Euler Analysis of Unsteady Flows in Turbomachinery.* PhD thesis, M.I.T., Sept 1987.

[16] R.-H. Ni and F. Sisto. *Numerical Computation of Nonstationary Aerodynamics of Flat Plate Cascades in Compressible Flow.* ASME Paper 75-GT-5, 1975.

TASK IV: THEORETICAL MODELLING OF STABILITY AND UNSTEADINESS IN TRANSONIC COMPRESSOR FLOW FIELDS
(Investigators: J.E. McCune, E. Imperatori)

Summary

In the past several months, we have focussed a renewed effort on understanding the flow structure in well-developed vortex streets, inlcuding substantial vortex cores similar to those believed to be occurring behind turbomachine blade rows. In earlier reports [1], [2], approximate analyses of the development of total temperature separation due to the inherent unsteadiness caused by such structured blade wakes were described. More recently, Kurosaka et al. [3] have reported more extensive analysis and calculations, based on work initiated under the present Grant, which elucidate these ideas with more precision. These calculations and the experimental evidence indicate the presence of relatively large vortex cores in the "street" whose size is a substantial fraction of the inter-vortex spacing. Some important features of this intra-wake structure are reported here.

I. Vortex Streets With Finite Cores

In order to emphasize understanding of the intra-wake vortex structure, we consider in Ref. [4] a classical vortex street of infinite extent in the through-flow direction. In ignoring the "development" phase of the actual vortex street, we lose primarily information relating the street parameters to the blade row behavior, which we have previously treated. Thus, we focus on the intra-wake structure itself. In particular, for close vortex spacing, we are able to assess the usefulness of the "radial-equilibrium" approximations previously used to determine presssure and static enthalpy variations centered on the cores. With these results, improved analysis and understanding of "total temperature" trends can be achieved.

In the work of Ref. [4], finite core size is postulated on the basis of

typical observed blade-wake thickness - a fraction of blade spacing. The intra-wake flow is treated as "mainly inviscid"; the inner core flow occurs almost without local shear stress (as with "solid-body" motion, for example) and the outer flow is potential and classical [5]. Between the outer flow and each "inner-flow" core, there is a viscous region or sheath, accounting for total pressure loss and the eventual sizing of the cores. The flow within the cores is determined by methods analogous to those of Batchelor [6], [7]. Details of this model are reported in Ref. [4] and also in the thesis of Weissbein [8].

II. Typical Results: Total Temperature Variations in a Vortex Street With Finite Cores

Some of the results of our calculations are illustrated in Figs. 4.1 to 4.10, extracted from Ref. [4].

In Fig. 4.1, the total temperature distribution in the wake (as defined in the laboratory - or observer-frame of reference) is illustrated in terms of total-temperature contours in a street of point vortices, ignoring the presence of the inner cores.

In Fig. 4.2, by contrast, similar contours are shown with the cores present, and the more realistic ultimate depth of the total temperature change, which occurs within the core, is shown. A magnified view of the contours within the core, for this case, is given in Fig. 4.3.

Variations of these effects with vortex intensity, as measured by $\Gamma/U_v a \equiv \Gamma'$, are illustrated in Figs. 4.4, 4.5 and 4.6. (Here, Γ is the vortex-centered circulation, while "U_v" is the street speed relative to the lab frame and "a" is the longitudinal inter-core spacing, see Fig. 4.7.) It will be seen that in each case the cores significantly limit the magnitude of total temperature separation.

Inspection of these results, together with more examples in Ref. [4], also reveals the existence of a maximum temperature-separation depth as a function of parameter $\Gamma/U_\infty a$. This can be readily explained as follows. We recall that, in a frame of reference moving with the vortex street (i.e., not the lab frame), the total temperature is constant in this model. In the lab frame, therefore, the total temperature varies in the wake in a manner determined by the symmetry properties of the street. Thus

$$\Delta H_{lab} \doteq U_v \Gamma / a$$

On the other hand, U_v also decreases with Γ, in the manner

$$U_v = U_\infty - c\Gamma/a$$

where c is a constant of order unity and U_∞ is the "throughflow" speed of the overall fluid. Thus

$$\frac{\Delta H_{lab}}{U_\infty^2} \doteq \frac{\Gamma}{U_\infty a}\left(1 - \frac{c\Gamma}{U_\infty a}\right)$$

implying the maximum observed.

III. Pressure Distribution in the Vortex Street

A very useful feature of the results obtained in this model is our ability to study specifically the static pressure variations in the street. Typical pressure contours are illustrated in Figs. 4.8 through 4.10, enabling us to assess the validity and usefulness of the vortex-centered "radial-equilibrium" approximation used in earlier analyses. In each case, the radial equilibrium model works very well near the vortex centers and, as expected, begins to fail in the intermediate regions between the cores.

IV. Next Steps

The vortex street model has enabled us to look in more detail at the intra-wake flow structure of a multiple-vortex pattern, and verify that earlier

approximate calculation techniques, including orbit calculations, are useful. To provide more realistic extensions, we now plan to limit the spatial extent of the wake model, including at its beginning the initial development phases associated with multiple vortex shedding at the blades.

References

1. E.M. Greitzer, A.H. Epstein, M.B. Giles, J.E. McCune, C.S. Tan, Annual Technical Report on Contract F49620-85-C-0018, "Fluid Dynamics of High Performance Turbomachines," November 1985.

2. E.M. Greitzer, A.H. Epstein, M.B. Giles, J.E. McCune, C.S. Tan, Annual Technical Report on Contract F49620-85-C-0018, "Fluid Dynamics of High Performance Turbomachines," November 1986.

3. Kurosaka, M. et al., "Energy Separation in a Vortex Street," J. Fluid Mech., Vol. 178, 1987, pp. 1-29.

4. Imperatori, E., "Total Temperature Separation in a Karman Vortex Street with Finite Vortex Cores," MIT S.M. Thesis, December 1987.

5. Milne-Thomson, L.M., Theoretical Hydrodynamics, 3rd edition, section 13.72, The Macmillan Company, 1955.

6. Batchelor, G.K., "On Steady Laminar Flow with Closed Streamlines at Large Reynolds Number," J. Fluid Mech., Vol. 1, 1956, pp. 177-190.

7. Batchelor, G.K., "A Proposal Concerning Laminar Wakes Behind Bluff Bodies at Large Reynolds Number," J. Fluid Mech., Vol. 1, 1956, pp. 388-398.

8. Weissbein, D., "Embedded Vortical Regions in Otherwise Irrotational Flow," MIT S.M. Thesis, June 1987.

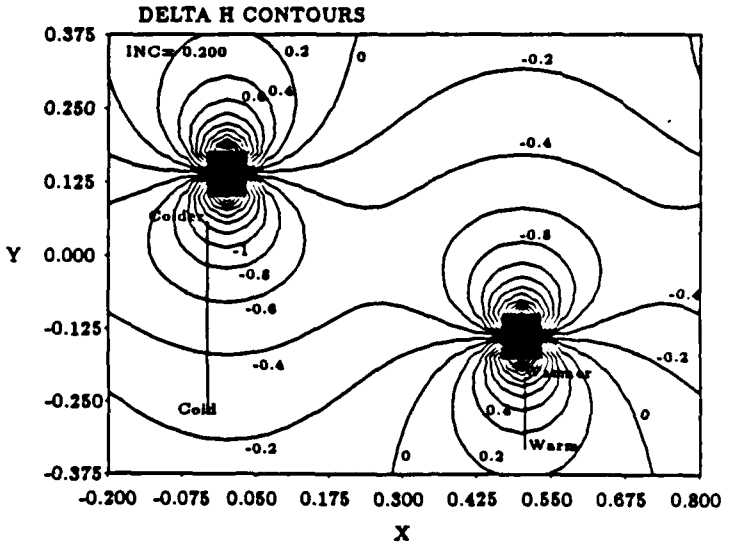

Fig. 4.1: Energy separation contours for a classical von Karman point vortex street: $\Gamma'_{pv} = 1$ and $U'_{\infty} = 1$

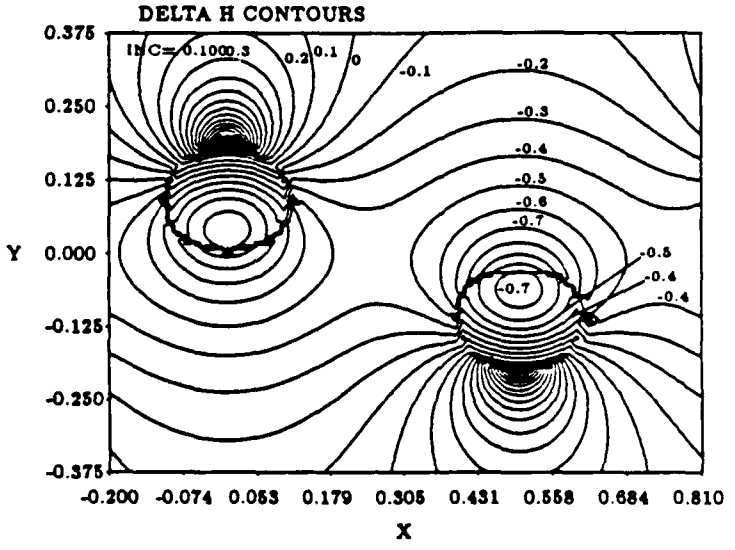

Fig. 4.2: Energy separation in a Karman finite vortex street with $\Gamma'_{FV} = 1$ and $U'_{\infty} = 1$

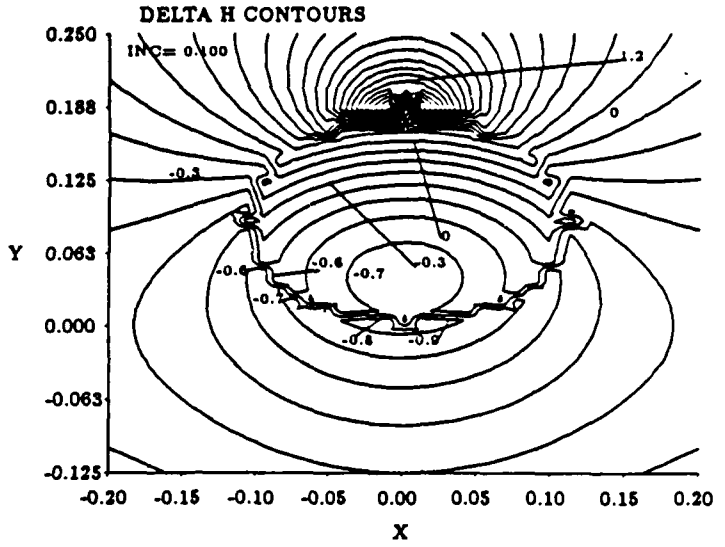

Fig. 4.3: Blown-up version of Fig. 4.2 for the vortex core rotating clockwise

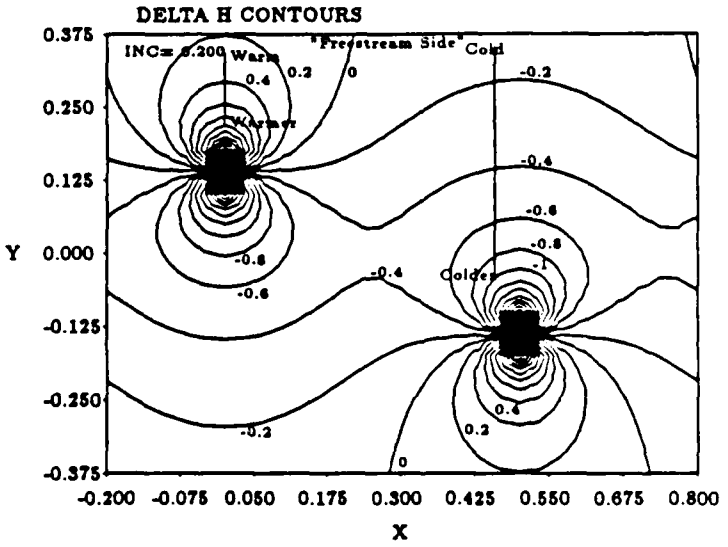

Fig. 4.4: Energy separation contours for a classical von Karman point vortex street: $\Gamma'_{pv} = 2$, $U'_\infty = 1$, and $t = \tau_k$

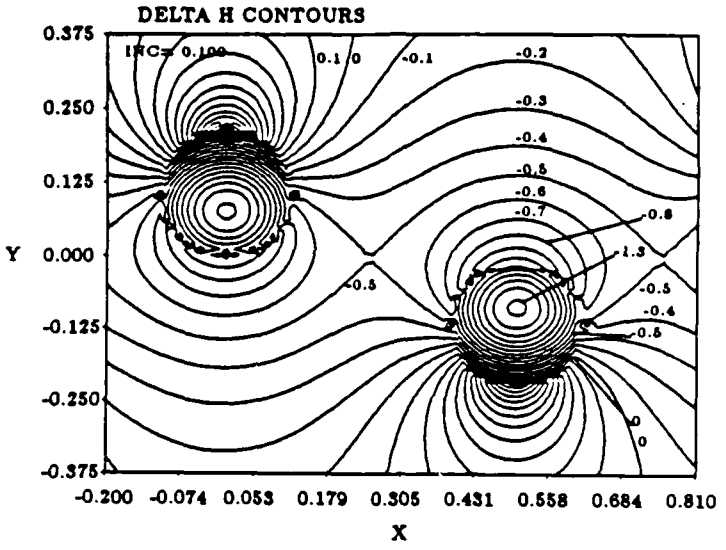

Fig. 4.5: Energy separation in a Karman finite vortex street with $\Gamma'_{FV} = \sqrt{2}$ and $U'_\infty = 1$

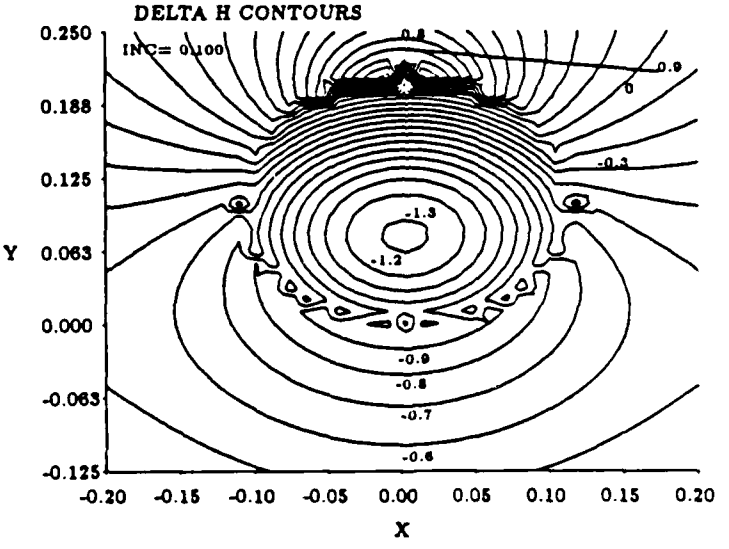

Fig. 4.6: Blown-up version of Fig. 4.5 for the vortex core rotating clockwise

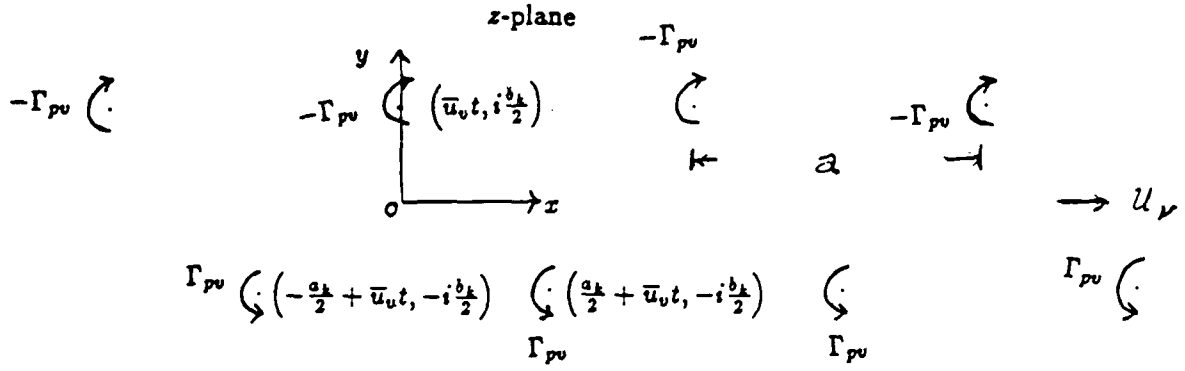

Fig. 4.7: Point vortex model of the classical von Karman street at time t = 0

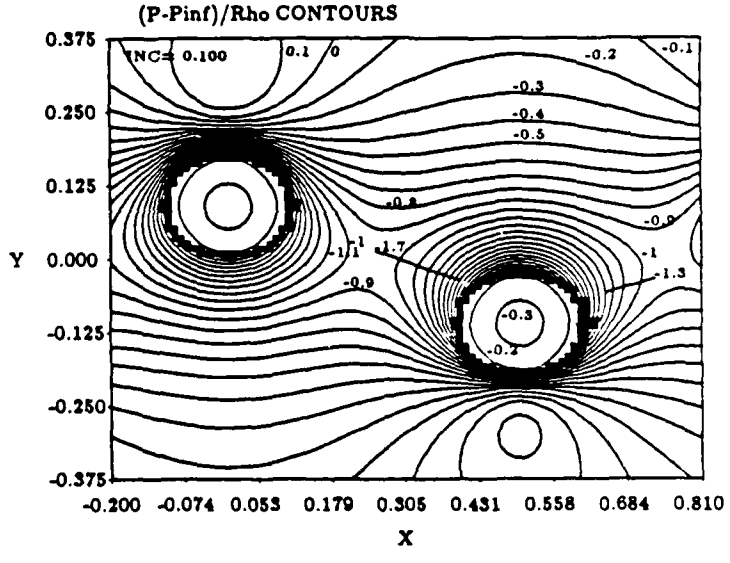

Fig. 4.8: Static pressure change in a Karman finite vortex street with $\Gamma'_{FV} = 1$ and $U'_\infty = 1$

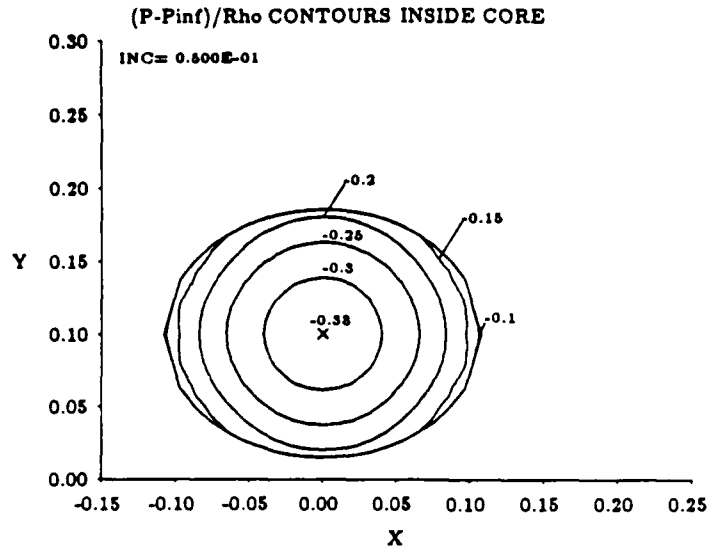

Fig. 4.9: Detail of the static pressure change in the vortex core rotating clockwise (for Fig. 4.8)

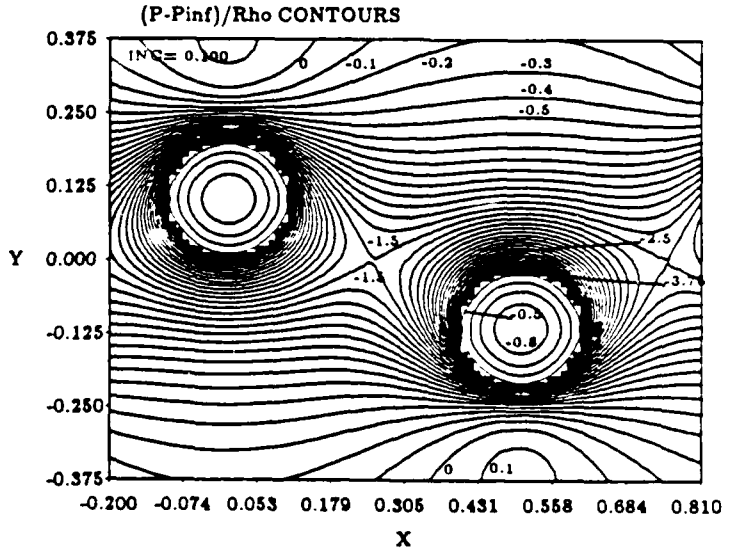

Fig. 4.10: Static pressure change in a Karman finite vortex street with $\Gamma'_{FV} = \sqrt{2}$ and $U'_\infty = 1$

3. OTHER ACTIVITIES ASSOCIATED WITH THIS PROGRAM

Air Force Research in Aero Propulsion Technology (AFRAPT) Program

The research at MIT is strongly tied in with the AFRAPT Program. At present, there are eleven students working in the Gas Turbine Laboratory under this training program. The students, advisors, and research projects are:

Trainee: Steven Allmaras
Advisor: Prof. M.B. Giles
Project: Computation Techniques for Turbomachines (Unsteady Flows in Turbomachinery) (AFOSR)

Trainee: Louis Cattafesta
Advisor: Prof. A.H. Epstein
Project: Fluid Physics of High Pressure Ratio Turbines (RRI)

Trainee: Victor Filipenco (new)
Advisor: Prof. E.M. Greitzer
Project: Unsteady Flows in Diffusers for High Performance Centrifugal Compressors (GE)

Trainee: Daniel Gysling (new)
Advisor: Prof. J. Dugundji
Project: Active Control of Aeromechanical Systems (AFOSR)

Trainee: Douglas Loose (new)
Advisor: Prof. Martinez-Sanchez
Project: Tip Clearance Excited Rotordynamic Instabilities (NASA LeRC)

Trainee: Knox Millsaps
Advisor: Prof. M. Martinez-Sanchez
Project: Rotor Dynamic Instability Due to Alford Forces (NASA MSFC)

Trainee: Judith Pinsley
Advisor: Prof. E.M. Greitzer
Project: Smart Engines - Active Stabilization of Aeromechanical Systems (ARO)

Trainee: Robert Plumley (new)
Advisor: Prof. E.M. Greitzer/Dr. C.S. Tan
Project: Unsteady Phenomena and Flow Instabilities in Multistage Turbomachines (AFOSR)

Trainee: Earl Renaud
Advisor: Dr. C.S. Tan
Project: Three-Dimensional Vortical Flows in Axial Turbines (NASA LeRC)

Trainee: William Steptoe (new)
Advisor: Prof. A.H. Epstein
Project: Influence of Radial Temperature Distribution Factor on Turbine Heat Transfer Aerodynamics (RRI)

In support of this program, considerable time was spent during the Spring of 1987 in selecting the new candidates for Fall 1987, and in reviewing the progress of the existing AFRAPT students. In addition, a visit was made to AFOSR in May by Professor Greitzer for a discussion of the program with AFOSR and with the other University/Industry representatives.

Tour of Turbomachinery Research Centers in Japan

As part of the effort under this Contract, Professor Greitzer visited several centers of turbomachinery research in Japan. Support for travel and lodging was provided by a Fellowship from the Japan Society for the Promotion of Science (JSPS). The host for the visit, and the nominator for the Fellowship, was Professor H. Takata of the Department of Aeronautics, University of Tokyo. Profesor Takata has carried out several very well-planned research projects on the topics of stability enhancement using casing treatment and compressor rotating stall, so there was a great deal of mutual interest.

In addition to spending time at the University of Tokyo, Professor Greitzer visited other university, government, and industry laboratories where fluid machinery research was taking place. A copy of a summary report written for the JSPS is enclosed which includes an itinerary. Three days were spent at the International Gas Turbine Congress, where an invited Special Lecture was presented entitled "Unsteady Flows in Turbomachines: Recent Advances and Opportunities for Control". A copy of this paper is also included.

The lecture summarized the progress that had been made over approximately the past decade, both experimentally and computationally, on the understanding of unsteady flow phenomena. The general theme was that there are many situations in which, although one thinks of the flow as steady-state, the behavior is in fact determined critically by unsteady effects. Examples of this were given. It was also pointed out that opportunities for flow control, leading to enhanced performance, often also require a knowledge of the unsteady fluid dynamical processes that occur in turbomachinery. To implement flow control, therefore, it is crucial to have a firm understanding of the unsteady fluid dynamics.

It is planned to give a report of this trip as a presentation at a society meeting or in one of the professional society magazines.

RESEARCH REPORT

Edward M. Greitzer
Professor, Aeronautics & Astronautics,
and Director, Gas Turbine Laboratory
Massachusetts Institute of Technology
Cambridge, Massachusetts, USA

Introduction and Overall Itinerary

This document comprises a report on my activities in Japan under a JSPS Fellowship during the period October 11, 1987 (arrival) to October 31, 1987 (departure). My host for the visit was Professor H. Takata, of the Department of Aeronautics, Tokyo University. The university, government and industrial laboratories visited during this period were as follows:

Week 1

October 12 - University of Tokyo, Department of Aeronautics
October 13 - University of Tokyo, Department of Aeronautics
October 14 - National Aerospace Laboratory
October 15 - University of Tokyo, Department of Aeronautics and Center for Interdisciplinary Research
October 16 - Aeroengine and Space Division, Ishikawajimi-Harima-Heavy Industries (IHI)

Week 2

October 21 - Osaka University, Department of Mechanical Engineering
October 22 - Takasago Research and Development Center, Mitsubishi Heavy Industries
October 23 - Kyushu University, Fukuoka, Institute for Advanced Material Study and Departments of Mechanical and Aeronautical Engineering

Week 3

October 26 - International Gas Turbine Congress (Tokyo)
October 27 - International Gas Turbine Congress (Tokyo)
October 28 - International Gas Turbine Congress (Tokyo)
October 29 - Mechanical Engineering Research Laboratory, Hitachi Company
October 30 - University of Tokyo, Department of Aeronautics

Given below is a summary of the technical interactions and activities during my visit. Due to lack of space, not all the individuals I met with can be mentioned. I have therefore limited the report to activities connected with those projects in which there was significant overlap between the work going on in Japan and that going on at MIT, so that the discussions were ones in which both parties had a strong mutual interest and there was good potential for further communication.

At all of the places that I visited, I gave a lecture which was an overview of all the work going on at the Gas Turbine Laboratory at MIT. At Osaka and Kyushu, I also presented some of the computations that we have made of post-stall compression system transients.

Description of Academic Activities

My host for this visit, and my principal contact, was Professor H. Takata of the Department of Aeronautics, Tokyo University. Professor Takata has been involved for a number of years on problems of unsteady flows in turbomachines. Two of his particular research projects have dealt with non-linear analyses of rotating stall in axial compressors, and with the mechanism of stability enhancement by compressor "casing treatment". I mention these because these are also two areas in which I have been actively investigating at the Gas Turbine Laboratory at MIT. There was thus considerable scope for interaction between Professor Takata and his students and myself. As described below, this was indeed what occurred.

During the first week, I spent three days at the University of Tokyo. The majority of this time was at the Department of Aeronautics, where there is research on the topic of unsteady flow in turbomachines, under the direction of Professors Takata and Kaji. In addition, I also visited the Institute of Interdisciplinary Reearch, where work on unsteady flow is also being conducted under the supervision of Professors Tanida, Hanamura, and Nagashima.

The exchange of technical information can perhaps be characterized on two levels. At the most basic, I spent from an hour to a whole morning or afternoon with various faculty who described their research. In addition, I presented an overview of the range of turbomachinery and propulsion activities that are being carried out at MIT. At a more detailed level, however, I spent some further time with Professor Takata and several of his graduate students for in-depth discussion of the casing treatment research and the computations of unsteady vortex flows. This also gave me the opportunity to show our latest results on compressor casing treatment as well.

I found the research being conducted of great interest. For the casing treatment work, the relative frame measurements that Takata's student is making appear to point to the tip leakage flow as the critical feature of the process that eventually results in rotating stall. We had formed the same conclusion, using a quite different experimental configuration. Takata and I also had a discussion as to what the next steps would be in trying to understand this complex flow, and I told him of our plans to see what can be learned from three-dimensional Navier-Stokes computations, which we are carrying out in conjunction with one of the American aircraft engine manufacturers.

During the first week that I was there, the student was just completing a series of measurements. When I returned at the end of the third week, he had finished these, and we had further discussions of his results and their interpretation. It is my hope that these initial contacts will lead to a continued technical dialogue between the University of Tokyo and MIT.

The work of Professors Tanida and Nagashima on unsteady separation was also related to work being carried out at MIT (by Professors Giles and Epstein). I was thus also quite interested in their results, which seemed complementary to the MIT work.

During this week, I visited IHI Aero-Engine and Space Operations Division

in Mizuho. My hosts were Mr. S. Nagano, Manager, Aerodynamics and Noise Group, whom I had met before on several occasions, and Mr. Aono, General Manager of the Research and Development Department. Technical discussions were carried on with the compressor and noise groups. A visit was also made to the National Aerospace Laboratory, with Dr. H. Kobayashi acting as my host.

During the second week, I visited two other universities, Osaka and Kyushu. My host at Osaka was Professor Miyake, who has an axial compressor experiment examining tip clearance flows and their effect on stall. He is also interested in design procedures for three-dimensional flows, and has examined the utility of a method developed jointly at MIT and Cambridge University. Another active researcher is Professor Tsujimoto, who is interested in fluid structure interaction in turbomachines. One of the topics he is looking at is the coupling between the structural dynamics and the onset of rotating stall, which is also close to the work going on at MIT.

I also visited Kyushu University. Professor Hayami, who is at the Institute for Advanced Material Study, has research programs on effects of tip clearance on centrifugal machines and on the use of low solidity vanes to enhance the performance of diffusers for centrifugal compressors. We are currently in the first stages of an investigation of the performance of diffusers in advanced centrifugal compressors, and this was an area of mutual interest.

Another area of mutual interest was that of endwall and tip clearance flows, which is being investigated by Professor Inoue in the Mechanical Engineering Department. He has obtained detailed measurements of the flow in the region between the blade end and the endwall. As mentioned above, I view this region as critical in setting the stall inception point. There is additional research in turbomachines being carried out by Professor Namba, in the Aeronautical Engineering Department, who is conducting work on predictions of flutter in turbomachine blading.

Visits were also made to two other laboratories which are involved in turbomachinery and gas turbine research, Takasago Research and Development Center of Mitsubishi and the Mechanical Engineering Research Laboratory of Hitachi. At the former, my hosts were Mr. Sato, the manager of the turbomachinery laboratory, and Mr. Kuramoto, the deputy general manager. Mr. Sato's group is engaged in work covering a large range of turbomachine types. They have very well equipped facilities, and are actively attacking a number of problems, ranging from application of casing treatment to industrial type blowers, to compressor endwall boundary layers, to application of three-dimensional computational methods to axial turbine design.

At the latter, my host was Dr. Kashiwabara. Some of the problems that were being examined at the Hitachi laboratory concerned compressor behavior in rotating stall. Mr. Ishii, in fact, is using a model for this phenomenon that is based on work that I did (with Professor F.K. Moore of Cornell) several years ago.

In addition to the technical interactions listed above, I also attended the International Gas Turbine Congress in Tokyo, where I presented a special lecture (arranged by Professor Takata) on "Unsteady Flows in Turbomachines:

together most of the principal Japanese researchers in the field and there was further opportunity for interchange of ideas.

Impressions About the State of Science in Japan in This Field

My impression is that a substantial amount of good work is being carried out, not only by the specific individuals named, but by others at these laboratories. I know first-hand, from serving on various American Society of Mechanical Engineers Honors and Awards Committees, that some of the Japanese papers are regarded quite highly indeed.

One aspect does seem very different from the situation in the United States and that was the level of involvement of the academic institutions with industry. In the U.S., it is not unusual for industry to financially support research at a university. At the Gas Turbine Laboratory, we encourage this and work at involving the industrial participants strongly in the research. This seems to be the exception in Japan, but it is my sense that this is a situation that may be starting to change. In any event, we (at MIT) find it very stimulating (from both a research and an educational point of view) to work jointly with industry.

Comments on the Fellowship Program

I am very pleased to have had the chance to interact and exchange ideas with researchers in Japan. The arrangements made by Professor Takata for doing this were excellent. I think that an extremely important effect of the JSPS Fellowship was the opportunity for contact with people in the same field on a more extended, and hence deeper, basis than would be possible at a technical conference. There were, for example, other participants at the Gas Turbine Congress from Western Europe or North America, and they were constrained much more in their opportunities to interact with Japanese scientists and engineers because of the limited duration of their stay. One of my purposes in making this trip was to explore possibilities for more contact between the research at MIT and that in Japan, by further mutual visits and by exchange of students. Programs such as this seem to be a very useful first step in starting such a process and I thank the JSPS for the chance to do this.

87 – TOKYO – IGTC – S2

Unsteady Flow in Turbomachines: Recent Advances and Opportunities for Control

E.M. Greitzer[1]

ABSTRACT

This review discusses some of the unsteady flow phenomena inherent in modern, high performance turbomachinery. The basic theme is that increases in this performance can be achieved through increased understanding and incorporation of unsteady flow effects into turbomachinery design. Within this theme, three main aspects are addressed: 1) the impact that unsteady phenomena can have on so-called steady state performance, 2) the considerable recent progress in one's ability to measure and to compute these flows, and 3) the new possibilities for using different types of non-uniformities (spatial as well as temporal) to control the flows of interest and thus to enhance the performance of advanced turbomachines.

INTRODUCTION

As recounted in many textbooks, turbomachines depend on unsteady fluid mechanic processes for operation, and turbomachinery flows are inherently unsteady. In spite of this, for the majority of current design procedures, unsteadiness tends either to be avoided, by adopting coordinate systems moving with the local blade row of interest, or neglected by assuming that the effects of upstream rows are "mixed out" and potential field effects are negligible for downstream rows. In situations where it is recognized that unsteadiness can impact performance, non-steady effects are often accounted for using correlative procedures, rather than by any truly unsteady calculation.

Work on unsteady fluid flow in turbomachines has thus been concentrated on areas where one cannot, even on the most basic level, avoid dealing with non-steady phenomena, for example aeroelasticity, flow instability, and noise. Even for these problems, however, much of the approach for "prediction" in the design process has been basically empirical. While the correlations thus developed provide very useful guidelines over certain regimes, they are often not well-based on a solid understanding of the fluid physics and hence not capable of extrapolation or extension.

There now appears to be growing recognition that to improve the performance of turbomachines further one will have to understand better the unsteady flow effects. In this paper, I will discuss some of the progress that has been made in the field over the past decade or so and some of the phenomena that subsequently affect turbomachinery operation. I will also attempt to highlight what I view as fruitful new research areas. The common thread throughout is the concept that increased performance can be obtained through a deeper understanding of unsteady effects. In view of the length restrictions, the paper is not an all-inclusive survey, but rather a more personal perspective on the topic, with examples chosen to illustrate the above concept in several different situations.

GENERAL BACKGROUND

During the mid 1970's, there were several good reviews of the state-of-the-art, e.g. [1], [2], and it is interesting to compare problems as well as approaches between then and now. There are clear differences in the "tool-kit" that is used to attack unsteady flow problems in turbomachines. First, the situation with respect to computations of unsteady flow has changed considerably. A decade ago, most unsteady computations were for inviscid flow past lightly loaded blades, with just the beginnings of procedures being developed to include loading. There now exist methods to compute (albeit with some questions concerning turbulence modelling) unsteady viscous flow past two- and even three-dimensional blade rows.

The difference in computational power is not just quantitative, e.g., a slightly better computation of pressure distribution. Rather, it means that one now has the ability to carry out "numerical experiments" in which the computation is used to interrogate the physical phenomena. This technique has been used for some time in other areas of fluid mechanics (two-dimensional vortex dynamics is one application) where the configurations are simpler, but the ability to do this in a turbomachine geometry is quite new. We will see below several examples where numerical computations have provided at least tentative conclusions about otherwise unexplained physical phenomena.

The situation is also different experimentally, where one now has the ability to store and reduce a large amount of unsteady flow data, as well as to conditionally sample an unsteady flow field so that data taking is keyed to times when interesting events occur. This has made it possible to examine items as diverse as the structure of rotating stall cells [3], [4], wake transport through blade passages [5], and unsteady transition in turbomachine boundary layers [6], [7].

A new area of considerable interest is that of flow control, applied to different types of unsteady fluid dynamic phenomena. Examples include active control of noise (anti-noise) [8] and turbomachinery

1 Gas Turbine Laboratory, MIT
Cambridge, Massachusetts, USA

Contributed by Gas Turbine Society of Japan for presentation at 1987 Tokyo International Gas Turbine Congress held in Tokyo, Japan on October 26th to 31st, 1987. Manuscript received at the Organizing Committee on Aug. 10th, 1987

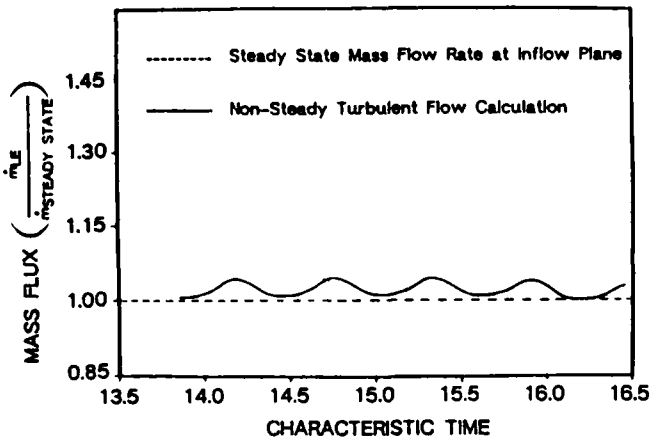

Fig. 1 Mass flow comparison at cascade leading edge plane [11]

and afterburner instabilities [9]. This interdisciplinary topic which includes control, unsteady fluid mechanics, and structures will also be discussed, as will the new area of mixing control and enhancement using axial vortex arrays [10].

In summary, from both experimental and theoretical/computational viewpoints, the situation appears qualitatively different than at the point of the reviews [1], [2]. We now examine some of the individual phenomena to see specifically where these differences lie.

UNSTEADY EFFECTS ON UNIFORM INLET FLOW PERFORMANCE

Even with nominally "uniform" inlet flow into a multi-row machine at the design point, it is apparent that there are sources of unsteadiness both upstream and downstream of a given row. There are also unsteady effects that are self-excited, such as vortex shedding and motion of the separation location; these can occur even in an isolated rotor.

For many of these effects, the reduced frequencies (defined essentially as (flow-through time / flow change time)) are of order unity or larger, and unsteadiness is important [1]. Significant pressure fluctuations can exist on blades and vanes, and the relative stagnation temperature of a fluid particle can be altered as the particle convects through the row. In modern compressors also, aspect ratios are tending to decrease so that both wake and potential flow effects (the latter of which scale as the blade pitch) have become more important.

One example of the impact of unsteadiness has been described in connection with the performance of transonic stages (stages where the rotor Mach number is greater than one over a significant portion of the span) in multistage compressors [11]. Instances are cited in which the flow into a stage was found to be too high by several percent. This is serious because the steepness of the speedlines in these types of stages means that overflowing leads to performance with low efficiency.

It was hypothesized that the higher flow capacity was linked to the circumferential non-uniformities at rotor inlet, seen by the rotor as an unsteady flow. A supporting circumstance was that the compressor had a low aspect ratio, which implied that the non-dimensional spacing between the blade rows was also low, so wakes have much less opportunity to mix out. (As pointed out in [11], for a given level of diffusion, compressor wake thickness scales as blade chord.)

To investigate this, two-dimensional, unsteady, viscous flow computations were carried out [12], using measured stator exit profiles as upstream conditions. The results of the computations (which one can regard as a numerical experiment in the spirit described above) are shown in Fig. 1, where flow capacity of a supersonic cascade is seen to be increased over the situation for uniform inlet flow with equivalent mass averaged conditions.

The significance of this result is discussed in [11] very well where the main theme of this paper is also expressed. Adverse consequences - here a mismatch of the stage - can result due to unsteadiness. Present design methods do not account for this, and the parametric dependence of the effect for new configurations is unknown.

Wake Effects on Boundary Layer Transition, Loss, and Heat Transfer

When wakes pass through a following blade row one can show from velocity triangles that they will have a cross-passage "slip" velocity relative to the mean flow. Wakes will thus impinge on the pressure side of a compressor blade passage and the suction side of a turbine blade. One effect of this wake transport is redistribution of stagnation enthalpy [1]. Another appears to be a strong influence on laminar-turbulent transition. It is argued in [6] and [7] that transition is due to the periodic variations in turbulence, from wake passing, which are impressed on the boundary layers. A very schematic representation of the process is given in Fig. 2, which shows sketches of laminar and turbulent velocity profiles, along with hot wire traces.

The unsteady transition process (for a turbine) has an effect on boundary layers and hence overall loss (as well as heat transfer). Comparison of losses for the same blade section tested in a linear cascade and in a turbine rotor showed the loss to be approximately fifty percent higher in the latter. Boundary layer measurement results are presented in Fig. 3, which shows the time averaged shape factor, H, on the suction surface, for the turbine rotor and the linear cascade [6]. Results from a turbulent boundary layer calculation are also plotted. Over much of the blade surface, the time averaged shape factor has a value

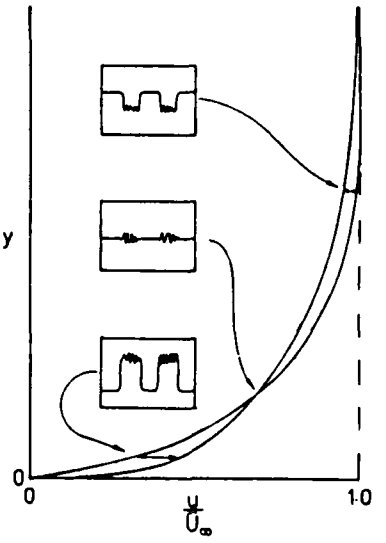

Fig. 2 Schematic representation of unsteady transition [6]

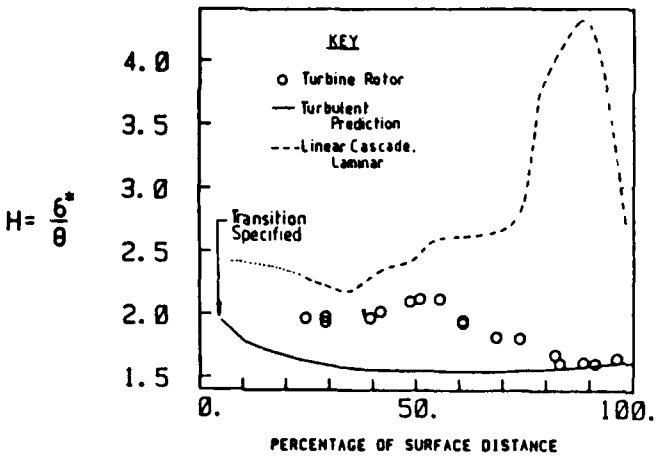

Fig. 3 Turbine blade suction surface boundary layer [6]

which is midway between the laminar and fully turbulent boundary layers.

At higher Mach numbers, unsteady shock impingement on the blades can also affect transition, not directly by shock wave-boundary layer interaction but by initiating a local separation which causes a turbulent "patch" that convects downstream [7]. An illustration of this is given in Fig. 4, which shows data from heat transfer gauges at different locations along an instrumented turbine blade. The wake and shock are from bars which are moved in front of the turbine cascade. Location x/s = 0 corresponds to the mean stagnation point.

The convection velocity of the turbulent patches due to wake and to the shock motion are found to be similar to those of turbulent spots. The former, however, are basically two-dimensional, while the latter occur irregularly across the span of the blades so the structures are not precisely alike.

This periodic transition process, which seems to be much more important for turbomachines than so-called natural transition, is also being examined for compressor blades in a specially designed large low-speed cascade with a grid of moving rods upstream of it [13]. Note that what is of interest is not only the overall results, e.g. losses, but perhaps even more importantly, the detailed information that can be obtained about the unsteady fluid mechanic processes on a more fundamental level. As remarked above, it is the latter that is needed to advance from correlations to real predictions.

PERFORMANCE IN DISTORTED INLET FLOW

One area in which unsteady effects have had to be addressed is engine response to inlet circumferential distortion. Although initial attempts to utilize quasi-steady ideas (in the basic parallel compressor theory) were very useful in developing an understanding of asymmetric flow, they did not capture the small effects on stall of distortions of narrow extent or of several sectors.

It was generally agreed that discrepancies between the quasi-steady parallel compressor model and this type of data are due to "unsteady response" although precisely what this meant was not clear. The need to include some description of the unsteady response spurred a considerable amount of work and a review of the present state of the art is given in [14].

To see another example of the effect of unsteadiness, we examine a compressor subjected to a rotating inlet distortion, such as might be caused by rotating stall in the low compressor imposed on the high compressor. Experimental results showing flow coefficient at stall versus distortion rotation speed are given in Fig. 5 [15]. There is a marked increase in the value of stall flow coefficient when the propagation speed of the distortion is close to the natural speed of stall propagation.

As will be shown below, it is clear that the decrease in stability is not an effect that one can predict form any steady theory, that it is associated with the behavior of the disturbance wave structure in the compressor annulus, and that its understanding and prediction at even a basic level involves unsteady flow effects.

The most important problem associated with inlet distortion is the change in the operating point at which flow instability occurs. One approach pursued recently as a joint MIT-Cambridge University effort is a rigorous stability analysis of the circumferentially nonuniform flow in a compressor, i.e., the stability (to small amplitude perturbations) of a steady circumferentially non-uniform flow field in an axial compressor [16], [17]. In this, the steady flow nonuniformity must come into the problem in a nonlinear manner, otherwise there is no interaction between distortion and unsteady perturbations. It is also necessary to include not just a description of the compressor, but the compression system as well, because

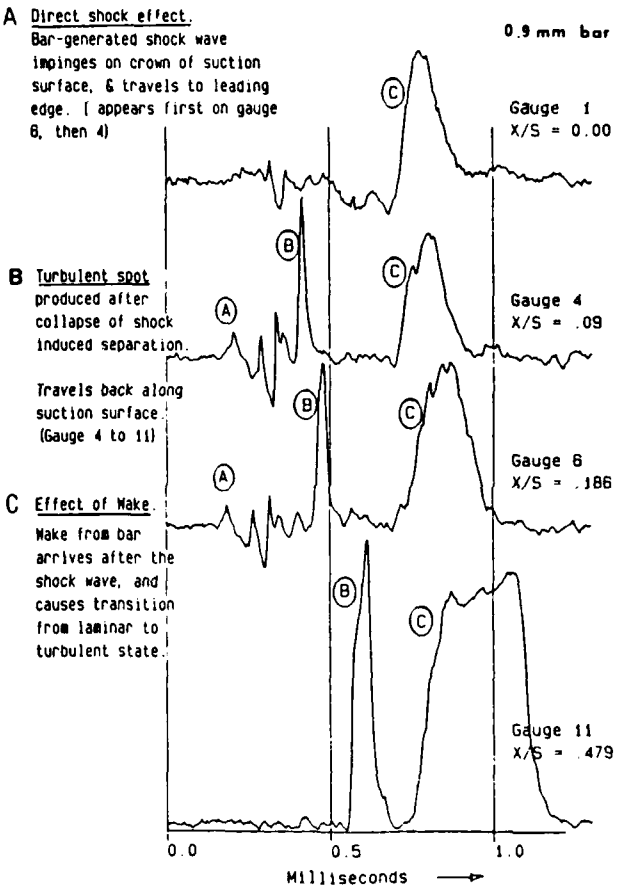

Fig. 4 Summary of effects of wakes and shock waves on turbine heat transfer [7]

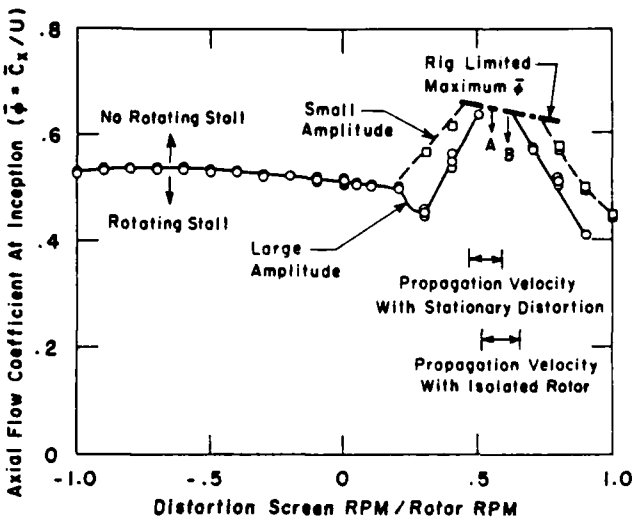

Fig. 5 Effect of distortion rotation rate on stall point [15]

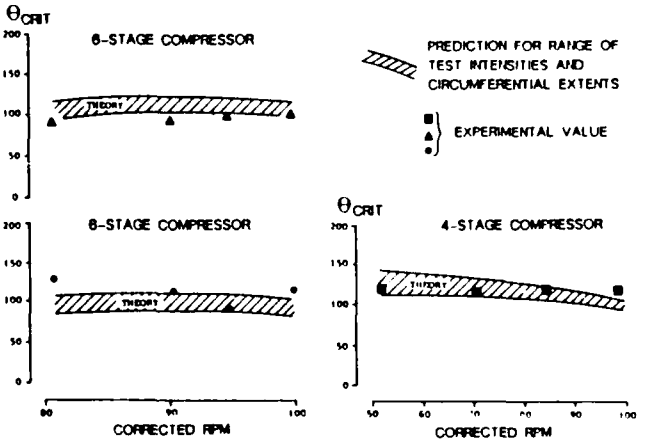

Fig. 6 Predicted and experimental critical sector angles [14]

the presence of a travelling wave perturbation in a distorted flow will cause changes in the annulus averaged flow quantities.

A key feature of the calculation procedure is a model for the fluid dynamic interaction between the spoiled and unspoiled sectors of the compressor. This, rather than any "critical resonance time" appears to be linked most closely to stability.

The analysis shows that there is a useful approximate stability criterion, annulus averaged slope of the compressor pressure rise characteristic equal to zero.

$$\int_0^{2\pi} \frac{d\psi}{d\phi}\, d\theta = 0 \quad ; \quad \psi = \text{non-dimensional pressure rise}, \quad \phi = \text{axial flow parameter}$$

This is valid in the many situations when the dynamics of the compressor distorted flow field do not couple strongly to the compression system or when the structure of the imposed distortion is not similar to that of the eigenmodes of the flow in the compressor annulus.

Application of this criterion to different multistage compressors is given in Fig. 6 [14]. The figure shows first-of-a-kind computations, based on the theoretical model, of θ_{crit}, which is a parameter used to modify the parallel compressor theory to correlate stall margin loss.

To understand the previously mentioned decrease in stability for rotating distortions, calculations have been carried out for distortions rotating at various fractions of rotor speed, f, from f = -0.6 (against rotor rotation) to f = 0.6. As in the experiments, rotation rate has a marked effect on the overall distorted flow compressor characteristic as well as the stall point. The results are shown in Fig. 7. As the distortion rotation rate is increased from zero to 0.3, there is a drop in the compressor performance and a shift in the stall point, and for f = 0.3, there is only a small regime in which the flow is stable. We view this as a (nonlinear) resonance between the inlet disturbance and the natural eigenmodes (i.e., the embryo propagating stall modes which have f ≈ 0.33) of the flow in the compressor annulus.

The analysis also indicates that with inlet distortion there will be a decrease in stability due to interactions between the compressor and the compression system, when the frequencies of the surge-like and rotating stall-like perturbations approach each other. The situation can be described in terms of an increased disturbance energy being fed in from the compressor due to the propagating disturbances forcing the system-type oscillations near their resonant regime.

As the final topic on inlet distortion, we describe a scheme for increasing the distortion tolerance using asymmetric stator staggering [18]. The basic idea can be discussed with reference to Fig. 8 which presents the arguments in terms of parallel compressor ideas although it is to be stressed that the computations carried out are much more general.

Three speedlines are shown for nominal vane stagger, and for staggers increased and decreased by $\Delta\gamma$. With an inlet total pressure distortion, ΔP_t, and the stagger uniform around the circumference, the low

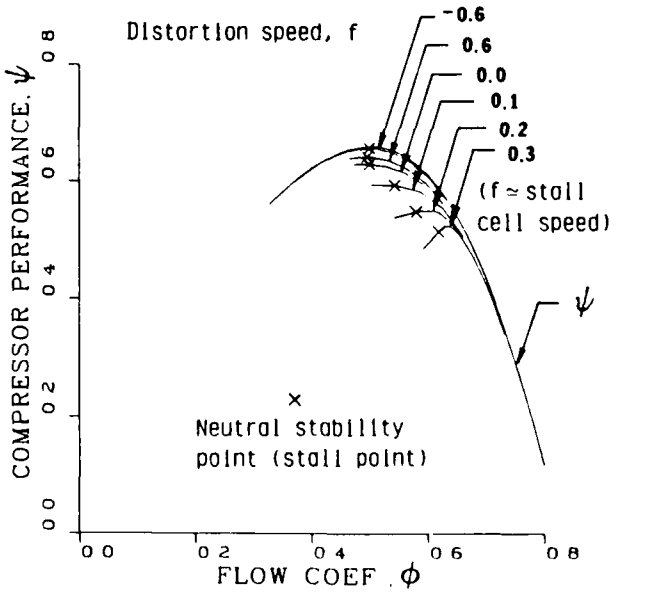

Fig. 7 Compressor performance with inlet distortion; effect of distortion rotation rate [17]

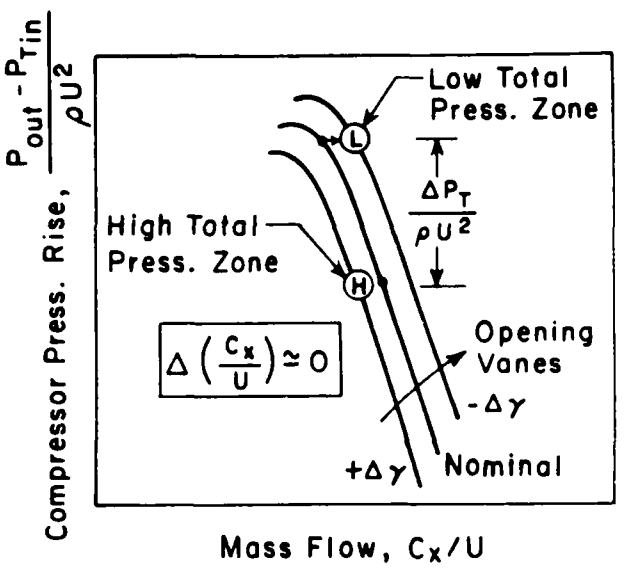

Fig. 8 Effect of asymmetric vane stagger on compressor response to circumferential distortion [18]

and high total pressure zones operate at the solid points.

Suppose one has the capability to vary the vane stagger asymmetrically about the circumference, open in the portion of the circumference that sees a low total pressure, and closed in the portion exposed to high total pressure. Such an action moves the low and high pressure zone operating points to the locations denoted by L' and H'.

There are two consequences of doing this. The axial velocity distortion presented to the compressor is greatly decreased, and the operating point of the low total pressure zone moves "down" the speedline relative to its position for the nominal stagger. This implies that there will be a smaller velocity distortion and an increased distortion tolerance due to the increased pressure rise capability of the speedline with opened vanes, with essentially no decrease in mean (annulus averaged) flow or pressure rise.

This strategy was described some time ago [19], but as far as we are aware, the computations in [18] are the first quantitative indications of the degree to which such a scheme is useful. Examination of the change in stability due to asymmetric stagger are given in Fig. 9, which shows calculated loss in stall pressure rise versus inlet distortion level. A two-sector vane stagger arrangement is used, and the curves refer to different amounts of vane motion. The stall pressure rise increases when the vanes are used because the velocity defect is decreased, so that the "average" operating point of the compressor becomes closer to the axisymmetric characteristic.

COMPRESSOR/COMPRESSION SYSTEM INSTABILITY

Although one still cannot predict the onset of instability in a turbomachine or engine flow field from a first principles basis, there has been significant progress in understanding the instabilities that are of practical concern in gas turbine engines.

As pointed out in [20], an important question is whether a given compression system will exhibit large amplitude oscillations of mass flow and pressure ratio (surge), or whether the system will operate in rotating stall where the annulus averaged mass flow and pressure ratio are essentially steady, but are greatly reduced from the pre-stall values. As a step towards answering this, the nonlinear system behavior has been analyzed, using a simple lumped parameter representation, with experiments carried out to validate the basic analysis. For a given compression system, there is an important nondimensional parameter, B, on which the system response depends:

$$B = \frac{U}{2\omega L_c}$$

where ω is the Helmholtz resonator frequency of the system, L_c is an "effective length" of the compressor duct, and U is the rotor speed. For a given compressor, there is a critical value of B which determines whether the mode of instability will be surge or rotating stall.

An examination of stall transients in compressors from a more general point of view, encompassing surge and rotating stall as special cases, is given in [21]. Nonlinear coupling exists between the (local) compressor performance and the (global) system behavior for two reasons. First, the rate of growth of the stall cell is dependent on the annulus averaged velocity at the compressor face, which is dependent on the system dynamic behavior. Second, the overall pressure rise depends on the shape (extent, amplitude, etc.) of the rotating stall cell which is a function of the unsteady compressor performance.

Calculations have been carried out to show the phenomena that can be captured by the analysis, as in Fig. 10 [21]. This is essentially a "time trace" representative of the local velocity (the velocity which would be seen by a single probe) and the annulus averaged velocity, at the compressor face, versus time, during surge. The amplitude of the rotating stall cell varies considerably during the surge cycle, as the compressor goes in and out of rotating stall. What is not evident from the figures, but what is nonetheless very important in understanding compressor post-stall transients, is that growth and decay of the stall cell does not occur in a quasi-steady manner and the instantaneous compressor pumping characteristic can be quite different from the quasi-steady one.

Another computation of a post-stall transient, during which a substantial reversed flow period is

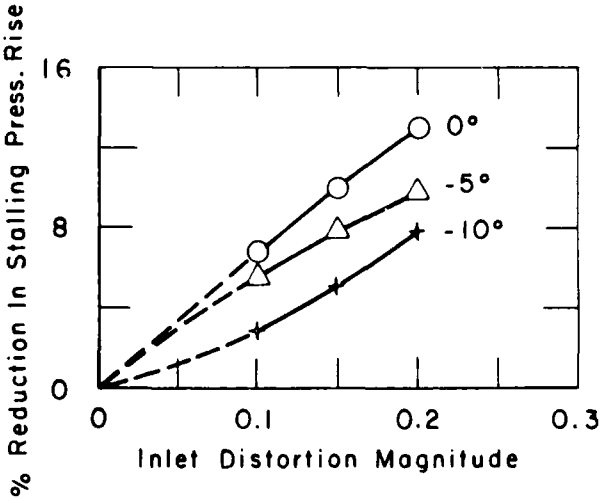

Fig. 9 Decrease in stall pressure rise versus magnitude of total pressure distortion [18]

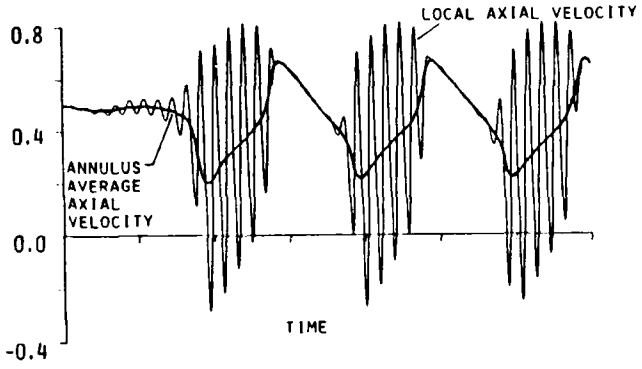

Fig. 10 Time history of local and annulus averaged axial velocities during surge [21]

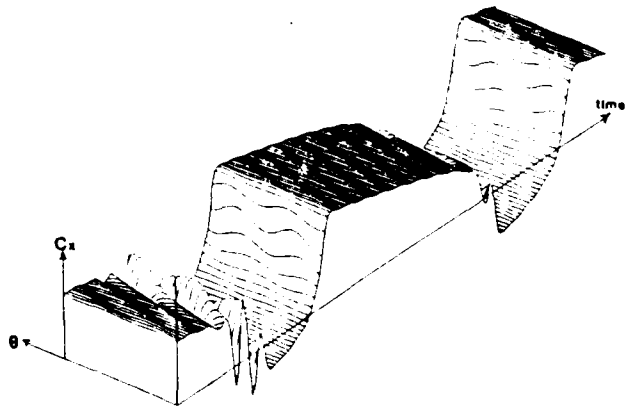

Fig. 11 Evolution of axial velocity wave during post-stall compressor transient

observed, is shown in Fig. 11. In the figure, θ measures distance around the circumference, C_x is axial velocity, and time is plotted along the long axis. The axial velocity waveform during the surge is quite complex and includes disturbances that propagate around the circumference, pulsations that are roughly planar, and a complicated admixture of both, at different times in the cycle. The post-stall transients seen in actual machines, however, appear to have many of these same features.

ACTIVE CONTROL OF UNSTEADY FLOWS IN TURBOMACHINES

An exciting new area of unsteady fluid mechanics is the use of integrated control in turbomachines to alter many of the aspects of operation from open loop to closed loop. One topic now being pursued is active stabilization, i.e., using unsteady effects to suppress aerodynamic instabilities, such as surge and rotating stall [22]. This work is still very much in its initial stages, and we show some simple calculations only, but it may have a significant potential for altering stall margin requirements.

The approach is fundamentally different from those that have been tried previously and is based on the recognition that the instabilities of interest are dynamic phenomena. If the aerodynamic damping (of these instabilities) were increased using active control, one might operate in a previously unstable, high performance region (as illustrated conceptually on the (deliberately provocative) compressor map in [22].)

Consider first the local instability, rotating stall, which we view as the growth of an unsteady propagating flow disturbance. The method of control is to sense this disturbance and generate an additional disturbance, possibly with a transducer system driven from processing data measured inside the turbomachine. The controlled system constitutes a machine of fundamentally different characteristics in which stable operation can be achieved under conditions which previously implied breakdown of the flow.

For the initial control strategies, an upstream velocity non-uniformity was generated of the form

$$(\delta C_x)_{\text{far upstream}} = Z(\delta C_x)_{\text{at compressor face}}$$

where δC_x denotes a perturbation in axial velocity and the control parameter, Z, is of the form $Z = Re^{i\beta}$.

Results of the calculations are shown in Fig. 12, based on parameters representative of a three-stage compressor. In the figure, Φ (mass flow) at instability is plotted versus β, the phase of the control parameter, Z, for different values of R, the modulus of Z. With no controller, the instability point is at Φ = 0.5, but with a controller, this is much altered.

Even for these fairly small values of R, there is a substantial movement of the stall point. If the controlled disturbance is considered to be put in by a row of far-upstream vanes that are wiggled, the local flow angle variation that has to be achieved for a one percent (vortical) velocity perturbation is approximately 1.5 degrees. Values of Z with modulus unity or higher are definitely possible.

For a multistage axial compressor, one must stabilize both local (compressor) and global (compression system) instabilities. For a centrifugal compressor, however (and perhaps for a single stage axial fan), the local instability that leads to rotating stall is often of less consequence than the system instability. If this is the situation, one can deal with the latter only.

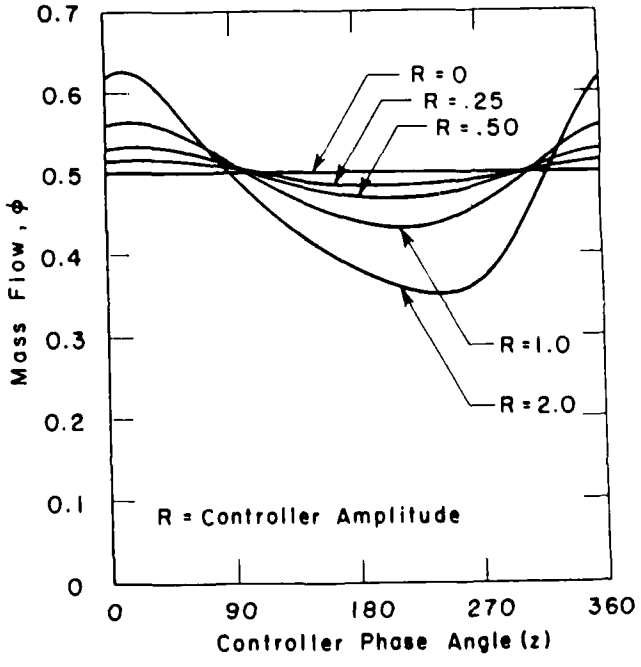

Fig. 12 Computed change in rotating stall inception point using active control [22]

Stabilization of surge oscillations has already been achieved for a turbocharger by Huang using a loudspeaker to alter plenum volume [23], and by Pinsley and Haldeman [24] using a downstream throttle. Stabilizing surge in a centrifugal compressor may be easier than suppressing rotating stall in an axial one because of the spatial uniformity and the low frequency of the oscillations and relatively slow growth rate of the instability.

To understand the mechanisms by which the controller suppresses the growth of oscillations, it is useful to examine production and dissipation of perturbation energy in the system. Detailed discussion of this is given in [22], but the important point is that it is the unsteady behavior (of the compressor, of the compression system, and of the controller) that must be understood to implement these schemes in an effective manner.

IMPLICATIONS FOR DATA ANALYSIS

Unsteady Structure in "Real" Turbomachine Wakes

Wakes are often viewed as constant pressure regions with a velocity defect. Actual wakes, however, generally have a well-defined unsteady vortical structure because the steady wake velocity profile is strongly unstable. The instability is inviscid, associated with the presence of a maximum of vorticity, and growth rates tend to be much larger than those associated with amplification of Tollmien-Schlichting waves. The situation downstream of the trailing edge is thus often as shown schematically in Fig. 13, with a vortex street forming downstream.

One result is that time resolved measurements of rotor exit flow will not show a periodic wake signal unless they are ensemble averaged. As example, Fig. 14 shows the relative flow angle determined by a high response probe at exit of a transonic rotor [25]. The upper trace is instantaneous data, the lower trace is for a 90 rotor revolution ensemble average.

Laser doppler anemometer measurements also reflect this unsteadiness, and can show a bimodal probability density distribution (p.p.d.) in the presence of vortex shedding, indicating that the wake may be more properly viewed as composed of two velocity states, one centered near the core flow velocity level and the other lower than the core flow level by nearly twice the time-mean wake velocity deficit.

Modelling the unsteady flowfield downstream of the rotor very simply as a two-dimensional vortex street appears to give a useful qualitative picture of the flowfield. This unsteady vortex model reproduces the wake shape and bimodal p.d.d., and accounts for the high level of blade to blade variation observed in several transonic compressors, which is now viewed as being due to intermittent sampling of the vortex street by the fixed frame probe [25].

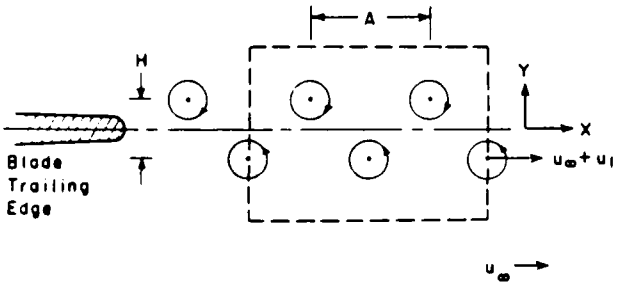

Fig. 13 Geometry of rotor blade vortex street

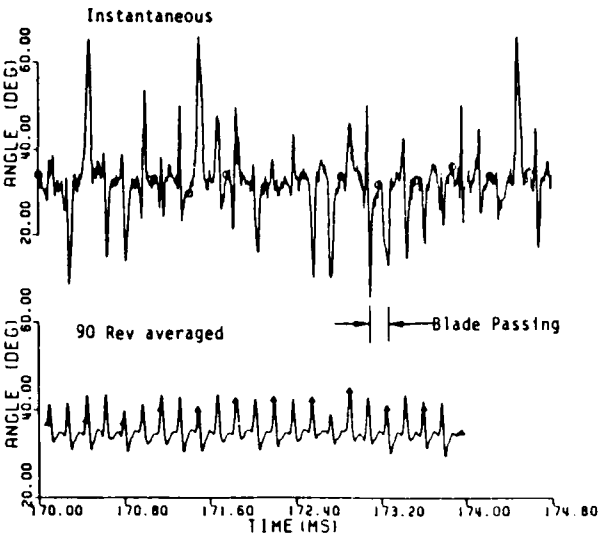

Fig. 14 Instantaneous and blade-by-blade ensemble average rotor exit angle measurements [25]

Energy Separation in Unsteady Flow

Another effect of the wake vortex structure is the creation of a nonuniform relative (i.e., as measured in the blade fixed system) total temperature [26]. The situation is similar to that analyzed in the seminal paper on this topic by Preston [27], and can be demonstrated by examining the kinematics of a vortex row. Close to any vortex, the streamlines n the vortex fixed coordinate system are roughly circular. Velocity magnitude, pressure and temperature are roughly constant on these streamlines. To a stationary observer, fluid particles on one side of the vortex row have a high velocity and those on the other a low velocity, so particles on one side of the row have a higher total temperature than those on the other. Unsteadiness due to the vortex row is thus tied to total temperature differences.

The top part of Fig. 15 shows a row of vortices moving to the right, and the solid line represents a particle path. Static pressure changes experienced by the particle are also shown. The terms "turbine" and "compressor" are appropriate because kinematically the vortices act like turbines for the passage of fluid across the row from the upper side and like compressors for the passage from below to above the row.

For a turbomachine wake which consists of two of these vortex rows, moving from the free stream to the wake has the same effect as going across a turbine blade row, i.e., a drop in total temperature (consider the circulation of the vortices shown in Fig. 15). Neglecting dissipation and heat transfer, the relative total temperature difference would be expected to be roughly $U_v \Gamma/h$, where U_v is the vortex velocity as seen in the blade fixed system, Γ is the circulation and h is the vortex spacing. As is evident from this basic discussion, the variations in temperature and pressure observed will scale approximately as relative Mach number squared.

The wake structure can affect the efficiency that one infers from high response measurements and, as indicated as shown in [28], can give rise to apparent differences of order 1% between machines which may actually have the same performance.

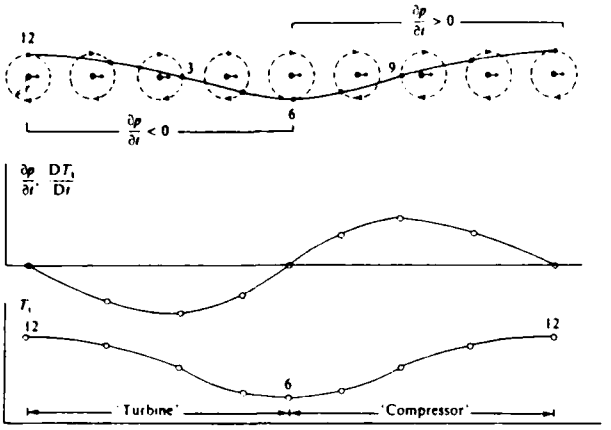

Fig. 15 Variation of T_t along pathline; moving row of vortices [26]

Unsteady Separation

The vortex shedding is a phenomenon with characteristic frequency of order ten kilohertz for a half meter diameter transonic fan. There are also much lower frequency sources of unsteadiness that exist, which may affect not only performance, but may be in a frequency range to excite blade vibrations.

To understand the cause of the low frequency unsteadiness, two-dimensional unsteady viscous calculations have been carried out [28] using the midspan geometry of a transonic rotor. The vortex shedding shows up quite clearly in the calculated trailing edge static pressure, Fig. 16, along with a lower frequency which modulates its amplitude and the frequency, similar to the modulation observed experimentally. The lower frequency correlates with the computed motion of the separation point along the suction surface and with axial motion of the passage shock. There is also a 30% fluctuation in blade moment at this frequency (~300Hz) which can be of concern structurally. The exact cause of this movement of the separation point is not yet clear but it does appear similar to instabilities observed in high speed diffusers [28].

The large fluctuations in frequency shown in the numerical simulation also tend to explain the difficulty often encountered in extracting a single, unambiguous frequency estimate from experimental measurements. Fluctuations of this magnitude may also blur the bimodal anemometer histograms. The point to be emphasized is that separation is generically an unsteady process and that there can be aerodynamic, as well as perhaps aeroelastic, consequences of this for turbomachines.

MIXING PROCESSES IN TURBOMACHINES AND OTHER PROPULSIVE DEVICES

In predicting the performance of a turbomachine, especially a multistage machine, it is important to be able to account for mixing processes that occur, such as radial transport of quantities from the endwall regions to near midspan. Mixing is included in the phenomena covered in this lecture because it is viewed here inherently as an unsteady process.

In this connection, we can briefly note some of the recent results concerning mixing in situations that are much simpler than turbomachines, for example, turbulent plane shear layers, where it is recognized that the "turbulence" has a definite organized unsteady vortical structure to it. Descriptions using this structure appear to provide a more fundamental picture of the flow than approaches which do not. In this instance, at least, it seems that there is an increase in insight if one recognizes the inherent unsteadiness of the phenomena, rather than tries to devise procedures which suppress the unsteadiness through some sort of averaging.

The mixing process in turbomachines is more complex and, in the past five years, two different descriptions have been put forth. One of these attributes the radial transport to an organized secondary flow [29], the second to "turbulent diffusion" [30]. Although the descriptions are based on totally different mechanistic ideas, they both appear to give good results when applied to multistage machines. (As stated in [11]: "One conclusion one might reach is that the introduction of any spanwise mixing model is better than none at all in attempting to predict multi-stage compressor performance.")

Some resolution of the two viewpoints has recently been made by Wisler [31], who showed that the real situation is actually a combination of both mechanisms. What is not well known is how mixing is influenced by compressor design parameters. If a turbulent-like process is indeed occurring, it would seem useful to examine it using some of the recent concepts concerning coherent turbulence structure, i.e., by again recognizing the unsteadiness and not trying to fit the process into a gradient transport framework. The whole topic of mixing in turbomachines is an area of unsteady flow which needs further exploration on a basic level.

Flow Control Using Embedded Streamwise Vorticity

A final topic, which is related to the two previously described areas of mixing and flow control, and which has been of considerable recent interest, is flow control using embedded streamwise vorticity. This differs from other phenomena that we have been discussing in that the process involved may not be intrinsically unsteady (at least on the larger scale of the motion involved). Nevertheless, it is appropriate to include it because of the potential offered for: decreasing base drag in subsonic flows (through the strong effect on the unsteady vortex shedding which is critical in setting the base pressure), suppressing airfoil separation, altering wake structure in turbomachines, reducing unsteadiness in

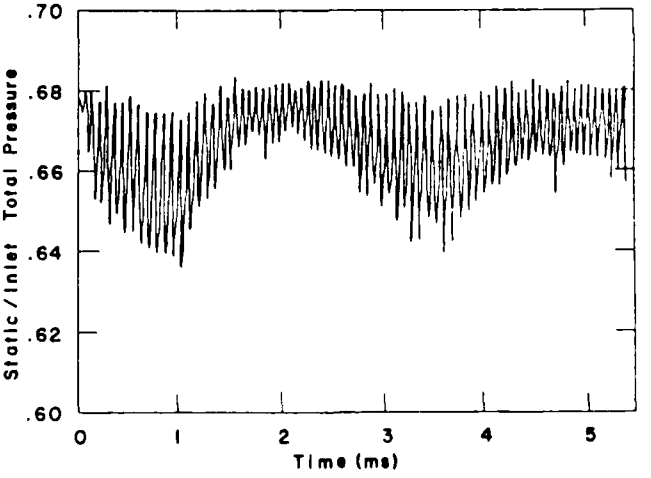

Fig. 16 Computed static pressure history at trailing edge of transonic compressor airfoil [28]

stall and diffusing passages, and enhancing mixing in a variety of propulsive devices.

The genesis of the idea arose from work done over a decade ago on forced mixer nozzles for turbofan engine noise reduction. A generic configuration is shown schematically in Fig. 17. The presence of convolutions or lobes, in the surface between two streams, creates trailing vorticity, similar to that from a finite wing. Streamwise vorticity in these flows can be much stronger than that seen in natural mixing layers between two streams.

Studies of the behavior of flow downstream of the lobes reveal an abrupt transition (as a function of downstream distance) from well-defined spiraling motion to a highly mixed state. Mixer nozzles, as well as other fluid dynmamic devices relying on mixing for their operation, can accomplish this much sooner than with natural mixing, i.e., with a splitter plate between them. One can thus drastically shorten an ejector, for example, and still obtain almost ideal performance. Strong streamwise vorticity can also inhibit coherence of spanwise vortex shedding, altering the flow in the base region of airfoils and decreasing base drag.

Application of this type of flow control is still in the early stages, but Fig. 18 presents sample results for an ejector tested with free and with convoluted splitters [10]. Secondary to primary flow rates (pumping) versus overall ejector lengths are shown. Calculations based on a simple control volume analysis are also indicated by the "ideal" line. Over the regime tested, the convoluted splitter increased injector pumping by over 100 percent, due to the greatly increased mixing. A major effect of the streamwise vortices was to improve the downstream diffuser performance because the large scale vortices sweep low energy boundary layers away from the outer wall surface.

The central problem of designing optimized lobes of this type can be posed as questions about: 1) what is the distribution of vorticity in the flow that will lead to the desired flow modification, and 2) how does one create this distribution. The substantial opportunity offered for improvements in turbomachinery performance using embedded streamwise vorticity make this an extremely fruitful subject for research.

CONCLUDING REMARKS

Unsteady flow phenomena affect a wide range of turbomachinery operation, from peak efficiency, to measurement interpretation, to performance with circumferential inlet distortion, and to stability and post-stall transients. In many of these, the unsteadiness is associated with a vortical structure. Design trends in modern turbomachines are such that unsteady effects are becoming even more important.

In the majority of current design procedures, the basic unsteady aspects of the flow are not recognized. Turbomachinery technology, however, appears to have advanced to a state where future improvements will come from understanding, and from the many opportunities for control, of these aspects. Inclusion of unsteady flow effects into design procedures in a rational, fundamental manner seems challenging but very worthwhile goal.

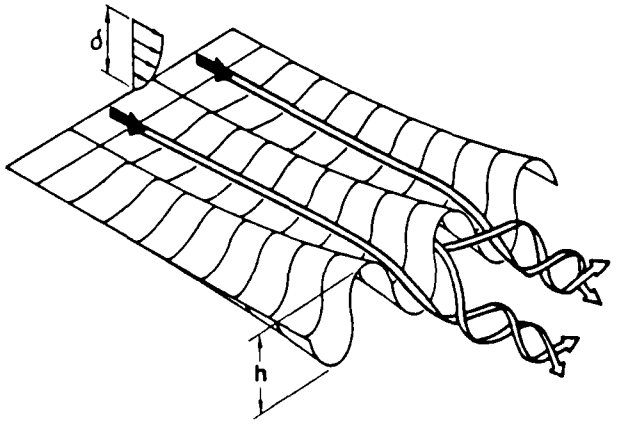

Fig. 17 Sketch of mixer lobe geometry [10]

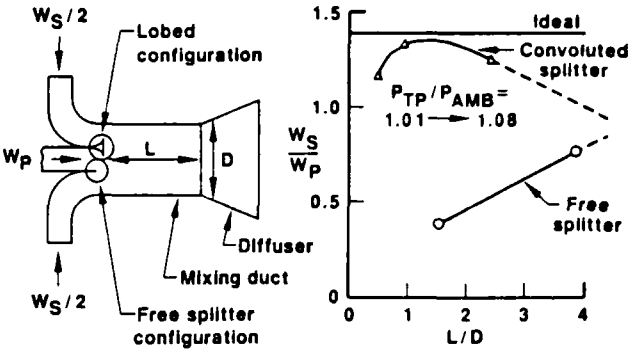

Fig. 18 Mixer ejector application [10]

ACKNOWLEDGEMENTS

The author is pleased to acknowledge the critical comments of Dr. C.S. Tan, which helped shape this lecture, and the useful suggestions of Prof. A.H. Epstein. Partial support for the preparation of the manuscript was furnished by the Air Force Office of Scientific Research, under Contract F49620-85-C-0018, J.D. Wilson Program Manager. This support is gratefully acknowledged.

REFERENCES

[1] Mikolajczak, A.A., "The Practical Importance of Unsteady Flow," Unsteady henomena in Turbomachinery, AGARD CP-177, 1975.

[2] Platzer, M.F., "Unsteady Flows in Turbomachines - A Review of Current Developments," in AGARD Conference Proceedings 227, Unsteady Aerodynamics, 1977.

[3] Day, I.J., and Cumpsty, N.A., "The Measurement and Interpretation of Flow Within Rotating Stall Cells in Axial Compressors," J. Mech. Eng. Science, Vol. 20, 1978, pp. 101-114.

[4] Lavrich, P.L., "Axial Compressor Stall Phenomena," Ph.D. Thesis, MIT, to be submitted 1987.

[5] Hodson, H.P., "Measurements of Wake Generated Unsteadiness in the Rotor Passages of Axial Flow Turbines," ASME Paper 84-GT-189, 1984.

[6] Hodson, H.P., "The Development of Unsteady Boundary Layers in the Rotor of an Axial-Flow Turbine," in AGARD Conference Proceedings No. 351, Viscous Effects in Turbomachines, 1983.

[7] Doorly, D.J. and Oldfield, M.L.G., "Simulation of the Effects of Shock Wave Passing on a Turbine Rotor Blade," ASME Paper 85-GT-112, 1985.

[8] Ffowcs Williams, J., "Anti-Noise," Proc. Royal Soc., A395, 1984, pp. 63-88.

[9] Ffowcs Williams, J., The Aerodynamic

Performance of Anti-Sound," 1986 Florence and Daniel Guggenheim Memorial Lecture.

[10] Werle, M.J., Paterson, R.W., and Presz, W.M., "Flow Structure in a Periodic Axial Vortex Array," AIAA Paper 87-0610, 1987.

[11] Wennerstrom, A.J., "Low Aspect Ratio Compressors: Why and What It Means," 1986 Cliff Garrett Lecture.

[12] Scott, J.N., and Hankey, W., "Navier-Stokes Solution of Unsteady Flow in a Compressor Rotor," ASME J. Turbomachinery, Vol. 108, 1986, pp. 206-215.

[13] Dong, Y., Personal Communication, 1987.

[14] Williams, D.D., "Review of Current Knowledge of Engine Response to Distorted Inflow Conditions," in Engine Response to Distorted Inflow Conditions, AGARD CP-400, 1987.

[15] Ludwig, G.R., Nenni, J.P., and Arendt, R.H., "Investigation of Rotating Stall in Axial Flow Compressors and Development of a Prototype Stall Control System," Technical Report USAF-APL-TR-73-45, 1973.

[16] Hynes, T.P. and Greitzer, E.M., "A Method for Assessing Effects of Inlet Flow Distortion on Compressor Stability," to be published in ASME J. Turbomachinery.

[17] Hynes, T.P., et al., "Calculations of Inlet Distortion Induced Compressor Flow Field Instability," in Engine Response to Distorted Inflow Conditions, AGARD CP-400, 1987.

[18] Chen, G.T., Greitzer, E.M., and Epstein, A.H., "Enhancing Compressor Distortion Tolerance by Asymmetric Stator Control," AIAA paper AIAA-87-2093, 1987.

[19] Wanger, R., and Smith, L.H., "Sector Control of Fan IGV Position," General Electric Company Preliminary Program Brief, 1971.

[20] Greitzer, E.M., "The Stability of Pumping Systems - The 1980 Freeman Scholar Lecture," ASME J. Fluids Eng., Vol. 103, 1980, pp. 193-243.

[21] Moore, F.K., and Greitzer, E.M., "A Theory of Post-Stall Transients in Axial Compression Systems, Parts I&II," ASME J. Gas Turbines and Power, Vol. 108, 1986, pp. 68-76 and pp. 231-240.

[22] Epstein, A.H., Ffowcs, Williams, J.E., and Greitzer, E.M., "Active Suppression of Compressor Instabilities," AIAA paper AIAA-86-1994, 1986.

[23] Huang, X., Personal Communication, 1987.

[24] Pinsley, J., and Haldeman, G., Personal Communication, 1987.

[25] Hathaway, M.D., Gertz, J.B., Epstein, A.H., and Strazisar, A.J., "Rotor Wake Characteristics of a Transonic Axial-Flow Fan," AIAA Journal, Vol. 24, 1986, pp. 1802-1810.

[26] Kurosaka, M., et al., Energy Separation in a Vortex Street," J. Fluid Mech., Vol. 178, 1987, pp. 1-29.

[27] Preston, J.H., "The Non-Steady Irrotational Flow of an Inviscid Incompressible Fluid, With Special Reference to Changes in Total Pressure Through Flow Machines," Aeronautical Quarterly, Nov. 1961, pp. 353-360.

[28] Epstein, A.H., Gertz, J.B., Owen, P.R., and Giles, M.B., "Vortex Shedding in Compressor Blade Wakes," in Flow in Supersonic Turbomachines, AGARD CP-401, 1987.

[29] Adkins, G.G., Jr., and Smith, L.H., Jr., "Spanwise Mixing in Axial-Flow Turbomachines," Trans. ASME, Journal of Engineering for Power, Vol. 104, January 1982, pp. 97-110.

[30] Gallimore, S.J., and Cumpsty, N.A., "Spanwise Mixing in Multistage Axial Flow Compressors: Part I - Experimental Investigation," Trans. ASME, Journal of Turbomachinery, Vol. 108, July 1986, pp. 2-9.

[31] Wisler, D.C., Bauer, R.C., and Okiishi, T.H., "Secondary Flow Turbulent Diffusion and Mixing in Axial Flow Compressors," ASME Paper GT-16, 1987.

4. PUBLICATIONS AND PRESENTATIONS

Giles, M.B., "Calculation of Unsteady Flow in Turbomachinery," presentation at Courant Institute, NYU, February 1987.

Greitzer, E.M., "Mechanisms of Inlet Vortex Formation," presented at Renssalaer Polytechnic Institute, Troy, NY, March 1987.

Allmaras, S.R. and Giles, M.B., "A Second Order Flux-Split Scheme for the Unsteady 2-D Euler Equations on Arbitrary Meshes," AIAA-87-1119-CP, presented at the AIAA 8th Computational Fluid Dynamics Conference, June 1987.

Giles, M.B., "Non-Reflecting Boundary Conditions," presentation at Oxford University, July 1987.

Johnson, M.C. and Greitzer, E.M., "Effects of Slotted Hub and Casing Treatments on Compressor Endwall Flow Fields,"ASME J. Turbomachinery, 109, July 1987, pp.

McCune, J.E., "Interactive Aerodynamics of Wings in Severe Maneuver," Proceedings of Workshop II on Unsteady Flow, United States Air Force Academy, July 1987. To be published.

Giles, M.B. and Drela, M., "A Two-Dimensional Transonic Aerodynamic Design Method," AIAA Journal, Vol. 25, No. 9, September 1987, pp. 1199-1206.

Drela, M. and Giles, M.B., "Viscous-Inviscid Analysis of Transonic and Low Reynolds Number Airfoils," AIAA Journal, Vol. 25, No. 10, October 1987, pp. 1347-1355.

Greitzer, E.M., "Unsteady Flows in Turbomachines: Recent Advances and Opportunities for Control," Invited Lecture presented at Tokyo Gas Turbine Congress, October 1987.

Greitzer, E.M., "Flow Instabilities in Turbomachines," chapter in Handbook of Fluid Dynamics, A. Fuhs, ed., to be published in 1987-1988 by John Wiley.

McCune, J.E. and Scott, M., "Nonlinear Aerodynamics of Two-Dimensional Airfoils in Severe Maneuver," to be presented at the AIAA 26th Aerospace Sciences Meeting, Reno, NV, January 1988.

McCune, J.E., Tavares, T.S., Lee, N.K.W., and Weissbein, D., "Slender Wing Theory Including Regions of Embedded Total Pressure Loss," to be presented at the AIAA 26th Aerospace Sciences Meeting, Reno, NV, January 1988.

5. PROGRAM PERSONNEL

Principal Investigator:

Edward M. Greitzer
Professor of Aeronautics and Astronautics
Director, Gas Turbine Laboratory

Co-Investigators:

Alan H. Epstein
Associate Professor of Aeronautics and Astronautics
Associate Director, Gas Turbine Laboratory

Michael B. Giles
Assistant Professor of Aeronautics and Astronautics

James E. McCune
Professor of Aeronautics and Astronautics

Choon S. Tan
Principal Research Engineer

Graduate Research Assistants:

9/83 - Present	Petros Kotidis*, "Investigation of the Radial Transport in a Transonic Compressor Rotor Stage" (thesis title)
9/84 - 5/87	Norman Lee*, "Effects of Compressor Endwall Suction and Blowing on Stability Enhancement" (thesis title)
9/85 - Present	Edward Imperatori
9/86 - Present	Steve Allmaras (AFRAPT student)
9/87 - Present	Rob Plumley

* S.M. Degree Completed
**Ph.D Thesis Completed

6. INTERACTIONS

There are considerable interactions between Gas Turbine Laboratory personnel and industry and government. One of these was the spending of a "Sabbatical" leave at the Gas Turbine Laboratory by Dr. A.J. Wennerstrom of the Air Force Aero Propulsion Laboratory (Fall 1987). We list below only those which involved discussions of AFOSR projects. It should be noted that a considerable amount of the research at the GTL is supported by the aircraft engine industry and this promotes a large amount of technical interaction between MIT and the sponsors.

Seminars and Technical Discussions

Seminar by E.M. Greitzer on "Active Control of Turbomachinery Instability" at United Technologies Research Center, January 1987.

Visit by E.M. Greitzer to Whittle Laboratory, Cambridge University, England, May 1987.

Presentation by M.B. Giles on "Research at MIT in Computational Fluid Dynamics" to Mitsubishi's Nagoya Aircraft Works, Japan, June 1987.

Presentation by M.B. Giles on "Research at MIT in Computational Fluid Dynamics" to National Aerospace Laboratory, Japan, June 1987.

Presentation by M.B. Giles on "Calculation of Unsteady Flow in Turbomachinery" to IHI, Japan, June 1987.

Visit by J.E. McCune to Whittle Laboratory, Cambridge University, England, June 1987.

Visit by J.E. McCune to DFVLR, University of Gottingen, Gottingen, West Germany, August 1987.

Four-day short course by A. Epstein, M. Giles, E. Greitzer, and C. Tan on "Unsteady and Three-Dimensional Flows in Turbomachines" at Concepts ETI, Norwich, VT, September 1987.

Presentation by M.B. Giles on "Calculation of Unsteady Flow in Turbomachinery" to United Technologies Research Center, October 1987.

The Gas Turbine Laboratory also has an active seminar program to increase interaction with industry and/or government by bringing speakers to MIT. During the period covered by this report, these have included:

Dr. W. Presz, United Technologies Research Center/Western New England College
"Performance and Mixing Enhancement Using Axial Vortex Arrays"

Dr. A.J. Wennerstrom, Air Force Aero Propulsion Laboratory
"Low Aspect Ratio Axial Flow Compressors: Why and What It Means"

Dr. J. Simonich, United Technologies Research Center
"Liquid Crystal Measurements of Heat Transfer in Turbulent Boundary Layers on Concave Surfaces"

Dr. T.J. Barber, United Technologies Research Center
"Hypersonic Flow Propulsion Systems: A Case Study for Applied CFD"

Dr. D.C. Wisler, General Electric Company, Aircraft Engine Business Group
"Mixing in Axial Compressors"

Dr. D.B. Hanson, Hamilton Standard Division, United Technologies Corporation
"Prop-Fan Aeroacoustics"

7. DISCOVERIES, INVENTIONS, AND SCIENTIFIC APPLICATIONS

During the present contract period, there have been no inventions.

8. CONCLUDING REMARKS: FUTURE EFFORTS

The main remarks here conern the thrust of the future work under this contract. As is evident from the discussions that we have had with AFOSR personnel, all of the investigators are in accord that it is the understanding of unsteady flow phenomena in turbomachines which is necessary to achieve the desired improvements in levels of performance. The overall research activity in the next year will therefore be focussed more strongly on this area. In particular, the four areas in which research will be conducted are:

1. Unsteady Flow in Compressors,
2. Numerical Investigation of Viscous Flow Instabilities,
3. Unsteady Phenomena, Inlet Distortion, and Flow Instabilities in Multistage Compressors, and
4. Unsteady Blade-Vortex Street Interactions in Transonic Cascades.

As stated before, we see as an important asset in dealing with these complex problems the existence of a "critical mass" of faculty and students in the Gas Turbine Laboratory whio share a strong interest in unsteady fluid phenomena. The multi-investigator format is extremely useful in enabling us to maintain this type of interactive research effort.

END

DATE

FILMED

5-88

DTIC